SEASONAL OSCILLATIONS IN A MID-LATITUDE OCEAN WITH BARRIERS TO DEEP FLOW

Eric Firing

S.B., Massachusetts Institute of Technology

(1973)

Submitted in Partial Fulfillment of the Requirements for the Degree of DOCTOR OF PHILOSOPHY

at the

Massachusetts Institute of Technology

and the

Woods Hole Oceanographic Institution

August, 1978

Signature of Author Eric Firing
Joint Program in Oceanography, Massachusetts Institute of Technology--Woods Hole Oceanographic Institution and Department of Meteorology, Massachusetts Institute of Technology, August, 1978.

Certified by Henry M. Stommel
Thesis Supervisor

Accepted by J. M. Edmond
Chairman, Joint Oceanography Committee in the Earth Sciences, Massachusetts Institute of Technology--Woods Hole Oceanographic Institution.

SEASONAL OSCILLATIONS IN A MID-LATITUDE OCEAN WITH BARRIERS TO DEEP FLOW

by

ERIC FIRING

Submitted to the Joint Oceanographic Committee in the Earth Sciences, Massachusetts Institute of Technology and Woods Hole Oceanographic Institution, on August 11, 1978, in Partial Fulfillment of the Requirements for the Degree of Doctor of Philosophy

ABSTRACT

A two-layer linear analytic model is used to study the response of the mid-latitude ocean to the seasonal variation of the windstress. The most important component of the response is a barotropic quasi-steady Sverdrup balance.

A meridional ridge such as the Antilles Arc is modeled as an infinitely thin meridional barrier that blocks the lower layer but does not protrude into the upper layer. It is found that such a barrier has little effect on the upper layer flow across the barrier. This result is obtained provided the frequency of the motion is low enough so that free short Rossby waves are essentially nondivergent. In this case there is little coupling between the layers for energy propagating to the east away from the barrier.

A study of the dynamics of flow over a sloping bottom is made and the results are used to determine the effect on seasonal oscillations of eastern boundary slopes and triangular

ridges. It is found that the presence of a slope at the eastern boundary has little effect. A meridional ridge that does not reach the interface may cause substantial scattering of free Rossby waves, but unless the ridge is steep its effect on the quasi-steady Sverdrup balance is minimal. However, if the ridge height is a substantial fraction of the lower layer depth and the width is comparable to the scale of free short Rossby waves, the ridge will tend to block flow in the lower layer, acting like the infinitely thin barrier. The theory suggests that the Antilles Arc should have the effect of a thin barrier, while the Mid-Atlantic Ridge should have little effect on the response of the ocean to seasonal wind variations.

Thesis Supervisor: Henry M. Stommel, Professor
Department of Meteorology
Massachusetts Institute of Technology

ACKNOWLEDGEMENTS

I am deeply grateful to Prof. Henry Stommel, who suggested the topic of this thesis as well as supervising the work. From the time of my first exposure to oceanography through the present he has been a source of ideas, inspiration, fun, and encouragement.

Although he was not involved in the work presented in this thesis, Dr. Robert Beardsley was responsible for my first research efforts. I owe much to his patience and guidance at that time.

Conversations with Drs. Joseph Pedlosky and Nelson Hogg were especially useful in the course of my work. Comments by Drs. James Luyten and Peter Rhines led to improvement in the manuscript. Dr. Lloyd Regier provided moral support.

Figures were drawn by Edna Coneybear and Jeffrey Zwinakis, and typing was done by Doris Haight. Their competence and patience are appreciated.

For three and a half years of generous financial support I am grateful to the John and Fannie Hertz Foundation, from which I received a Graduate Fellowship. Research money and other support were provided by the National Science Foundation under contract OCE 77 15600.

Table of Contents

List of Figures

List of Figures (Contd)

List of Figures (Contd)

List of Figures (Contd)

List of Tables

List of Tables (Contd)

List of Tables (Contd)

Chapter I

Introduction

The seasonal variation of the wind over the mid-latitude oceans is comparable in magnitude to the mean wind, which is the primary driving force of the mean ocean circulation. What seasonal variations in the ocean circulation are driven by the seasonal variations in the wind? This is the central question that motivates this thesis.

Lighthill (1971) discusses time-dependent ocean response in general, including the reasons why it is of interest. There are several reasons why the annual cycle is of particular importance. It occupies a point on the frequency spectrum that may be thought of as intermediate, between "climate" with its timescales of years to thousands of years, and "weather" with its timescales of days to weeks. The concentration of seasonal forcing at a few discrete frequencies affords a valuable opportunity to discover the connection between forcing and response. Like tidal motion but unlike most other time-varying motions, the regularity of the seasonal cycle means that historical data taken at irregular intervals can be used to accurately determine amplitude and phase of both the forcing and the response.

As a practical matter, it is important to know the annual cycle of ocean currents and properties in order to interpret historical data and design monitoring programs. For example,

oceanographic cruises may tend to be concentrated in the milder seasons. How much bias does this introduce when estimating time averages of properties? Understanding the ocean response to annual forcing is also a necessary step in understanding the seasonal cycle of the coupled ocean-atmosphere system, and in understanding the fluctuations of that cycle from year to year. In addition, there is the possibility that the annual cycle may lead directly to mean transports of mass and/or other quantities.

An early study of the response of the ocean to periodic forcing was made by Veronis and Stommel (1956). Using an unbounded two-layer beta-plane model with forcing independent of latitude and periodic in longitude they explored the wide range of motions from fast inertial waves to slow Rossby waves. Their main finding relevant to the present study was that in mid-latitudes the barotropic response predominates at higher frequencies while the baroclinic response becomes important at low frequencies. Motions of annual period are near the crossover between barotropic and baroclinic dominance. In the limit of low frequency the two modes occur in combination such that the response is limited to the upper layer.

Phillips (1966) developed bounded beta-plane models, both homogeneous and two-layer, driven by forcing periodic in time and in the meridional direction. Bottom friction

was included so the response was in the form of damped basin modes. At annual frequencies the barotropic response in terms of meridional velocity was small except very close to the western boundary. In the two-layer model the upper layer meridional velocity dropped much less rapidly with distance from the western boundary, since the bottom friction was inefficient in damping low frequency upper layer motion. At periods shorter than 250 days, for which there were no propagating baroclinic waves, there was little difference between the homogeneous and the two-layer results. The phase of the response was not discussed, since Phillips was interested in explaining the observed power spectrum of currents near Bermuda. Recently Leetmaa (1978) has re-evaluated both the observations and the (barotropic) model to conclude that a regular cycle of forcing at harmonics of the annual frequency may indeed account for much of the observed energy at those frequencies.

Other studies of the response of a homogeneous beta-plane model to periodic forcing include the analytic work of Pedlosky (1965a) and the numerical work of Veronis (1970). Both calculated nonlinear effects and found significant mean flow generation by periodic forcing.

Longuet-Higgins (1965a) studied the effect of periodic and localized forcing patterns on a stratified unbounded beta-plane model. His main concern was the generation of Rossby waves by stationary or moving wind systems, so he

emphasized smaller spatial and shorter time scales than those of interest here.

Another approach to the study of time-dependent response is the use of forcing with a step function time dependence. All frequencies are present so the results are not immediately applicable to the case of periodic forcing, but useful insights may be obtained. In some cases the annual cycle of forcing may be so rich in higher harmonics that a spin-up model is superior to a periodic one. This idea is implicit in Lighthill's (1969) application of a spin-up model to the generation of the Somali Current by the Southwest Monsoon. Since the region is equatorial, the barotropic and baroclinic responses have comparable time scales, in constrast to the mid-latitude situation. Spin-up at mid-latitudes due to both wind stress curl and to long-shore stress is treated by Anderson and Gill (1975).

There are two papers that are explicitly concerned with mid-latitude annual response. That of Gill and Niiler (1973) emphasizes the factors involved in sea level variations. Scaling arguments are used to show that the barotropic response of the ocean interior should be in accord with the Sverdrup balance. White (1977) uses a reduced gravity model to show that the baroclinic response to annual wind curl variations consists of two parts: a displacement of the thermocline by Ekman pumping, and a free baroclinic wave generated at the eastern boundary.

All of the previous work mentioned so far (with the partial exception of Gill and Niiler, 1973) involves models with flat bottoms; but the ocean bottom is far from flat. Hence our central question of the response of the ocean to annual wind variations leads to a second question: How do the characteristic major topographic features of the oceans - the continental slopes, the mid-ocean ridges, the island arcs - affect the dynamics of the annual circulation?

The effect of topography on steady homogeneous flow on a beta-plane is fairly well understood. See, for example, Welander (1969) for calculations of the deep North Atlantic flow that might be driven by a uniform vertical velocity in the thermocline. The essential idea is that geostrophic flow may occur freely along geostrophic contours (constant f/H), but forcing in the form of a vertical velocity or torque is required to allow flow to cross contours. In a model with two immiscible layers there can be no steady vertical velocity of the interface, so motion in the lower layer can be induced only through interfacial friction. A model of this type is considered by Welander (1968).

Waves in a homogeneous fluid on a beta-plane over topography have been studied by, among others, Rhines (1969). He calculated the effect of simple step and ridge topographies on incident Rossby waves. He found that a step reflects waves if its fractional height is large compared to the (nondimensionalized) frequency. A wide ridge will also cause reflection,

but a ridge that is narrow relative to the length scale of the wave has little effect. Each slope generates vorticity of the opposite sign, so cancellation occurs.

Waves in a stratified fluid on a beta plane over a slope have also been studied by Rhines (1970). In a two-layer system with a north-south slope he found that the usual barotropic and baroclinic vertical modes are replaced by one mode concentrated in the upper layer and a second concentrated in the lower layer. With continuous stratification, Rhines finds that a slope brings forth a bottom intensified mode and a set of baroclinic modes that are influenced but little by the slope. These waves are investigated further by Suarèz (1971). The scattering of incident barotropic and first mode baroclinic waves by low topography in both continuous and two layer systems has been studied by Hall (1976). He concludes that scattering is strongest when a ridge is a few internal Rossby radii across and when the group velocity of the incident wave is at a shallow angle to the ridge axis.

The present investigation begins with the development in Chapter II of scaled linear equations for periodic flow on a beta-plane over topography. Two-layer stratification is used. The scaling is tailored to the problem at hand: oscillations due to annual wind varations. The north-south scale is assumed fixed by the forcing pattern, while the east-west scale is left free to be selected by the forcing or the

dynamics as required. With the slope terms set to zero, a unified theory of annual oscillations without topography is developed. The model is bounded in the east and west but is open to the north and south. Emphasis is placed on forcing that is zonally uniform, but more general forcing is also considered.

In Chapter III we examine the effects of some simple topographic features on the annual circulation. We start with a model inspired by the Antilles Arc in the Atlantic and the Ryukyu Arc in the Pacific. The model has an infinitely thin meridional barrier that blocks the lower layer without impeding the upper layer. In section B of Chapter III we consider the properties of flow over an east-west slope. Two types of analysis are made. The first analysis uses constant-coefficient approximations of the vorticity equations to find plane wave descriptions of all the various types of motion. The second analysis uses scaling arguments to find approximate vorticity equations that are appropriate to each different type of motion. This gives a better understanding of the dynamics, but the solutions are too complicated to be used in calculating the effects of isolated features. Accordingly, in section C we use the plane wave solutions to calculate the effects of three topographic features: a sloping region at the eastern boundary; a triangular meridional ridge; and the same ridge combined with a lower layer barrier. Last, in section D we extend the thin

barrier model of section A to a multi-layer fluid. Examples with eight layers and barriers of various heights are presented.

Chapter IV is a survey of observations of the annual cycle of both winds and currents in the North Atlantic. The relation of these observations to the theory is discussed.

In Chapter V we summarize and discuss the results of the investigation and suggest areas in need of further study.

Chapter II

THE TWO-LAYER MODEL

A. Primary model equations

We are interested in low frequency, large scale motions in the ocean, and in particular, in the effects of topography on these motions. Suspecting that homogeneous models may be inadequate to display even some of the simplest physics, we are led to a two-layer model as a first step in discovering the role of stratification. The model will be limited from the outset to small amplitude oscillations in the absence of mean motion; quadratic terms in the dynamic variables will be omitted.

1. Scaled momentum equations

Consider a fluid of two imiscible layers with a small density difference $\Delta\rho$ and mean density ρ_0. With the traditional Boussinesq and hydrostatic approximations, the linearized momentum and continuity equations for the i^{th} layer are

$$u_{it} - f v_i = -\frac{1}{\rho_0} p_{ix} + F_i^{(x)} \qquad (2.A.1a)$$

$$v_{it} + f u_i = -\frac{1}{\rho_0} p_{iy} + F_i^{(y)} \qquad (2.A.1b)$$

$$p_2 - p_1 = g \Delta\rho \eta \qquad (2.A.1c)$$

$$u_{ix} + v_{iy} + w_{iz} = 0 \qquad (2.A.1d)$$

where (u_i, v_i) is the horizontal velocity vector in a Cartesian coordinate system with y positive northward and x positive eastward. The interface is perturbed by the motion to lie a distance η from its equilibrium position at $z = -H_1$. The velocity components are functions of x, y, and z. The vector $(F_i^{(x)}, F_i^{(y)})$ represents the dissipative forces, due primarily to turbulent motions. There is no adequate theory of such dissipation, so we will use the traditional device of introducing different eddy viscosities, ν_H and ν_V, in the horizontal and vertical directions:

$$(F_i^{(x)}, F_i^{(y)}) = \left(\frac{\partial}{\partial z}\nu_V \frac{\partial}{\partial z} + \nu_H \nabla^2\right)(u_i, v_i) \qquad (2.A.2)$$

where ∇^2 here and elsewhere refers to the horizontal Laplacian.

For simplicity, a rigid lid boundary condition will be used at the upper surface:

$$w_1 = 0 \quad \text{at} \quad z = 0 \qquad (2.A.3)$$

This rigid lid approximation is good so long as there is a scale of the motion, L, such that $L^2 << \lambda_R^2$ where $\lambda_R \equiv (gH)^{1/2}/f$ is the external Rossby radius of deformation. A typical mid-latitude value of λ_R is 3500 km. At the lower boundary, the condition of no flow through the boundary is

$$\underset{\sim}{u}_2 \cdot \nabla H_2 + w_2 = 0 \qquad \text{at} \quad z = -H_1 - H_2(x,y) \tag{2.A.4}$$

The lower boundary may come arbitrarily close to the interface, but must not pierce it. At the interface between layers, the linearized boundary condition is

$$w_1 = w_2 = \eta_t \qquad \text{at} \quad z = -H_1 \tag{2.A.5}$$

Interfacial friction will be neglected; we let ν_v go to zero except near the top and bottom boundaries. At the top boundary, we will specify the wind stress, $(\tau^{(x)}, \tau^{(y)})$. At the bottom boundary a no-slip condition will produce an Ekman layer. For most motions we will consider, this bottom Ekman layer is negligible. Likewise, the lateral friction term will be significant only in special instances.

All variables will now be non-dimensionalized by dividing them by appropriate scales. The meridional length scale, L, will be externally imposed, while the zonal scale, W, will be selected by the dynamics. The ratio $A \equiv W/L$ will be $O(1)$ or smaller. Since we are interested in periodic motion, all forcing terms and dependent variables can be expressed in the form $\mathrm{Re}[g(x,y,z)e^{-i\omega t}]$ where g is a complex amplitude. The operator $\frac{\partial}{\partial t}$ then becomes $-i\omega$, and the $e^{-i\omega t}$ factors out of each equation. The Coriolis parameter will be approximated by a linear function of y: $f = f_0 + \beta y$. Temporarily denoting non-dimensionalized variables with primes, we set

$$
\begin{aligned}
x &= W x' \\
y &= L y' \\
z &= H_1 z' \\
t &= \omega^{-1} t' \\
u_i &= \hat{u}\, u_i' e^{-i\omega t} \\
v_i &= \hat{u} A^{-1} v_i' e^{-i\omega t} \\
p_i &= \rho_0 f_0 L \hat{u}\, p_i' e^{-i\omega t} \equiv \hat{p}\, p_i' e^{-i\omega t} \\
\eta &= (\hat{p}/g\Delta\rho)\, \eta' e^{-i\omega t} \equiv \hat{\eta}\, \eta' e^{-i\omega t} \\
w_i &= \omega \hat{\eta}\, w_i' e^{-i\omega t} \\
H_2 &= H_{20}\, h(x',y') = H_1 \delta^{-1} h(x',y')
\end{aligned}
\qquad \text{(2.A.6)}
$$

In terms of these new variables, (2.A.1a-c), (2.A.3), (2.A.4), and (2.A.5) become (dropping the primes)

$$-iA\sigma u_i - f v_i = -p_{ix} + A F(u_i) \tag{2.A.7a}$$

$$-iA^{-1}\sigma v_i + f u_i = -p_{iy} + A^{-1} F(v_i) \tag{2.A.7b}$$

$$p_2 - p_1 = \eta \tag{2.A.7c}$$

$$u_x + v_y + \sigma \lambda^{-2} A w_z = 0 \tag{2.A.7d}$$

$$w_1 = 0 \quad at \quad z = 0 \tag{2.A.7e}$$

$$\left(u_2 \frac{\partial}{\partial x} + v_2 \frac{\partial}{\partial y}\right) h - \sigma A \delta \lambda^{-2} w_2 = 0 \quad at \quad z = -1 - \delta^{-1} h \tag{2.A.7f}$$

$$w_1 = w_2 = -i\eta \quad at \quad z = -1 \tag{2.A.7g}$$

with the following definitions of parameters:

$$\sigma \equiv \omega / f_0$$
$$f \equiv f / f_0 = 1 + by$$
$$b \equiv \beta L / f_0 \qquad (2.A.8)$$
$$\lambda^2 \equiv (H_1 g \Delta\rho/\rho_0) / (f_0^2 L^2)$$

The friction terms are now expressed in terms of the operator

$$F = \left[\frac{\partial}{\partial y} E_V \frac{\partial}{\partial y} + E_H \left(A^{-2} \frac{\partial^2}{\partial x^2} + \frac{\partial^2}{\partial y^2} \right) \right] \qquad (2.A.9)$$

where E_V and E_H are Ekman numbers

$$E_V \equiv \frac{\nu_V}{f_0 H_1^2}, \qquad E_H \equiv \frac{\nu_H}{f_0 L^2} \qquad (2.A.10)$$

Both Ekman numbers are very small. For example, if $\nu_V = 10^{-3}\ m^2\ sec^{-1}$, $f_0 = 5 \times 10^{-5}\ sec^{-1}$ and $H_1 = 500\ m$ then $E_V \approx 10^{-4}$; and with $\nu_H = 10\ m^2\ sec^{-1}$, the range of L from 10^4 to 10^6 gives $E_H = 2 \times 10^{-3}$ to 2×10^{-7}. Hence lateral friction is of no importance in (2.A.7a,b) except possibly in thin boundary layers where a large value of A^{-3} (meaning a small zonal scale) can make the product $A^{-3} E_H = O(1)$. For small A, the dominant balance in (2.A.7a) is geostrophic, so the only potentially

significant lateral friction term, found in (2.A.7b), may be written $A^{-3} E_H f^{-1} p_{i\alpha\alpha\alpha}$.

The smallness of E_V ensures that the Ekman boundary layers are thin, so the bulk of the flow in each layer is independent of depth. Let this depth-independent velocity be denoted (u^*, v^*), and let the Ekman layer correction be $(\tilde{u}, \tilde{v})$. Then, provided $\sigma \ll 1$, $E_H \ll 1$, and $|\nabla h| \ll 1$, a standard Ekman layer calculation (e.g., Greenspan, 1969) yields the bottom stress, $(\tau_B^{(x)}, \tau_B^{(y)}) = E_V \frac{\partial}{\partial y}(u_2, v_2)$, in terms of (u^*, v^*):

$$\tau_B^{(x)} = \left(\frac{E_V f}{2}\right)^{1/2} (u^* A - v^*) \qquad \text{(2.A.11a)}$$

$$\tau_B^{(y)} = \left(\frac{E_V f}{2}\right)^{1/2} (u^* A + v^*) \qquad \text{(2.A.11b)}$$

The depth-independent velocity is governed by (2.A.7a,b) with $E_V = 0$. Since we restrict $A \leq O(1)$, $\sigma \ll 1$, and $E_H \ll 1$, deviations from geostrophic balance in (2.A.7a) are small, and $v^* \simeq f^{-1} p_{2x}$. If A is small, there may be significant ageostrophy in (2.A.7b); but u^* in (2.A.12a,b) is multiplied by A , so the ageostrophic contribution to the bottom stress from u^* is also small, and we may substitute $u^* \simeq -f^{-1} p_{2y}$ in (2.A.11a,b) to get expressions for the bottom stress in terms of the pressure:

$$\tau_B^{(x)} \simeq \left(\frac{E_v}{2f}\right)^{1/2}\left(-A p_{2y} - p_{2x}\right) \equiv E_v^{1/2}\,\tilde{\tau}_B^{(x)} \qquad (2.A.12a)$$

$$\tau_B^{(y)} \simeq \left(\frac{E_v}{2f}\right)^{1/2}\left(-A p_{2y} + p_{2x}\right) \equiv E_v^{1/2}\,\tilde{\tau}_B^{(y)} \qquad (2.A.12b)$$

Although the bottom boundary layer flux is of order $E_v^{1/2}$, the flux in the surface Ekman layer is determined by the imposed wind stress, $(\tau_w^{(x)}, \tau_w^{(y)})$, and may therefore be as large as $O(1)$ regardless of the value of E_v. Since the wind stress is externally imposed, both components, unlike the velocity, have been scaled by the same factor: $\hat{\tau} \equiv \rho_0 f_0 H_1 \sigma \lambda^{-2} \hat{u}$. This scale is chosen to balance the divergence of the Ekman flux by vortex stretching in the upper layer, as will be seen.

Now that the friction terms have been simplified, we may vertically integrate (2.A.7a,b,d) over the depth of each layer to get

$$-iA\sigma U_1 - fV_1 = -p_{1x} + A\sigma\lambda^{-2}\tau_w^{(x)} \qquad (2.A.13a)$$

$$-iA^{-1}\sigma V_1 + fU_1 = -p_{1y} + \sigma\lambda^{-2}\tau_w^{(y)} + A^{-3}E_H f^{-1} p_{1xxx} \qquad (2.A.13b)$$

$$U_{1x} + V_{1y} = -iA\sigma\lambda^{-2}\eta \qquad (2.A.13c)$$

$$-iA\sigma U_2 - fV_2 = -\delta^{-1}h\,p_{2x} - E_V^{1/2}\tilde{\tau}_\sigma^{(x)} \qquad (2.A.13d)$$

$$-iA^{-1}\sigma V_2 + fU_2 = -\delta^{-1}h\,p_{2y} - A^{-1}E_V^{1/2}\tilde{\tau}_B^{(y)} + A^{-3}E_H\,\delta^{-1}h\,f^{-1}p_{2xxx} \qquad (2.A.13e)$$

$$U_{2x} + V_{2y} = iA\sigma\alpha^{-2}\eta \qquad (2.A.13f)$$

where

$$(U_1, V_1) \equiv \int_{-1}^{0} (u_1, v_1)\,dy$$

$$(U_2, V_2) \equiv \int_{-1-\delta^{-1}h}^{-1} (u_2, v_2)\,dy \qquad (2.A.14)$$

Before proceeding to the derivation of vorticity equations, let us review some of the features of (2.A.13a-f), which govern the depth-integrated velocity in each of two fluid layers on a beta plane over topography.

First, the scales have been chosen in anticipation of a strong geostrophic balance. The frequency, σ, is small: $.4 \times 10^{-2}$ for motions of annual period at 20° N, for example. The frequency and the meridional scale are externally imposed, for example by a seasonal variation of wind stress. The zonal scales (there may be more than one zonal scale in a single region) must be determined by the dynamics, and may be different in different regions, due,

for example, to changes in topography. We will be considering topography that is primarily a function of x, and therefore does not introduce its own meridional scale. Anisotropic length scaling requires anisotropic velocity scaling if the geostrophic balance is to have $O(1)$ coefficients. Hence, the scales of v_i and V_i are inversely proportional to the zonal length scale.

Second, we specify that the eddy viscosities are small, so friction will be important only where there are especially large velocity gradients. The meridional scales chosen will be too large to create such gradients, so friction appears only as a result of locally small zonal scales, and therefore only in the meridional momentum equation.

Finally, note that the coefficient on the right hand sides of (2.A.13c,f) may be written as $\sigma \frac{\beta_0^2 L W}{g' H_1}$. Thus the horizontal divergence of the flow diminishes as the frequency or either of the length scales is reduced.

2. Vorticity equations

Through standard manipulations, (2.A.13a-f) with (2.A.7c) can be reduced to two coupled equations for the pressure in each layer. Define

$$D_i \equiv U_{ix} + V_{iy} \tag{2.A.15a}$$

$$Z_i \equiv A^{-1} V_{ix} - A U_{iy} \tag{2.A.15b}$$

$$\nabla_s \times \tau_w \equiv A^{-1} \frac{\partial}{\partial x} \tau_w^{(y)} - \frac{\partial}{\partial y} \tau_w^{(x)} \tag{2.A.15c}$$

$$\nabla_s \cdot \equiv A^{-1} \frac{\partial}{\partial x} + \frac{\partial}{\partial y} \tag{2.A.15d}$$

$$\nabla_s^2 \equiv A^{-1} \frac{\partial^2}{\partial x^2} + A \frac{\partial^2}{\partial y^2} \tag{2.A.15e}$$

Then

$$-i\sigma Z_1 + f D_1 + b V_1 = \sigma \lambda^{-2} A \nabla_s \times \tilde{\tau}_w + A^{-3} E_H f^{-1} p_{1xxxx} \tag{2.A.16a}$$

$$-i\sigma D_1 - f Z_1 + bA U_1 = -\nabla_s^2 p_1 + \sigma \lambda^{-2} A \nabla_s \cdot \tilde{\tau}_w + A^{-2} E_H (f^{-1} p_{1xxx})_y \tag{2.A.16b}$$

$$-i\sigma Z_2 + f D_2 + b V_2 = \delta^{-1} [(h p_{2x})_y - (h p_{2y})_x] - \left(\frac{E_v}{2}\right)^{1/2} \left[f^{-1/2} \nabla_s^2 p_2 - \tfrac{1}{2} b f^{-3/2} p_{2x} \right] + A^{-3} E_H f^{-1} \delta^{-1} (h p_{xxxx})_x \tag{2.A.16c}$$

$$-i\sigma D_2 - f Z_2 + bA U_2 = -\delta^{-1} [A^{-1} (h p_{2x})_x + A (h p_{2y})_y] + E_v^{1/2} \nabla \cdot \tilde{\tilde{\tau}}_B + A^{-2} E_H \delta^{-1} \left(\frac{h}{f} p_{2xxx} \right)_y . \tag{2.A.16d}$$

Elimination of Z_i gives

$$(f^2-\sigma^2)D_1 + b(-i\sigma A U_1 + f V_1) = i\sigma \mathcal{V}_s^2 p_1 + A^{-3} E_H p_{1xxxx} - i\sigma E_H (f^{-1} p_{1xxx})_y + \sigma \lambda^{-2} A (f \mathcal{V}_s \times \tau_w - i\sigma \mathcal{V}_s \cdot \tau_w) \qquad (2.A.17a)$$

$$(f^2-\sigma^2)D_2 + b(-i\sigma A U_2 + f V_2) = i\sigma \delta^{-1}[A^{-1}(h p_{2x})_x + A(h p_{2y})_y] + f\delta^{-1}[(h p_{2x})_y - (h p_{2y})_x] + \left(\frac{E_v}{2}\right)^{1/2}\left(f^{1/2}\mathcal{V}_s^2 p_2 - \tfrac{1}{2} b f^{-1/2} p_{2x}\right) + A^{-3} E_H \delta^{-1}(h p_{xxx})_x - i\sigma\left[E_v^{1/2}\mathcal{V}\cdot\tilde{\tau}_0 + A^{-2} E_H \delta^{-1}\left(\frac{h}{f} p_{2xxx}\right)_y\right] \qquad (2.A.17b)$$

Since σ is small, σ^2 can be neglected relative to f^2, and the friction and forcing terms on the right hand sides can be neglected when multiplied by σ. Assuming $\sigma A \ll 1$, the first term multiplied by b can be neglected relative to the second, and from (2.A.13a,d) we approximate

$$f V_1 \simeq p_{1x} - \tau_w^{(x)} A \sigma \lambda^{-2} \qquad (2.A.18a)$$

$$f V_2 \simeq \delta^{-1} h p_{2x} \qquad (2.A.18b)$$

In addition, the term $\left(\frac{E_v}{2f}\right)^{1/2} \frac{b}{2} p_{2x}$ is small compared to $f b V_2$, and will be dropped. With these approximations and the use of (2.A.13c,f) and (2.A.7c), we find

$$-i\sigma \upsilon_s^2 p_1 - i\sigma \alpha^{-2} A f^2 (p_2 - p_1) + b p_{1x} = \sigma \alpha^{-2} A \left(f \upsilon_s \times \tau_w + b \tau_w^{(x)}\right) + A^{-3} E_H p_{1xxxx} \qquad (2.A.19a)$$

$$-i\sigma h \upsilon_s^2 p_2 - i\sigma \left(A^{-1} p_{2x} h_x + A p_{2y} h_y\right) + i\sigma \alpha^{-2} A \delta f^2 (p_2 - p_1) + b h p_{2x} + f\left(h_x p_{2y} - h_y p_{2x}\right) = -\delta \left(\frac{E_v f}{2}\right)^{1/2} \upsilon_s^2 p_2 + A^{-3} E_H \left(h p_{2xxx}\right)_x \qquad (2.A.19b)$$

In the special case of $h = 1$ (flat bottom), (2.A.19b) reduces to

$$-i\sigma \upsilon_s^2 p_2 + i\sigma \alpha^{-2} A \delta f^2 (p_2 - p_1) + b p_{2x} = -\left(\frac{E_v f}{2}\right)^{1/2} \upsilon_s^2 p_2 + A^{-3} E_H p_{2xxxx} \qquad (2.A.20)$$

3. Parameters

To understand the dependence of a model on its parameters, it is helpful to have specific numerical examples. The main focus of this thesis is on seasonal oscillations,

so for one numerical example we choose motions of annual period and a meridional length scale of 1000 km. As a second example, at the limits of validity of the theory, we choose eddy scales: a length scale of 100 km and a period of about three months.

The descriptive parameters of the model must also be given numerical values. Let the basic layer depths be $H_1 = 500\ m$, $H_2 = 3500\ m$, so that $\delta = 1/7$. A convenient value of the reduced gravity is $g\,\Delta\rho/\rho_0 = 2\times10^{-2}\ m\ sec$ which could result from a temperature difference of about 10 C. As a central latitude we choose 20° N, making $f_0 = 5\times10^{-5}\ sec^{-1}$ and $\beta = 2\times10^{-11}\ m^{-1}\ sec^{-1}$.

Now the essential non-dimensional dynamical parameters of the model are determined for the two examples. For the annual oscillation, $\sigma = .4\times10^{-2}$, $b = .4$, and $\lambda^{-2} = 2.5\times10^{2}$. For the eddy, $\sigma = 1.6\times10^{-2}$, $b = .04$, and $\lambda^{-2} = 2.5$. In both examples, σ is clearly a small parameter. The beta parameter, b, is small for the eddy but not so small for the annual oscillation. Nevertheless, we will sometimes be forced to treat b as a small parameter in the latter example. The accuracy of the theory will then suffer, but it will still be capable of giving some qualitative information.

B. Behavior of the model without topography

In the remainder of this chapter, we will review the theory of two-layer flow over a flat bottom, and apply the theory to the problem of the oceanic response to seasonal wind variations. This will provide a frame of reference in which to develop a theory of flow over topography.

The flat-bottom problem is greatly simplified by the ease with which the inviscid versions of (2.A.19a) and (2.A.20) can be combined to give a pair of decoupled equations for the two vertical normal modes of the system. Using subscripts T and C to denote barotropic and baroclinic modes, and defining

$$\begin{aligned} p_T &\equiv p_1 + \delta^{-1} p_2 \\ p_C &\equiv p_1 - p_2 \end{aligned} \tag{2.B.1}$$

linear combinations of (2.A.19a) and (2.A.20) yield

$$-i\sigma \mathcal{O}_s^2 p_T + b p_{T\alpha} = \sigma \lambda^{-2} A G + A^{-3} E_H p_{T\alpha\alpha\alpha\alpha} - \left(\frac{E_v f}{2}\right)^{1/2} \delta^{-1} \mathcal{O}_s^2 p_2 \tag{2.B.2a}$$

$$-i\sigma\left(\mathcal{O}_s^2 p_C - \lambda_C^{-2} A f^2 p_C\right) + b p_{C\alpha} = \sigma \lambda^{-2} A G + A^{-3} E_H p_{C\alpha\alpha\alpha\alpha} + \left(\frac{E_v f}{2}\right)^{1/2} \mathcal{O}_s^2 p_2 \tag{2.B.2b}$$

with

$$G \equiv f \nabla_s \times \tau_w + b \tau_w^{(x)} = f^2 \nabla_s \times \left(\frac{\tau_w}{f}\right) \qquad (2.B.3)$$

$$\lambda_c^{-2} \equiv \lambda^{-2}(1+\delta).$$

In the limit $E_v \to 0$, these equations are uncoupled.

1. Free waves

Now, with $G=0$, and $E_v = E_H = 0$, consider the possible free barotropic wave motions governed by the left hand side of (2.B.2a):

$$-i\sigma\left(A p_{Tyy} + A^{-1} p_{Txx}\right) + b p_{Tx} = 0 \qquad (2.B.4)$$

This can be solved exactly, setting $A = 1$, by plane waves (Longuet-Higgins, 1964b)

$$p_T = e^{i(kx+ly)} \qquad (2.B.5)$$

where k and l satisfy the dispersion relation

$$k^2 + \frac{b}{\sigma} k + l^2 = 0 \qquad (2.B.6)$$

The two roots of the dispersion relation give the zonal wavenumbers of the long and short Rossby waves:

$$k_{TW} = \frac{1}{2}\left[-\frac{b}{\sigma} + \left(\left(\frac{b}{\sigma}\right)^2 - 4l^2\right)^{1/2}\right] \quad (2.B.7a)$$

$$k_{TE} = \frac{1}{2}\left[-\frac{b}{\sigma} - \left(\left(\frac{b}{\sigma}\right)^2 - 4l^2\right)^{1/2}\right] \quad (2.B.7b)$$

Subscripts W and E denote westward and eastward group velocities of the long and short waves, respectively. The group velocity components are

$$C_g^{(x)} \equiv \frac{1}{\sigma}\frac{\partial \sigma}{\partial k} = \frac{b(k^2-l^2)}{\sigma(k^2+l^2)^2} = \frac{\sigma}{b}\left(1 - \frac{l^2}{k^2}\right) \quad (2.B.8a)$$

$$C_g^{(y)} \equiv \frac{1}{\sigma}\frac{\partial \sigma}{\partial l} = \frac{2bkl}{\sigma(k^2+l^2)^2} = \frac{\sigma}{b}\left(-2\frac{l}{k}\right) \quad (2.B.8b)$$

The factor of σ^{-1} in the definition is included to make the scale factor $\hat{C}_g = \frac{L}{T} = L\omega$, consistent with the use of ω^{-1} rather than f_0^{-1} as the basic time scale.

Many of the characteristics of Rossby waves are clearly displayed in a plot of the dispersion relation in wavenumber space with the frequency fixed (Longuet-Higgins, 1964). Figure 2.B-1a shows the dispersion relation for barotropic waves of annual and semiannual period. Note that the zonal wavenumber is insensitive to the value of the meridional wavenumber until the latter becomes rather large. Even with $l = 10$, so the meridional scale is 100 km, the chord $\overline{AB}$ is almost the length of the diameter of the circle and the long and short waves are widely separated in their zonal scales. This difference of scales will be of central

importance throughout this thesis. Furthermore, note that the direction of the group velocity (AC for short waves, BC for long waves) is very nearly zonal if the meridional scale is greater than about 100 km for annual motions, or 200 km for semiannual motions. This means that the effects of an annual localized barotropic disturbance of scale greater than 100 km will be felt at remote longitudes primarily in the same latitude band as the disturbance. The ocean at a given point gets its annual information mainly from points due east.

Given that $\ell = O(1)$, the only parameter controlling nondivergent barotropic Rossby waves is the ratio σ/b. When $\sigma/b = O(1)$, all the terms in (2.B.4) are important. The zonal scale is the same order as the meridional scale, and the short and long waves have comparable zonal scales and group velocities. At $\sigma/b = |2\ell|^{-1}$, the zonal component of the group velocity goes to zero, and for $\sigma/b > |2\ell|^{-1}$ only zonally decaying solutions exist. These solutions are trapped to a meridional boundary. In the opposite limit, $\sigma/b \ll 1$, the zonal scales of the long and short waves become increasingly disparate. Equations (2.B.7a,b) become approximately

$$k_{TW} \simeq -\ell^2 \frac{\sigma}{b}\left(1 + \left(\frac{\ell\sigma}{b}\right)^2 + \ldots\right) \qquad (2.B.9a)$$

$$k_{TE} \simeq -\frac{b}{\sigma}\left(1 - \left(\frac{\ell\sigma}{b}\right)^2 + \ldots\right) \qquad (2.B.9b)$$

The first term in each of these expressions is an excellent approximation for seasonal oscillations, since $\frac{\sigma}{b} = O(10^{-2})$. For long waves, the zonal scale is $A_{TW} = b/\sigma$, while for short waves it is $A_{TE} = \sigma/b$. In dimensional terms, for annual oscillations the short wave scale is a mere 10 km while the long wave scale is 10^5 km, or $A_{TW} = 10^2$. However, this is much larger than the zonal extent of any ocean basin, so in fact A is limited to, say, 10. This means that the long wave balance in (2.B.4) is approximately $p_{Tx} = 0$. The annual large scale barotropic long wave is so fast that there is negligible phase change from one side of an ocean to the other.

Baroclinic Rossby waves are slowed by the need to move the thermocline. With $G = E_V = E_H = 0$, (2.B.2b) becomes

$$-i\sigma\left(A^{-1}p_{cxx} + A p_{cyy}\right) + i\sigma\lambda_c^{-2} A f^2 p_c + b p_{cx} = 0 \qquad (2.B.10)$$

This equation, unlike (2.B.4), has non-constant coefficients, so it does not admit pure plane wave solutions. However, in the parameter range with which we are concerned, (2.B.10) may be replaced by approximations in which the non-constant coefficient occurs at worst parametrically.

First, consider the case $b \ll 1$. Then we may treat b as a small expansion parameter, with $f^2 = 1 + 2by + b^2y^2$. To lowest order, $f^2 \simeq 1$, so all coefficients are constant.

Setting $A=1$ and substituting plane wave solutions $p_c = e^{i(kx+ly)}$ yields the dispersion relation (Longuet-Higgins, 1965b)

$$k^2 + \frac{b}{\sigma} k + l^2 + \lambda_c^{-2} = 0 \qquad (2.B.11)$$

The roots corresponding to the long and short waves are

$$k_{cw} = \tfrac{1}{2}\left\{ -\frac{b}{\sigma} + \left[\left(\frac{b}{\sigma}\right)^2 - 4\left(l^2 + \lambda_c^{-2}\right)\right]^{1/2} \right\} \qquad (2.B.12a)$$

$$k_{cE} = \tfrac{1}{2}\left\{ -\frac{b}{\sigma} - \left[\left(\frac{b}{\sigma}\right)^2 - 4\left(l^2 + \lambda_c^{-2}\right)\right]^{1/2} \right\} \qquad (2.B.12b)$$

and the group velocity components are

$$C_g^{(x)} = \frac{b}{\sigma} \frac{k^2 - l^2 - \lambda_c^{-2}}{\left(k^2 + l^2 + \lambda_c^{-2}\right)^2} = \frac{\sigma}{b}\left(1 - \frac{l^2 + \lambda_c^{-2}}{k^2}\right)$$

$$C_g^{(y)} = \frac{2bkl}{\sigma\left(k^2 + l^2 + \lambda_c^{-2}\right)} = -2\frac{\sigma}{b}\frac{l}{k} \qquad (2.B.13)$$

The critical value of b/σ at which $C_g^{(x)} \to 0$ is now $b/\sigma = 2\left(l^2 + \lambda_c^{-2}\right)^{1/2}$. Hence for a given b and l, the critical frequency for baroclinic waves is lower than for barotropic waves, often much lower, since λ_c^{-2} can be $O(10^2)$. From (2.B.10) we see that λ_c^{-2} determines the relative importance of vortex stretching compared to the u_{yt} part of the vorticity change. In the long wave, one or both of these is primarily balanced by beta. In

the short wave, the v_{xt} term is the largest counterbalance to beta.

It is important to note that the above approximation making use of the smallness of b is valid only when $y = O(1)$. Neglect of the variation of the radius of deformation is valid only so long as that variation is small over the whole area of interest.

Figure 2.B-1b shows the baroclinic dispersion relation in wavenumber space. The wavenumbers clearly depend very critically on the radius of deformation and the frequency. At the annual period, the length of the chord $\overline{AB}$ is similar for the barotropic and baroclinic waves if the radius of deformation is greater than about 40 km. Likewise, the direction of the group velocity vector remains nearly zonal unless l is large. However, as the radius of deformation decreases, the circle in wavenumber space rapidly shrinks until there are no longer any free propagating baroclinic waves. The minimum radius of deformation for which free baroclinic waves exist is 20 km at the annual period and 40 km at the semiannual period (with $\beta = 2 \times 10^{-11} m^{-1} sec^{-1}$).

If the meridional length scale of the motion, L, is large so that b approaches 1, then, for reasonable values of layer thickness and stratification, $\lambda_c^{-2} >> 1$. As was pointed out by White (1977) this means the term $A p_{cyy}$ can be neglected relative to $\lambda_c^{-2} A f^2 p_c$, leaving

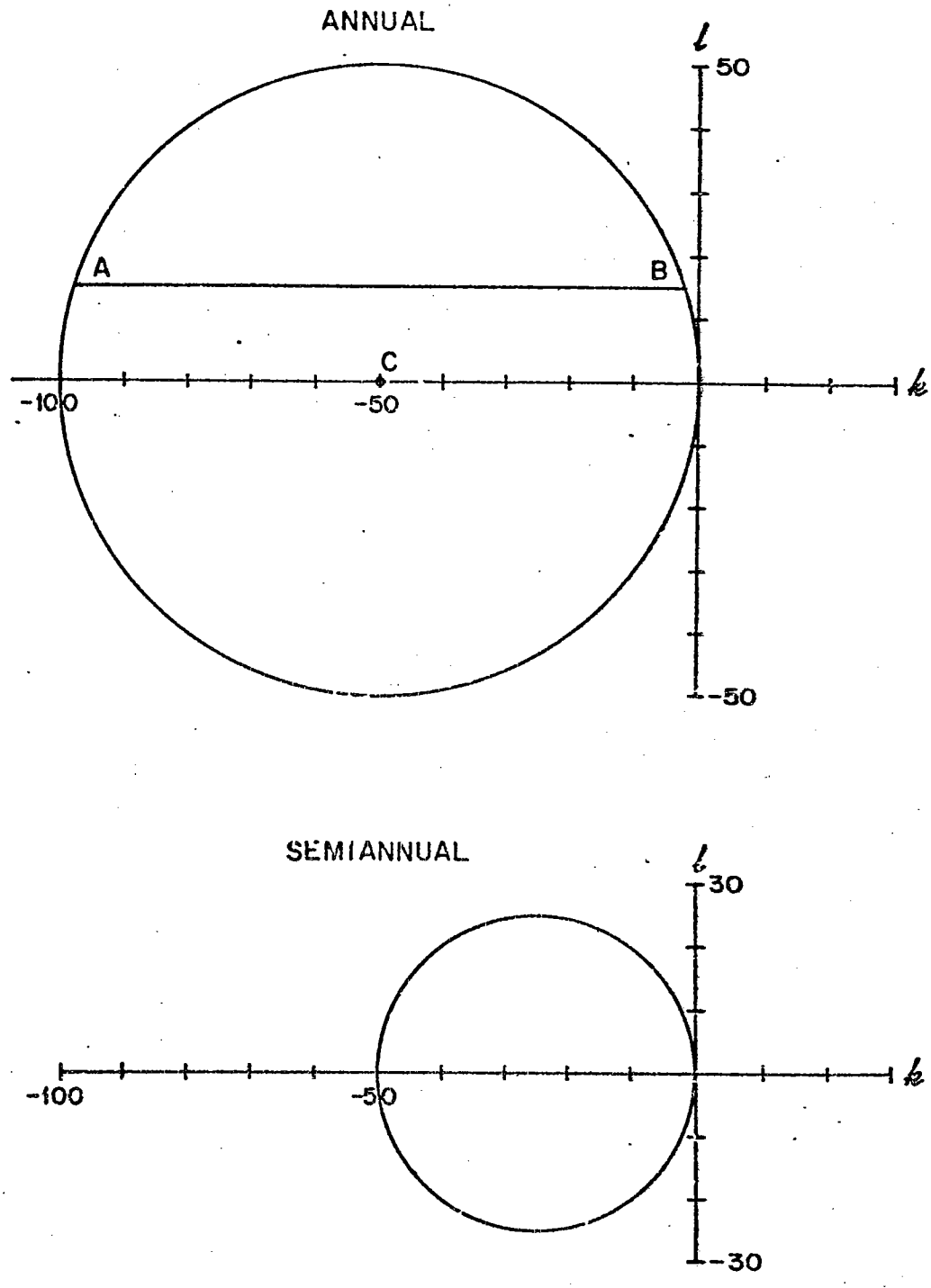

Figure 2.B-1a. Wavenumber vectors for barotropic Rossby waves of annual period (top) and semiannual period (bottom). The length scale is $L = 10^6$ m.

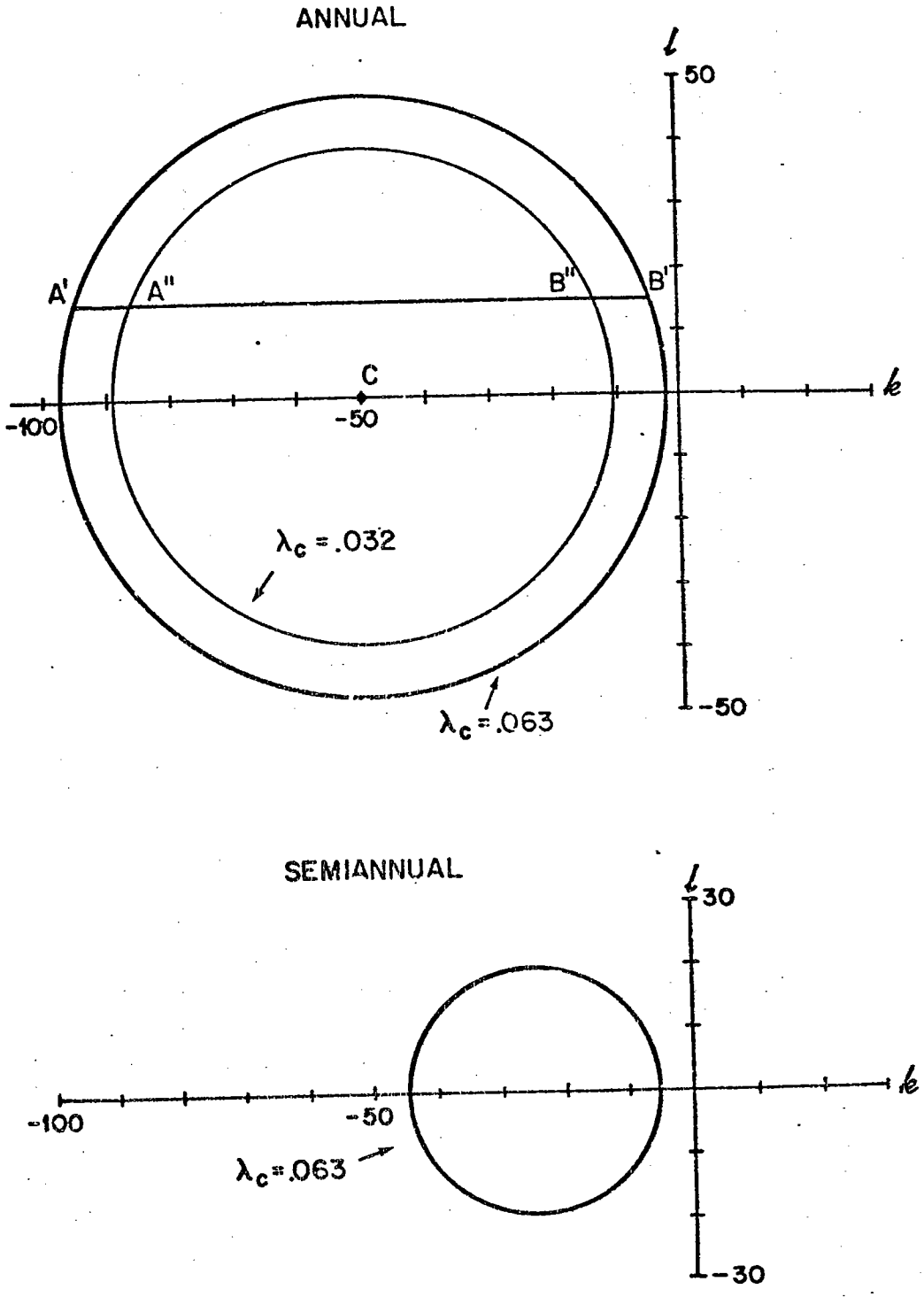

Figure 2.B-1b. Wavenumber vectors for baroclinic Rossby waves. In the case of annual period the wavenumbers are shown for radii of deformation 63 km and 32 km.

$$-A^{-1} p_{cxx} + \lambda_c^{-2} A f^2 p_c + \frac{b}{i\sigma} p_{cx} = 0 \qquad (2.B.14)$$

which has no y derivatives. Hence the variation of f may be taken into account parametrically. Solutions of (2.B.14) have the form

$$p_c = g(y)\, e^{ik(y)x} \qquad (2.B.15)$$

The function $g(y)$ is subject only to the restrictions that $\frac{dg}{dy} \leq O(1)$ and $\frac{d^2g}{dy^2} \leq O(1)$. With $A=1$ the dispersion relation for k is

$$k^2 + \frac{b}{\sigma} k + \lambda_c^{-2} f^2 = 0 \qquad (2.B.16)$$

The long and short wave roots are

$$k_{cw} = \frac{1}{2}\left\{ -\frac{b}{\sigma} + \left[\left(\frac{b}{\sigma}\right)^2 - 4\lambda_c^{-2} f^2 \right]^{1/2} \right\} \qquad (2.B.17a)$$

$$k_{cR} = \frac{1}{2}\left\{ -\frac{b}{\sigma} - \left[\left(\frac{b}{\sigma}\right)^2 - 4\lambda_c^{-2} f^2 \right]^{1/2} \right\} \qquad (2.B.17b)$$

If $\left(\frac{b}{\sigma}\right)^2 >> 4\lambda_c^{-2}$, the roots are approximately

$$k_{cw} \simeq -\lambda_c^{-2} \frac{\sigma}{b} f^2 \left(1 + \lambda_c^{-2} \left(\frac{\sigma}{b}\right)^2 f^2 + \ldots \right)$$
$$k_{cR} \simeq -\frac{b}{\sigma} \left(1 - \lambda_c^{-2} \left(\frac{\sigma}{b}\right)^2 f^2 + \ldots \right) \qquad (2.B.18)$$

For annual oscillations, the first term in each of these expressions is a good approximation, since $\lambda_c^{-2}\left(\frac{\sigma}{b}\right)^2 \simeq 2.5 \times 10^{-2}$

The long waves result from a balance between vortex stretching and beta, with the wavelength increasing as the latitude is decreased. Therefore a line of constant phase that starts out oriented north-south will gradually be refracted as it travels west, taking on a northeast-southwest slant. The short baroclinic waves are almost identical in scale to the short barotropic waves, both resulting from a balance between beta and the ν_{xt} part of the vorticity change. Because of the small zonal scale, $A = \sigma/b$, the radius of deformation is not an important parameter. From (2.A.13c,f) we see that the annual short wave motion is almost non-divergent. Hence the layers are only weakly coupled. This fact will be seen in the next chapter to have important implications.

2. Forced motion

Now we will look for particular solutions of (2.B.2a,b) with $E_H = E_V = 0$ but with $G \neq 0$. Since the equations are linear, we restrict our attention to simple forcing patterns, $G = e^{il\eta} e^{ik\chi}$. In the absence of boundaries, the scales of the forced response are exactly those of the forcing. Then l and k can be restricted to the values +1 and -1 depending on the direction of phase propagation of the forcing. The parameter A becomes the ratio of zonal to meridional scales of forcing. If the forcing is

independent of x, then there is no zonal scale, and the response in the absence of boundaries is also zonally uniform. It is found by setting the x-derivative terms in (2.B.2a,b) equal to zero, in which case the parameter A is common to all remaining terms and drops out of the equation. This is the same result as can be obtained by taking the limit of (2.B.2a,b) as $A \to \infty$.

a. Zonally uniform forcing

Since the patterns of seasonally varying wind stress and stress curl are much stronger functions of latitude than of longitude, they may, as a first approximation, be taken to be independent of x. Therefore we consider first the case $G = e^{ily}$.

The barotropic response obeys

$$-i\sigma p_{Tyy} = \sigma \lambda^{-2} e^{ily} \qquad (2.B.19)$$

which can immediately be integrated to give

$$p_T = -\lambda^{-2} l^{-2} i e^{ily} \qquad (2.B.20)$$

Without loss of generality, we may set $l^{-2} = 1$. For scales $L >> 100$ km, $\lambda^{-2} >> 1$, so the barotropic response

is large. All of the torque supplied by the wind must go into changing u_y .

Now, suppose there is a boundary at $x = 0$ and we are interested in the flow to the west, at negative x . The boundary condition $u_T = 0$ at $x = 0$ can be approximated $p_T = \sigma\lambda^{-2}\int \tau_w^{(y)} dy$ at $x = 0$, since the only important departure from geostrophy is due to the wind stress. Free waves with group velocity away from the boundary are added to (2.B.20) to meet the boundary condition. In this case, the barotropic long waves with wavenumber given by (2.B.7a) are appropriate. A complete solution is then

$$p_T = -\lambda^{-2} i e^{ily}\left(1 - e^{ik_{Tw}x}\right) + \sigma\lambda^{-2}\int \tau^{(y)} dy\, e^{ik_{Tw}x} . \qquad (2.B.21)$$

For convenience, it is assumed that $\tau^{(y)} \sim e^{ily}$. Note that there is an ambiguity in (2.B.21); the constant of integration is undetermined in the present model.

As we have seen, the zonal scale of the barotropic long waves is $A_{Tw} = \frac{b}{\sigma}$ which is large compared to the width of an ocean basin. Hence (2.B.21) is approximately

$$p_T \cong -\lambda^{-2} k_{Tw} x\, e^{ily} + \sigma\lambda^{-2}\int \tau^{(y)} dy \qquad (2.B.22)$$

and the complete response is $O(\lambda^{-2}\frac{\sigma}{b}) = O(1)$ for $x = O(1)$ This means the Sverdrup balance holds. The torque applied by the wind is balanced by the beta effect. This result can be seen directly from (2.B.2a) without going through the formal procedure of adding a free wave to a directly forced solution. The smallest zonal scale in the problem is set by the width of the basin, so let that scale determine A. Then, so long as $A\sigma << b$, the relative vorticity term is small compared to the beta term, giving the primary balance found by Gill and Niiler (1973)

$$b p_{Tx} \simeq \sigma \lambda^{-2} A e^{ily} \qquad (2.B.23)$$

which can be integrated to give (2.B.22), remembering that $k_{Tw} \simeq -\sigma/b$. The condition for the validity of this approximation, $A\sigma << b$, is, in dimensional terms, $L >> \left(\frac{\omega W_0}{\beta}\right)^{1/2} \simeq 200\ km$ for annual period with $W_0 = 4000\ km$ as the width of the basin. In the Sverdrup balance, the response is in phase with the forcing, in the sense that the maximum northward velocity coincides in time and space with the maximum wind stress curl. As L decreases and the $-i\sigma A p_y$ term gains importance, the response begins to lag behind the forcing. At $L = \left(\frac{\omega W_0}{\beta}\right)^{1/2}$, this phase lag is half a radian.

Calculation of the baroclinic component of the response to a forcing $G = e^{ily}$ proceeds along the same lines as the barotropic analysis above. However, there is a major difference in the results, due to the additional physical process, vortex stretching described by the $i\sigma\lambda_c^{-2} A f^2 p_c$ term. For $L \gtrsim 50$ km, this term dominates $-i\sigma A p_{cyy}$; vortex stretching due to thermocline displacement is more important than relative vorticity change. Vortex stretching also establishes a free wave scale shorter than an ocean's width, so the Sverdrup-type balance can hold for the baroclinic mode only near the eastern boundary.

As in our earlier discussion of baroclinic free waves, there are two cases to consider, depending on whether L is small enough to allow the approximation $f^2 \simeq 1$. First, consider the limit $b \ll 1$, or $L \ll b^0/\beta = 2500$ km. From (2.B.2b) we extract

$$-i\sigma\left(A^{-1} p_{cxx} + A p_{cyy} - A\lambda_c^{-2} p_c\right) + b p_{cx} = A\sigma\lambda^{-2} e^{ily} \qquad (2.B.24)$$

which has the solution

$$p_c = \frac{-i\lambda^{-2}}{l^2 + \lambda_c^{-2}}\left(1 - e^{ik_{cw}x}\right) e^{ily} + \sigma\lambda^{-2}\int \tau_w^{(y)}\, dy\, e^{ik_{cw}x} \qquad (2.B.25)$$

satisfying the boundary condition $p_c = \sigma\lambda^{-2}\int \tau_w^{(y)} dy$ at $x = 0$. The scale factor A has been set to one, and k_{cw} is determined from (2.B.12b). Similarly, in the case where $b = O(1)$, (2.B.2b) becomes

$$i\sigma\lambda_c^{-2} A f^2 p_c + b p_{cx} = A\sigma\lambda^{-2} e^{ily} \qquad (2.B.26)$$

which has the solution

$$p_c = -i\left(\frac{\lambda_c}{\lambda f}\right)^2 \left(1 - e^{ik_{cw}(y)x}\right) e^{ily} + \sigma\lambda^{-2}\int \tau_w^{(y)} dy\, e^{ik_{cw}(y)x} \qquad (2.B.27)$$

with k_{cw} here determined from (2.B.18a):

$$k_{cw} \simeq -\frac{\sigma}{b}\lambda_c^{-2} f^2. \qquad (2.B.28)$$

Near the boundary, where $|k_{cw} x| << 1$, (2.B.27) is approximately

$$p_c \simeq \frac{\sigma}{b}\lambda^{-2} x\, e^{ily} + \sigma\lambda^{-2}\int \tau_w^{(y)} dy. \qquad (2.B.29)$$

In the same region, the barotropic flow, from (2.B.22), is identical, since $k_{Tw} \simeq -\frac{\sigma}{b}$:

$$p_T \to p_c \quad \text{as} \quad |x| \to 0. \tag{2.B.30}$$

But (2.B.1) implies

$$p_1 = \left(p_T + \delta^{-1} p_c \right) \left(1 + \delta^{-1} \right)^{-1}$$
$$p_2 = \left(p_T - p_c \right) \left(1 + \delta^{-1} \right)^{-1} \tag{2.B.31}$$

so near the eastern boundary there is no flow in the lower layer. In the upper layer, $p_1 \simeq p_T$. This means that the upper layer alone carries the total transport required by the Sverdrup balance. Further from the boundary the total transport still satisfies the Sverdrup balance, but it is no longer confined to the upper layer.

The baroclinic response, (2.B.27), can be re-written (with $\tilde{\tau}_w^{(y)} = 0$)

$$p_c = -2 \left(\frac{\lambda_c}{\lambda f} \right)^2 \sin \frac{k_{cw} x}{2} \, e^{i \frac{k_{cw} x}{2}} \, e^{i l y} \tag{2.B.32}$$

so the phase lag is $-k_{cw} x/2$. For annual oscillations, this means a lag of one week at about 100 km from the eastern boundary at 20° N. At 10° N, a one-week lag occurs about 400 km from the coast. Equation (2.B.32) shows that

the baroclinic response takes the form of a wave propagating at twice the free wave speed, modulated by a sinusoidal amplitude with the same wavelength. This behavior is shown in Figure (2.B.2). As one goes west from $x = 0$, amplitude and phase lag increase until $k_{cw} x = \pi$, where the phase lag is $\pi/2$ and the amplitude is a maximum. Then the phase lag continues to increase while the amplitude decreases, going to zero at $k_{cw} x = 2\pi$, where the phase lag is π. Further west, the amplitude increases again, and the phase lag increases from zero. Hence the phase lag is always between zero and π, and the motion is greatest where the lag is $\pi/2$. There the free wave from the eastern boundary is in phase with the directly forced response.

This behavior of the baroclinic response to seasonal wind variations has been described by White (1977), who has found observational evidence of its existence in the Pacific. Data from a grid of hydrographic stations occupied monthly for 15 months near Hawaii show westward phase propagation and a phase lag that increases from south to north due to the decrease in baroclinic phase speed with increasing Coriolis parameter. Earlier Meyers (1975), using the same data, had shown that the average thermocline displacement from its mean value lagged the wind stress curl by about $\pi/2$. He concluded that this demonstrated that the thermocline was simply moving up and down with the vertical velocity induced by surface Ekman pumping. While this is

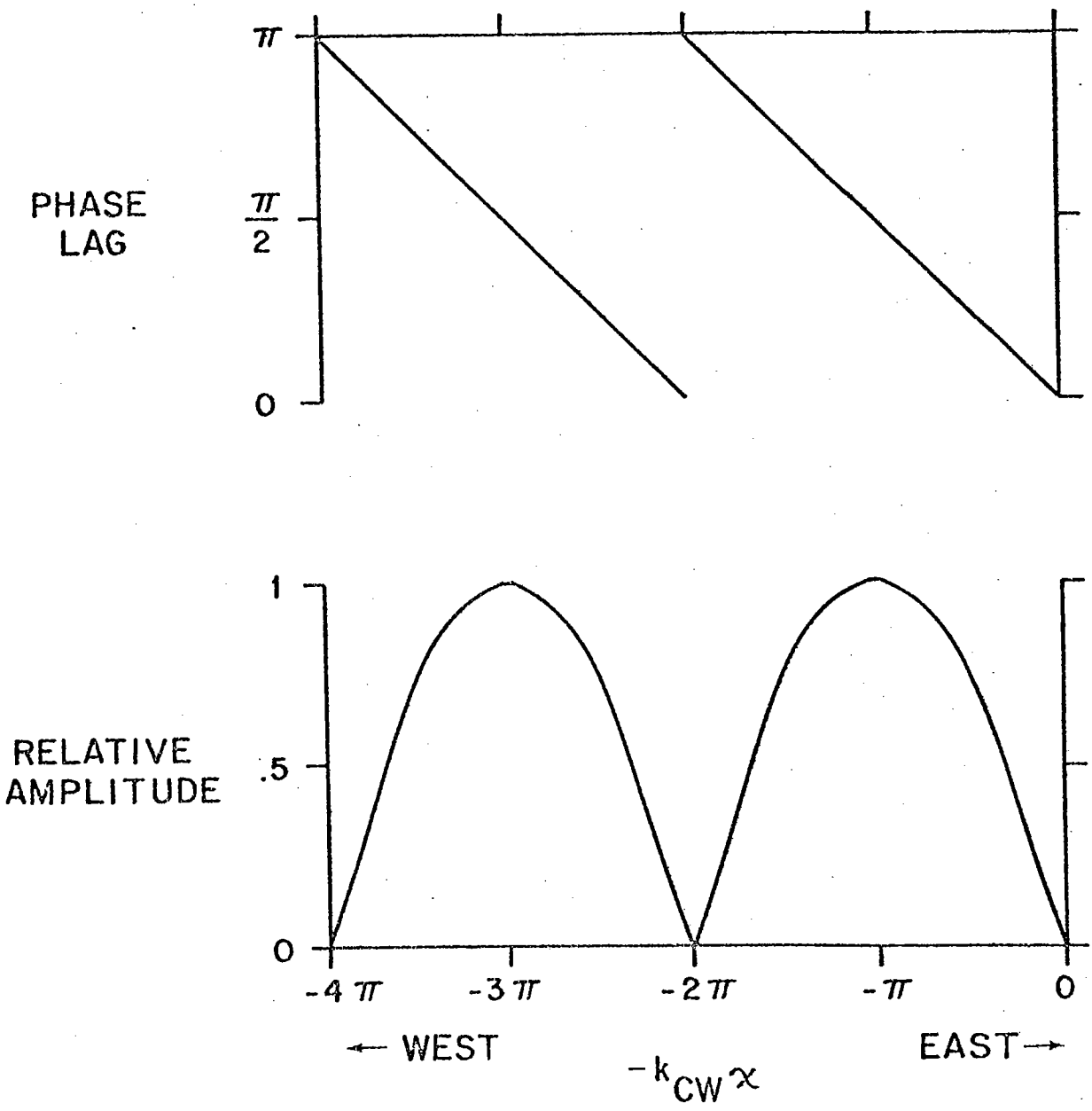

Figure 2.B-2. Variation with distance from the eastern boundary of the baroclinic response to forcing (2.B.32).

true if one considers an average over an integral number of baroclinic free wavelengths, it is not true locally. As demonstrated by White, the free wave from the eastern boundary plays an important part in the complete response.

b. General forcing

When the forcing function takes the more general form $G = e^{ily} e^{ikx}$ the response is a bit more complicated but is governed by the same principles as in the case of zonally uniform forcing. Solutions for an unbounded ocean were found by Longuet-Higgins (1965). Here we will briefly sketch the theory for the case of an ocean with an eastern boundary.

As previously, the barotropic response is simplest. The equation to be solved is

$$-i\sigma\left(A^{-1}p_{Txx} + A p_{Tyy}\right) + b p_{Tx} = \sigma\alpha^{-2} A e^{ily} e^{ikx} \qquad (2.B.33)$$

An exact solution with $A = 1$ and $p_T = 0$ at $x = 0$ is

$$p_T = \frac{-i\sigma\alpha^{-2} e^{ily}}{k^2 + l^2 + \frac{bk}{\sigma}} \left(e^{ikx} - e^{ik_T x}\right) \qquad (2.B.34)$$

Alternatively, we can examine the scales in (2.B.33) by setting l and k equal to ± 1. Then, so long as $\frac{b}{\sigma} >> A$ and $\frac{b}{\sigma} >> A^{-1}$, the relative vorticity term is small

compared to the beta term. The same is true for the barotropic long wave on ocean-wide scales. What is left is just the Sverdrup balance, which can be directly integrated to give

$$p_T \simeq -i \frac{\sigma}{b} \lambda^{-2} A k^{-1} \left(e^{ikx} - 1 \right) e^{ily} \qquad (2.B.35)$$

Baroclinic behavior is complicated slightly by the presence of the vortex stretching term, which is generally important and may have a variable coefficient. However, as was shown earlier, the variability of f^2 does not really present a great difficulty, since whenever the variation of f^2 is significant, the y-derivative term is small, and f^2 becomes merely a varying parameter. Using this fact, a general approximate solution to

$$-i\sigma \left(A^{-1} p_{cxx} + A p_{cyy} - \lambda_c^{-2} f^2 A p_c \right) + p_{cx} = \sigma \lambda^{-2} A e^{ily} e^{ikx} \qquad (2.B.36)$$

is

$$p_c \simeq -i \lambda^{-2} \left(l^2 + \lambda_c^{-2} f^2 + A^{-2} k^2 + A^{-1} \frac{b}{\sigma} k \right)^{-1} \left(e^{ikx} - e^{ik_c x} \right) e^{ily} \qquad (2.B.37)$$

The response is larger for westward propagating forcing, since it more nearly matches the free long wave solutions. At resonance, $k = k_{cw}$ or k_{cE}, (2.B.37) is no longer valid and must be replaced by

$$p_c \simeq \frac{\sigma \lambda^{-2}(x - x_0)}{\sigma k_{c_E^W} + 1} e^{i k_{c_E^W} x} e^{ily} \qquad (2.B.38)$$

If the resonance is at the short wavelength $(k = k_{cE})$ free short waves must be added to meet the $p_c = 0$ boundary condition at the western, not the eastern, boundary. This is done by making x_0 the longitude of the western rather than the eastern boundary. Resonant response is stronger at the short wavelength; the group velocity is smaller, so a wave has more time to gather energy while traveling a given distance.

The dependence of the baroclinic forced response on the direction of propagation has an interesting consequence if the forcing is a standing wave in the zonal direction: $G = e^{ily} \cos x$. The response analogous to the directly forced part of (2.B.37) is (assuming $\lambda_c^{-2} >> 1$)

$$p_c \simeq \frac{-\lambda^{-2} e^{ily}}{\lambda_c^{-4} f^4 - A^{-2}\left(\frac{b}{\sigma}\right)^2} \qquad (2.B.39)$$

$$\left(A^{-1}\frac{b}{\sigma} \sin x + i\lambda_c^{-2} f^2 \cos x\right)$$

The first part of (2.B.39) is in phase with the forcing in time, but 90° out of phase in x ; while the second part is 90° out of phase in time, but in phase in space. The first term dominates as the frequency and length scales are decreased, and vise versa for the second term. The two terms are the same size at resonance. When the first term dominates, the zonal scale is small enough to allow a Sverdrup balance, between $b p_x$ and the forcing. Although p in this case is spatially out of phase with G, $v \simeq p_x$ is in phase with G. When the second term dominates, beta is ineffective, and the wind stress curl produces local vortex stretching.

3. The western boundary

So far, little has been said about the western boundary. The response of the ocean interior has been calculated as the sum of local effects and waves generated at the eastern boundary. The justification for this asymmetric development of the theory is the anisotropic nature of Rossby waves. As pointed out by Pedlosky (1965b), the Rossby waves generated at the western boundary at a given frequency have shorter wavelengths and slower group velocities than those generated at the eastern boundary. The short waves tend to be rapidly dissipated, and so their effects are confined to a western boundary layer.

In the present model, the damping can be provided by horizontal or bottom friction, or both. We are not interested here in the details of the oscillating western boundary layer, but in its general characteristics, primarily its width and transport. Let us very briefly consider, then, how each type of friction modifies short wave dynamics at the western boundary. Of interest are large scale motions with periods of three months and longer.

a. Bottom friction

Since bottom friction acts directly only on the lower layer, the normal modes in the vertical are no longer the simple barotropic and baroclinic modes. If the friction is small and the layers are closely coupled, the short wave solutions will differ only slightly from inviscid short waves; but if friction is larger and coupling is weak, the short wave solutions will consist of an essentially undamped wave concentrated in the upper layer, and an independent damped wave in the lower layer. These types of behavior can be demonstrated by a couple of simple perturbation expansions.

From (2.B.2a,b) with $E_H = 0$ and $A = \frac{\sigma}{b}$ chosen as the scale appropriate to short waves, we have approximately

$$-i p_{1xx} + p_{1x} + \Gamma i (p_1 - p_2) = 0 \qquad (2.B.40a)$$

$$-i p_{2xx} + p_{2x} + \Gamma \delta i (p_2 - p_1) + F_v p_{2xx} = 0 \qquad (2.B.40b)$$

where $\Gamma \equiv \left(\frac{\sigma f}{b\lambda}\right)^2 = \frac{\omega^2 f^2}{\beta^2 g' H_1}$ and $F_v \equiv \left(\frac{E_v f}{2}\right)^{1/2} \delta \sigma^{-1}$. Consider first the case $\Gamma = O(1)$, $F_v << 1$. Then solutions of (2.B.40) can be sought in the form

$$p_1 = e^{ikx}$$

$$p_2 = \left(p_2^0 + F_v p_2' + F_v^2 p_2^2 + \ldots\right) e^{ikx} \qquad (2.B.41)$$

with $k = k^0 + F_v k' + \ldots$ For the modified barotropic mode, we find

$$p_{2T} = 1 - \frac{i F_v}{\Gamma(1+\delta)} + O(F_v^2)$$

$$k_T = -1 + \frac{i F_v}{1+\delta} + O(F_v^2) \qquad (2.B.42)$$

and for the modified baroclinic mode

$$p_{2c} = -\delta - \frac{i F_v k_c^{0\,2} \delta}{\Gamma(1+\delta)} + O(F_v^2)$$

$$k_c = k_c^0 + \frac{i k_c^{0\,2} F_v \delta}{[1 - 4\Gamma(1+\delta)]^{1/2}(1+\delta)} + O(F_v^2) \qquad (2.B.43)$$

$$k_c^0 = -\tfrac{1}{2}\left[1 + \left(1 - 4\Gamma(1+\delta)\right)^{1/2}\right]$$

To lowest order, the solutions are just damped barotropic and baroclinic short waves, decaying to the west. The barotropic decay scale is $O(F_v)$ while the baroclinic scale is $O(F_v\delta)$; not surprisingly, the damping is weaker for the baroclinic mode, with its smaller bottom velocity. The first order frictional correction to the lower layer velocity is in each case 90° out of phase with the zero-order velocity. Note that the correction varies as Γ^{-1}, and so the expansion is valid only for $F_v/\Gamma \ll 1$.

Now, suppose $\Gamma \ll 1$ and $F_v = O(1)$. Then we find that there are two solutions, one with no zero-order flow in the lower layer, the other with no zero-order flow in the upper layer. These can be expressed in the forms

$$p_1 = e^{ik_u x}$$
$$p_2 = \left(\frac{-\Gamma\delta}{F_v} + O(\Gamma^2) \right) e^{ik_u x} \qquad \text{(2.B.44)}$$
$$k_u = -1 + \Gamma + \Gamma^2 \left(1 + \frac{i\delta}{F_v} \right) + O(\Gamma^3)$$

and

$$p_1 = \left\{ \Gamma \left[-2 + \frac{i}{F_v} \left(1 - F_v^2 \right) \right] + O(\Gamma^2) \right\} e^{ik_L x}$$
$$p_2 = e^{ik_L x} \qquad \text{(2.B.45)}$$
$$k_L = \left(-1 + iF_v \right) \left(1 + F_v^2 \right)^{-1} + O(\Gamma)$$

The first solution is a short wave that is heavily concentrated in the upper layer and is damped only at $O(\Gamma^2)$. The lower layer velocity is 90° out of phase with the upper layer. The second solution is a heavily damped wave concentrated in the lower layer. Bottom friction has detuned the two layers so that they act almost independently. Because of the small scale of the motion, the coupling between layers via interface deformation is weak, and energy in the upper layer is lost to bottom friction only very slowly. In fact, this energy loss decreases as the friction parameter F_v is increased, since $\delta m(k_u) \simeq \Gamma^2\delta/F_v$. This type of behavior has previously been found by Foo (1976) and Rooth (1978).

For oscillations of annual period, with $E_v = 10^{-4}$, we find $F_v \simeq .25$ and $\Gamma \simeq .04$, while at a period of three months $F_v \simeq .06$ and $\Gamma \simeq .63$. Thus the three-month oscillations can have a western boundary layer governed by (2.B.42) and (2.B.43), whereas the annual oscillations are in the parameter range for which (2.B.44) and (2.B.45) are appropriate. For the annual oscillations, then, the upper and lower layers are only weakly coupled at the western boundary, and the short waves in the upper layer are free to propagate energy eastward with minimal damping. In order to damp these waves, we may invoke lateral friction.

b. Lateral friction

Lateral friction does not cause any direct coupling between barotropic and baroclinic modes, so the appropriate

equations, taken from (2.B.2a,b) with $A = \frac{\sigma}{b}$ and $E_V = 0$ are

$$-i p_{T\alpha\alpha} + p_{T\alpha} - F_H p_{T\alpha\alpha\alpha\alpha} = 0$$

$$-i p_{c\alpha\alpha} + p_{c\alpha} + i\Gamma_c p_c - F_H p_{c\alpha\alpha\alpha\alpha} = 0 \qquad (2.B.46)$$

with $\Gamma_c \equiv \left(\frac{\sigma f}{b \lambda_c}\right)^2$ and $F_H \equiv E_H \frac{b^2}{\sigma^3}$. For small F_H, the effect of the friction term is to introduce a damping of order F_H in the short waves, and to introduce a new and smaller scale motion that decays rapidly. Substituting $p_c = e^{ik\alpha}$ in (2.B.46b) gives

$$i\left(k^2 + k + \Gamma_c\right) - F_H k^4 = 0 \qquad (2.B.47)$$

The damped short wave solution is

$$k_E = k_E^0 - F_H \frac{i k_E^{0\,4}}{2 k_E^0 + 1} + O(F_H^2)$$

$$k_E^0 = -\tfrac{1}{2}\left[1 + (1 - 4\Gamma_c)^{1/2}\right] \qquad (2.B.48)$$

and the other solution that decays to the east is

$$k_F \simeq F_H^{-1/2} \frac{1+i}{\sqrt{2}} + \frac{1}{2} + O\left(F_H^{1/2}\right) \qquad (2.B.49)$$

The solutions for the barotropic mode are obtained from those above by setting $\Gamma_c = 0$.

When lateral friction is present, an additional boundary condition is needed. The no-slip condition implies $p_x = 0$ at the boundary, since the flow along the western boundary is very nearly geostrophic. Furthermore, since the zonal scales of the boundary layer flows are much smaller than those of the interior solution for $\frac{\sigma}{b} << \lambda^{-2}$, the no-slip condition can be applied to the boundary layer solution alone with little loss of accuracy. This determines the ratio of the two solutions (2.B.48) and (2.B.49), so the lateral friction layer becomes

$$\tilde{p} = \tilde{p}_0 \left(e^{ik_E x} - \frac{k_E}{k_F} e^{ik_F x} \right) \qquad (2.B.50)$$

with only the constant $\tilde{p}_0$ to be determined by the interior solution to satisfy the condition of no normal flow at the boundary.

If $\Gamma << 1$ but $F_H >> 1$, the two solutions of (2.B.47) that decay to the east will have $k = O(F_H^{-1/3})$ as in the steady western boundary solution of Munk (1950), so the zonal scale increases slowly as the horizontal friction increases. For annual oscillations with $\nu_H = 10^2 m^2 sec^{-1}$, $F_H \simeq .5$. With this value of F_H , the boundary layer is not very accurately described by the small F_H expansion, but the main physical processes are

indicated: The short waves that are added to the interior solution to satisfy the condition of no flow through the boundary are damped by friction, and a rapidly decaying frictional layer is added at the boundary to satisfy the no-slip condition.

If both lateral and bottom friction are important in the boundary layer, the structure becomes more complicated but the essential features remain. The layer is always barotropically non-divergent, and as the frequency is decreased it becomes baroclinically non-divergent as well.

c. Matching the interior solution

The conditions $u_i = 0$ at the boundary are, from (2.A.13a,b,d,f)

$$\begin{aligned} -ibf^{-1}\tilde{p}_{1x} - bF_H f^{-1}\tilde{p}_{1xxx} \\ + \tilde{p}_{1y} + p_{I1y} = \sigma\lambda^{-2}\tau_w^{(y)} \\ -ibf^{-1}\tilde{p}_{2x} - bF_H f^{-1}\tilde{p}_{2xxx} + bF_V\tilde{p}_{2x} \\ + \tilde{p}_{2y} + p_{I2y} = 0 \end{aligned} \qquad (2.B.51)$$

The tilde denotes boundary layer variables, the subscript I interior solutions. Use has been made of the condition $A = \sigma/b \ll 1$. If b is taken as a small parameter, then the boundary condition to lowest order is a balance between geostrophic and Ekman interior flow into the boundary and geostrophic boundary layer flow in the opposite

direction. The friction and acceleration terms enter as $O(b)$ departures of the boundary layer flow from geostrophy. These terms can be simplified with the help of the boundary vorticity equations, similar to (2.B.40) but with lateral friction included:

$$-i\tilde{p}_{1xx} + \tilde{p}_{1x} + \Gamma i(\tilde{p}_1 - \tilde{p}_2) - F_H \tilde{p}_{1xxxx} = 0$$

$$-i\tilde{p}_{2xx} + \tilde{p}_{2x} + \Gamma i(\tilde{p}_2 - \tilde{p}_1)\delta - F_H \tilde{p}_{2xxxx} - F_V \tilde{p}_{2xx} = 0. \qquad (2.B.52)$$

Integrating once from $x = \infty$, where $\tilde{p}$ and its derivatives are zero, to $x = 0$, the western boundary, gives

$$\left(i\tilde{p}_{1x} + F_H \tilde{p}_{1xxx}\right)\Big|_{x=0} = \tilde{p}_1\Big|_{x=0} + \Gamma i\int_{-\infty}^{0}(\tilde{p}_1 - \tilde{p}_2)\,dx \qquad (2.B.53)$$

$$\left[(i + F_V)\tilde{p}_{2x} + F_H \tilde{p}_{2xxx}\right]\Big|_{x=0} = \tilde{p}_2\Big|_{x=0} + \Gamma\delta i\int_{-\infty}^{0}(\tilde{p}_2 - \tilde{p}_1)\,dx.$$

Substituting these in (2.B.51) gives, at $x = 0$,

$$-bf^{-1}\Gamma i\int_{-\infty}^{0}(\tilde{p}_1 - \tilde{p}_2)\,dx + f\frac{\partial}{\partial y}\left(\frac{\tilde{p}_1}{f}\right) + p_{I1y} = \sigma\lambda^{-2}\tau_w^{(y)} \qquad (2.B.54a)$$

$$-bf^{-1}\Gamma\delta i\int_{-\infty}^{0}(\tilde{p}_2 - \tilde{p}_1)\,dx + f\frac{\partial}{\partial y}\left(\frac{\tilde{p}_2}{f}\right) + p_{I2y} = 0. \qquad (2.B.54b)$$

Since the meridional transport in the boundary layer is geostrophic, $f^{-1}\tilde{p}_i$ is just the total boundary layer volume flux. Also, p_{Iy}/f is the geostrophic interior flux into the boundary layer. Hence, (2.B.54a,b) merely state that the geostrophic and Ekman influxes into the boundary layer go to change the transport and the volume of the layer. To the extent that Γ is small, the layer is baroclinically non-divergent, and the change in transport in each vertical layer can be computed from the influx into the layer. Equations (2.B.54a,b) can also be derived by integrating the continuity equations (2.A.13c,f) and substituting geostrophic approximations for (U_i, V_i).

For the barotropic mode, (2.B.54a,b) become

$$f\frac{\partial}{\partial y}\left(\frac{\tilde{p}_T}{f}\right) + p_{ITy} = \sigma\lambda^{-2}\tau_w^{(y)} \qquad (2.B.55)$$

This implies that, with $\tau_w^{(y)} = 0$, the point of maximum boundary current transport is displaced to the north of the point of maximum interior geostrophic transport. However, if the interior transport is governed by the Sverdrup balance and driven by some $(\tau_w^{(x)}, \tau_w^{(y)})$, then

$$p_{ITy} = \left(\frac{\sigma}{b\lambda}\right)^2 \int \frac{\partial}{\partial y}\left(f^2 \nabla_s \times \frac{\tau}{f}\right) dx + \sigma\lambda^{-2}\tau_w^{(y)} \qquad (2.B.56)$$

Substituting this in (2.B.55) yields, after minor manipulations,

$$\frac{d}{dy}\left[\tilde{p}_T + f\left(\frac{\sigma}{b\lambda}\right)^2 \int \nabla_s \times \tilde{\tau}_w \, dx\right] = 0 \qquad (2.B.57)$$

where we have kept $A = \frac{\sigma}{b}$, and the integration is from one side of the basin to the other. Thus, to within a constant of integration, the barotropic western boundary current transport is determined solely by the curl of the wind stress integrated across the ocean. The component of wind stress along the boundary does not affect the transport except insofar as it contributes to the curl of the stress. In other words, local forcing does not produce significant barotropic western boundary current transports at low frequencies. The meridional wind stress is balanced by a pressure gradient at each coast. The fast barotropic long wave causes this pressure gradient to propagate rapidly across the ocean, so there is everywhere a geostrophic barotropic transport equal and opposite to the zonal Ekman drift, resulting in zero net barotropic transport.

Calculation of the baroclinic response of the western boundary current is much more difficult than calculation of the barotropic part. In the first place, the divergence terms in (2.B.54a,b) depend on the

detailed dynamics of the boundary region. In the second place, even if the divergence terms are negligible (which they may often be), it is difficult to determine $f^{-1} p_{Icy}$, the interior geostrophic flow into the boundary. Due to the slowness of the baroclinic long waves, information from the eastern boundary may take years to reach the west. The phase of a wave then depends critically on details of the geometry and hydrography of the basin.

Subtracting (2.B.54b) from (2.B.54a) gives

$$b f^{-1} \Gamma (1+\delta) i \int_0^\infty \tilde{p}_c \, dx + f \frac{\partial}{\partial y}\left(\frac{\tilde{p}_c}{f}\right) + p_{Icy} = \sigma \lambda^{-2} \tau_w^{(y)} \tag{2.B.58}$$

If $p_{Ic} = 0$ and $\Gamma << 1$, then $\left(\frac{\tilde{p}_c}{f}\right)_y \simeq \sigma \lambda^{-2} \frac{\tau_w^{(y)}}{f}$; zonal Ekman flux at the coast supplies the baroclinic boundary current. As in the barotropic case there is a balance at the coast between wind stress and pressure gradient, but in the baroclinic case this balance does not exist uniformly across the ocean. At the eastern boundary it generates a baroclinic long wave, and at the western boundary it generates a boundary current. The baroclinic long wave upon arriving in the west will itself generate a boundary current, but the phase of this contribution is uncertain.

The part of the baroclinic western boundary transport due to the wind stress curl in the interior, ignoring the wave from the eastern boundary, can also be calculated in the limit $\Gamma \ll 1$. For example, if $\nabla_s \times \left(\frac{\tau_w}{f}\right)$ is a function of latitude only, then from (2.B.2b), (2.B.3), and (2.B.27) the directly forced part of p_{IC} is approximately $-i(1+\delta)\nabla_s \times \left(\frac{\tau_w}{f}\right)$. Use of (2.B.58) then gives the result

$$p_c \simeq -i(1+\delta) f \int f^{-1} \nabla_s \times \left(\frac{\tau_w}{f}\right) dy \qquad (2.B.59)$$

This reiterates the increasing importance of the baroclinic mode as one goes towards the equator (Lighthill, 1969; Gill and Niiler, 1973; White, 1977); the response in terms of transport goes as f^{-2}, while the barotropic transport is independent of f.

In the calculation of both baroclinic and barotropic western boundary responses, we find that there is a constant of integration that is not constrained by the model. The model is valid only over a restricted range of latitudes, but it has not been closed off by zonal boundaries. The undetermined constants of integration represent boundary current transports through the region of validity of the model due to processes outside that region, or of a scale for which the model is invalid.

Another shortcoming of this model is its neglect of mean currents and dynamic topography. Qualitatively, a mean flow toward the western boundary will aid boundary layer formation by slowing the short wave radiation of energy away from the boundary. Similarly, a mean flow away from the boundary will widen the boundary layer or prevent its formation entirely. This may limit the applicability of our simple model to regions where the zonal component of mean flow is small or to the west, say from the southern edge of the North Equatorial Current to Cape Hatteras, for example.

Chapter III

FLOW OVER TOPOGRAPHY

A. The two-layer barrier problem

In the last chapter we saw how short Rossby waves, or their counterparts modified by friction, are generated at the western boundary to satisfy the condition of no normal flow into the boundary. Now we ask, what happens if the condition of no zonal flow is applied only in the lower layer? If the lower layer is blocked by a meridional ridge, but the upper layer is unimpeded, does a boundary layer form in the upper layer as well as in the lower?

These questions are motivated in part by consideration of the topography of the North Atlantic. The Antilles Arc, separating the Caribbean from the Atlantic, has a maximum sill depth of less than 2000 m, and an average depth of far less than that. The Mid-Atlantic Ridge is less extreme, but still represents a sizeable barrier to deep zonal flow. Instead of modeling the Antilles and the Mid-Atlantic Ridge as infinitesimal perturbations to an otherwise flat bottom, one may go to the other extreme; suppose a meridional ridge extends close enough to the interface in the two-layer model to completely block flow in the lower layer. If realism in modeling the horizontal direction is sacrificed by making the barrier an infinitely thin wall, the problem can be simplified to the point where a closed form analytic solution is possible.

Since the value of this model lies in its simplicity rather than its realism, let us keep it stripped to its essentials. Explicit lateral and bottom friction will be ignored, so free waves will be used to meet matching and boundary conditions at the barrier. This allows the vertical structure of the solution to be represented by normal modes. Furthermore, in order to have equations with constant coefficients, we will consider only the lowest order solution in an implicit expansion in the beta parameter, b. This yields the usual beta-plane approximation in which the Coriolis parameter is considered constant except where differentiated. Since we also restrict attention to low frequencies, the lowest order momentum equations contain only the geostrophic balance.

The vorticity equations under these conditions are (2.B.4) and (2.B.10) with $f=1$ and $A=1$. The geostrophic balance in terms of velocity (not transport per unit width) is

$$u_i = -p_{iy}$$
$$v_i = p_{ix} \qquad (3.A.1)$$

This with (2.B.31) gives the relation between layer velocities and mode amplitudes:

$$\vec{u}_1 = (1+\delta^{-1})^{-1}(\vec{u}_T + \delta^{-1}\vec{u}_c)$$
$$\vec{u}_2 = (1+\delta^{-1})^{-1}(\vec{u}_T - \vec{u}_c) \qquad (3.A.2)$$

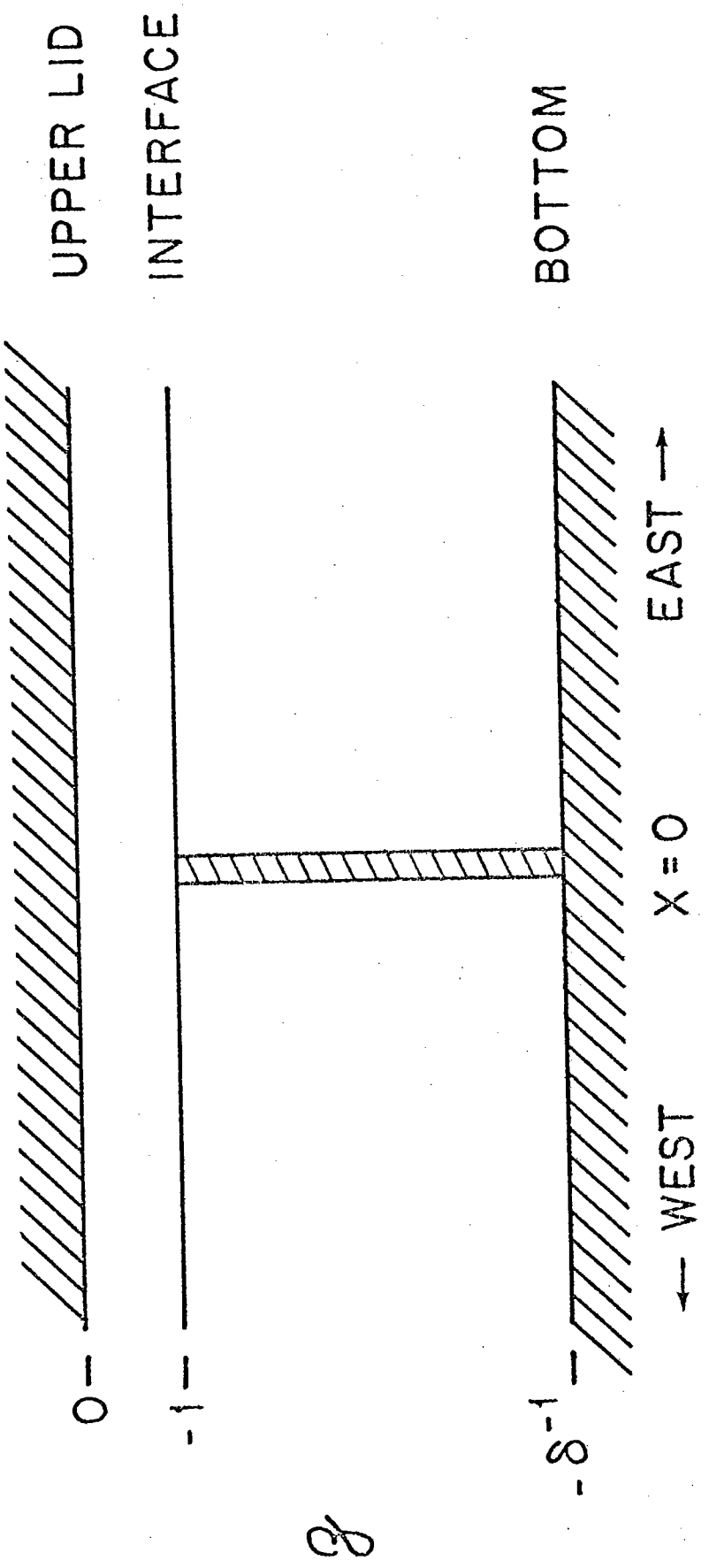

Figure 3.A-1. Barrier Model.

Let there be an infinite meridional barrier in the lower layer at $x = 0$, dividing the plane into two regions (Fig. 3.A-1). In both regions there is an initial flow, denoted by subscript I, that could exist alone if the barrier were absent. The initial flow might be any combination of free or forced solutions of the barotropic and baroclinic vorticity equations, and is continuous at $x = 0$. If the barrier is present, then free wave solutions of the vorticity equations (2.B.4) and (2.B.10), denoted by the subscript B, must be added to the initial flow in order to bring the lower layer zonal velocity to zero at the barrier. The appropriate free wave solutions are those that either have a zonal component of group velocity away from the barrier, or decay away from the barrier. To the east of the barrier these are the short waves, $p_{BTE}\, e^{ik_{TE}x}$ and $p_{BCE}\, e^{ik_{CE}x}$; and to the west, the long waves, $p_{BTW}\, e^{ik_{TW}x}$ and $p_{BCW}\, e^{ik_{CW}x}$. The common factor $e^{ily}\, e^{-it}$ is omitted. The wavenumbers are determined by (2.B.7) and (2.B.12).

There are four matching conditions at the barrier that determine the amplitudes of the four free waves:

$$u_2 = 0 \quad at \quad x = 0^+ \tag{3.A.3a}$$

$$u_2 = 0 \quad at \quad x = 0^- \tag{3.A.3b}$$

$$u_1\big|_{x=0^+} = u_1\big|_{x=0^-} \tag{3.A.3c}$$

$$v_1|_{x=0+} = v_1|_{x=0-} \qquad (3.A.3d)$$

The first two conditions are the obvious requirements of no flow through the barrier, and the third condition is the equally obvious condition of flux continuity over the barrier. The fourth condition is equivalent to saying that there is no singular source of vorticity in the upper layer. The barrier does not penetrate into the upper layer, so it cannot cause a vortex sheet there. Note that the third and fourth conditions are satisfied independently by the initial flow, since it is assumed continuous at the barrier. Therefore only the initial zonal velocity at $x = 0$ enters the matching conditions.

If the initial lower layer pressure is $p_{I2}(x)\, e^{ily}\, e^{-it}$, then the matching conditions become

$$(p_{BTE} - p_{BCE})(1+\delta^{-1}) + p_{I2}(0) = 0 \qquad (3.A.4a)$$

$$(p_{BTW} - p_{BCW})(1+\delta^{-1}) + p_{I2}(0) = 0 \qquad (3.A.4b)$$

$$p_{BTE} + \delta^{-1} p_{BCE} = p_{BTW} + \delta^{-1} p_{BCW} \qquad (3.A.4c)$$

$$k_{TE}\, p_{BTE} + \delta^{-1} k_{CE}\, p_{BCE} = k_{TW}\, p_{BTW} + \delta^{-1} k_{CW}\, p_{BCW} \qquad (3.A.4d)$$

The first three conditions say that the pressure is the same on either side of the barrier in both layers, so the amplitude of each mode must be the same on either side. The solution for the amplitudes is

$$p_{BTE} = p_{BTW} = -p_{I2}(0)(1+\delta^{-1})\frac{K}{\delta}\left(1+\frac{K}{\delta}\right)^{-1} \qquad (3.A.5a)$$

$$p_{BCE} = p_{BCW} = p_{I2}(0)\left(1+\delta^{-1}\right)\left(1+\frac{K}{\delta}\right)^{-1} \qquad (3.A.5b)$$

where

$$K \equiv \frac{k_{cE}-k_{cW}}{k_{TE}-k_{TW}} = \left[\frac{1-4\left(\frac{\sigma}{b}\right)^2\left(\lambda_i^{-2}+\ell^2\right)}{1-4\left(\frac{\sigma\ell}{b}\right)^2}\right]^{1/2} \qquad (3.A.6)$$

The upper layer pressure at $x=0$ is therefore

$$p_{B1} = p_{I2}(0)\,\delta^{-1}\left(1+\frac{K}{\delta}\right)^{-1}(1-K) \qquad (3.A.7)$$

which goes to zero as K goes to 1. This means that if $K \simeq 1$, the waves induced by the barrier sum to zero in the upper layer at $x=0$. The barrier in this limit has no effect on the flux of upper layer water across the barrier. The limit $K \to 1$ occurs when $k_{cE} \to k_{TE}$, which means that

the baroclinic and barotropic modes to the east of the barrier will change their relative phases only very slowly. If $p_1 \simeq 0$ at the barrier, then $p_1 \simeq 0$ for many short wavelengths east of the barrier. If the short waves are dissipated within a few wavelengths, then for $\alpha > 0$ the effect of the barrier is entirely confined to the lower layer.

In order to show the effect of dissipation without adding undue complexity we may introduce a Rayleigh friction, proportional to velocity. If d is the dissipation parameter then the dispersion relations (2.B.6) and (2.B.11) become

$$k^2 + \frac{b}{\sigma_d} k + l^2 = 0$$

$$k^2 + \frac{b}{\sigma_d} k + l^2 + \frac{\sigma}{\sigma_d} \lambda_c^{-2} = 0$$

with

$$\sigma_d \equiv \sigma (1 - i d)$$

Note that d^{-1} is a barotropic spindown time nondimensionalized by the time scale of the wave.

Figure 3.A-2a shows the pressure in each layer due to a barotropic long wave ($p_1 = p_2 = 3 \cos (k_{TW} x + l y - t)$) incident on the barrier. The wave is of semiannual period and has a 200 km meridional scale. With a 63 km radius of deformation this implies $k = .76$, which is not very close to the limiting value $k = 1$ but provides a clearer picture of

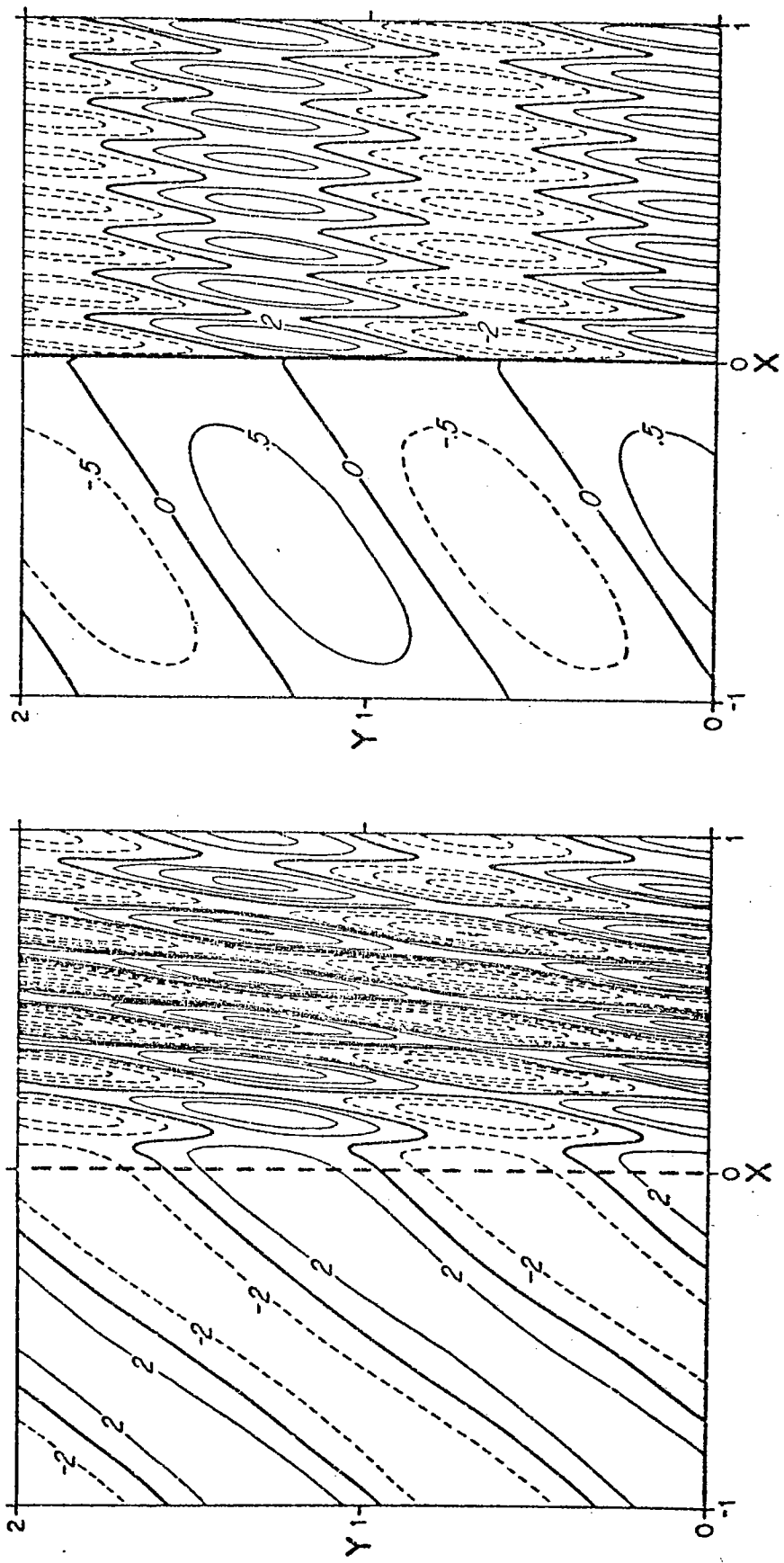

Figure 3.A-2a. Pressure in the upper layer (left) and the lower layer (right) due to a barotropic long wave incident on the lower layer barrier; without dissipation.

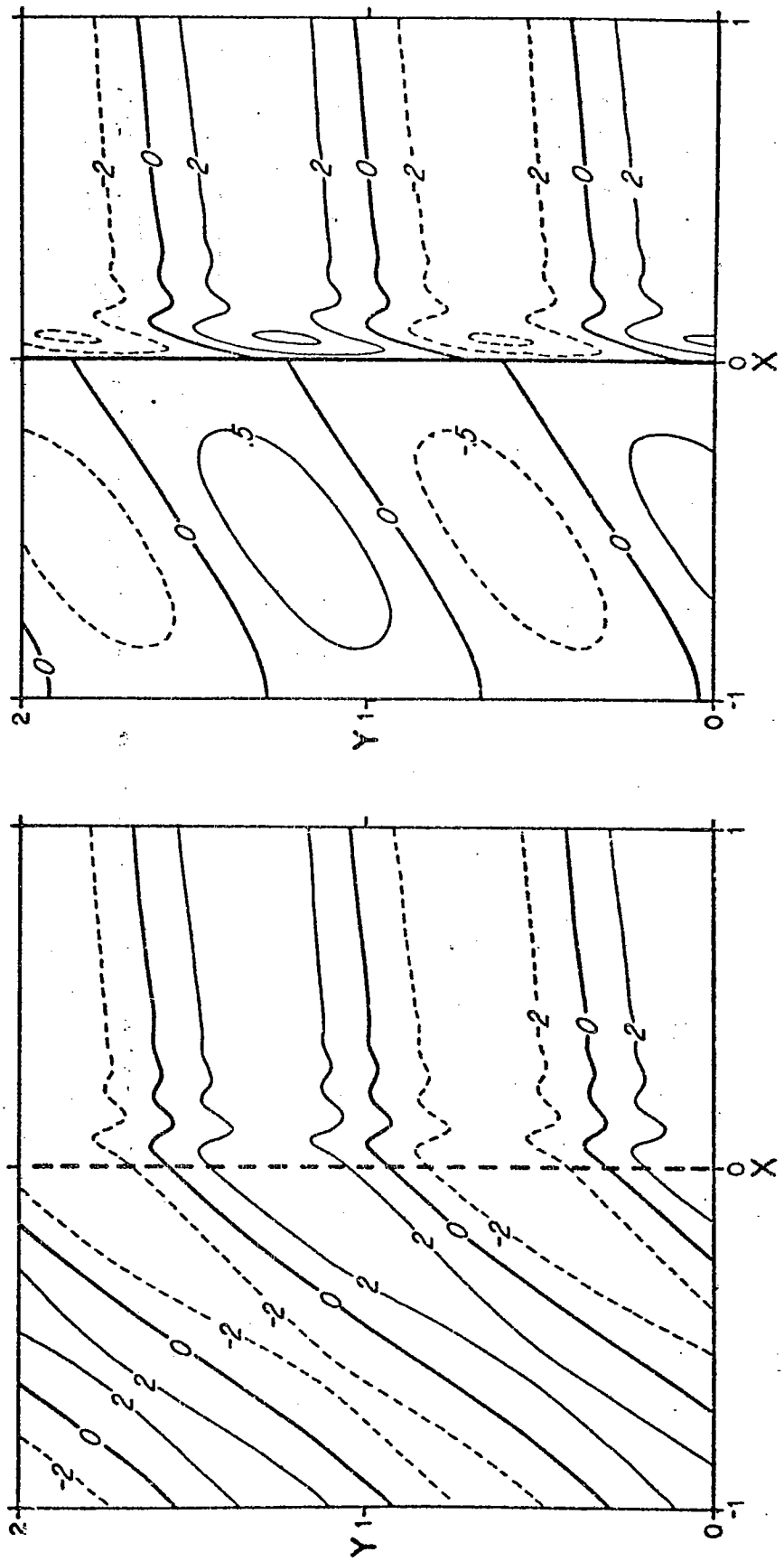

Figure 3.A-2b. Pressure in the upper layer (left) and the lower layer (right) due to a barotropic long wave incident on the lower layer barrier; with dissipation, d = .25.

the structure of the solution than would a more extreme example. Note the slow oscillation of the upper layer short wave amplitude due to the difference in wavelength of the barotropic and baroclinic short waves.

Figure 2.A-2b is perhaps a more realistic picture of the flow. Everything is the same as in the previous example except that dissipation with $d = .25$ has been added. Since the short waves have large particle velocities and small group velocities, they are damped within a short distance of the barrier. This short distance is insufficinet for a large transfer of energy from the lower layer to the upper, so the upper layer is only slightly disturbed east of the barrier. West of the barrier the flow is nearly the same with and without dissipation. Most of the energy is in a baroclinic long wave, which accounts for the diagonal phase lines. Waviness of the upper layer phase lines and the closed pressure contours in the lower layer are due to interference between the baroclinic and barotropic long waves.

This limiting case $K \simeq 1$ occurs when $\lambda_c^{-2} >> l^2$ and $\left(\frac{2\sigma}{b\lambda_c}\right)^2 << 1$ so that $K \simeq 1 - 2\left(\frac{\sigma}{b\lambda_c}\right)^2$. Physically, these conditions mean that the short wave scale, σ/b, is small compared to the radius of deformation. The stretching term in the short wave vorticity equation is then small compared to the vorticity change term, and the layers become decoupled.

Since the barrier is in the lower layer alone, it can affect the upper layer only to the extent that the layers are dynamically coupled by the waves that radiate away from the barrier. Although the short waves may involve little coupling between the layers, in long waves the layers are strongly coupled, so the barrier has a substantial effect on both layers to the west. The barotropic and baroclinic long waves from the barrier sum to zero at $x = 0$ in the limit $K = 1$, but they soon get out of phase to the west.

As the frequency of the oscillations increases, K decreases to zero and then becomes imaginary. As K decreases, the baroclinic waves become more important and the barotropic waves diminish. This has the effect of shifting the initial lower layer zonal transport to the upper layer. When $K = 0$, the total zonal transport at the barrier is exactly what it would be if only the initial flow were present, but it is all carried in the upper layer. When K is imaginary, phase shifts occur between the initial flow and the waves.

The parameter K can be defined in terms of the circle-diagrams of the Rossby wave dispersion relations, Figures 2.B-1a,b. It is just the ratio $\overline{A'B'}/\overline{AB}$ of the chords of the wavenumber circles for baroclinic and barotropic waves, respectively, at a given frequency and meridional wavenumber. Hence the limit $K = 1$ requires that the radii of the wavenumber circles in the diagrams be similar, and that the

meridional wavenumber not be too large. The restriction on ℓ is more severe as the radius of deformation decreases and the baroclinic wavenumber circle shrinks.

The group velocities of the free waves are predominantly zonal when $K \gtrsim 1$, but become icnreasingly meridional as K decreases. At $K=0$ the baroclinic group velocity is purely meridional, and when K is imaginary the baroclinic waves are trapped in the zonal direction. These factors limit the usefulness of the model as K decreases. The model has assumed periodic solutions in y, but is valid only for $y = O(1)$, or for $by \ll 1$. The model should therefore depend only on conditions local in y, and not on energy that propagates in along the barrier from $y = \pm\infty$. However, since the solutions depend in no way on the sign of ℓ, zonal boundaries could easily be added to the model, say at $y = \pm 1$, with the initial flow and all solutions proportional to $\sin n\pi y$. Then the trapped baroclinic waves would be able to reflect back and forth between the zonal boundaries without adding or removing energy from the system.

As was seen in the previous chapter, the condition $\left(\frac{\sigma}{b\lambda_c}\right)^2 \ll 1$ is satisfied by annual oscillations, so the $K \simeq 1$ limit is applicable. Values of K as a function of σ and λ_c are shown in Fig. 3.A-3. Since the radius of deformation decreases with increasing latitude, σ is restricted to smaller values at higher latitudes if the limit $K=1$ is

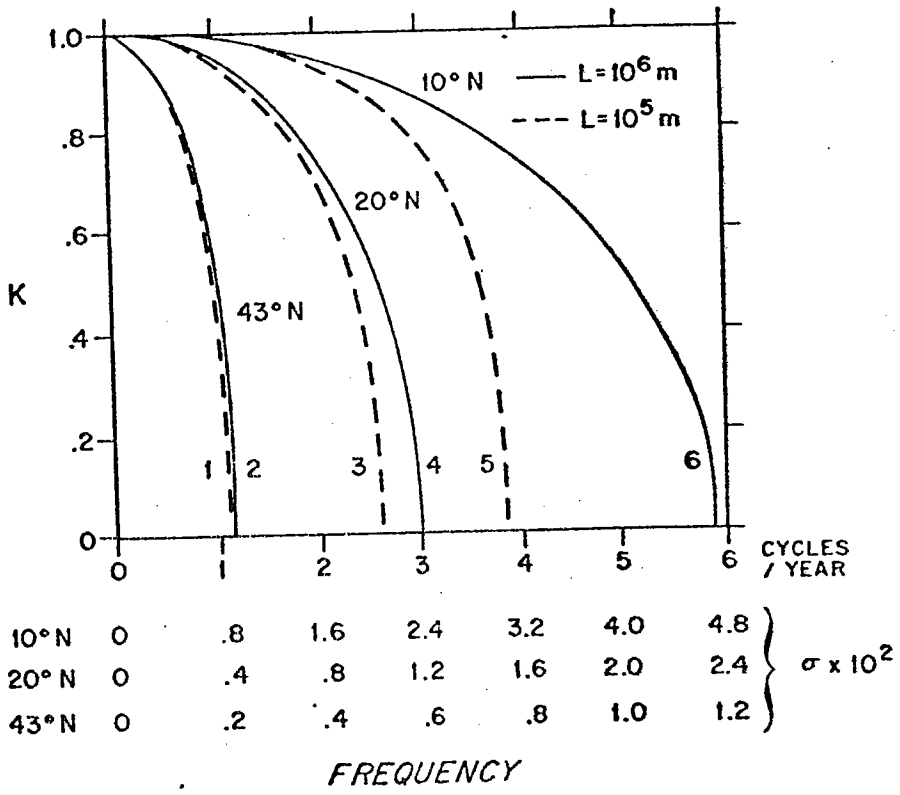

Figure 3.A-3. Variation of the barrier model parameter K with frequency.

required. For annual oscillations $K \simeq 1$ is a fair approximation as far as 40°N, but for semiannual oscillations the approximation breaks down around 20°N. With a doubling in frequency, K changes from about .87 to zero; hence for most of the frequency range over which propagating barotropic and baroclinic waves exist, K is near its limiting value of one. At the eddy scales of $L = 100$ km, there is no baroclinic zonal propagation at periods of 3 months at 20°N, so K is imaginary.

If the initial flow consists of a free wave, then it is instructive to recast the solution (3.A.5) in terms of incident, transmitted, and reflected waves. Suppose, for example, that the initial flow is a barotropic long wave. Then the incident wave is the initial flow east of the barrier. The transmitted wave is the sum of the initial flow and the barotropic long wave induced by the barrier to the west of the barrier. The reflected wave is the barotropic short wave induced by the barrier. The baroclinic waves contain energy scattered from the incident barotropic wave. The energy flux of the baroclinic short wave can be added to that of the barotropic short wave to give the total reflected energy flux, and similarly for the long waves and the total transmitted energy flux.

The average energy densities of barotropic and baroclinic waves (Longuet-Higgins, 1964a) are proportional to $p_T^2 \left(k_T^2 \frac{\varepsilon}{\omega}\right.$ and $p_c^2 \delta^{-1} \left(k_c^2 \frac{\varepsilon}{\omega} + l^2 + \lambda_c^{-2}\right)$, respectively. The factor of

δ^{-1} in the baroclinic energy density is due to the way in which the vertical modes are normalized. The energy fluxes are defined as the energy densities times the group velocities. Using the expressions (2.B.8a) and (2.B.13a) for the group velocities, along with the dispersion relations (2.B.7) and (2.B.12), it follows that the magnitudes of the zonal energy fluxes are proportional to $p_T^2 (k_{TW} - k_{TE})$ and $p_c^2 \delta^{-1} (k_{cW} - k_{cE})$ for both long and short waves.

Table 3A-1 gives the energy flux ratios for incident barotropic and baroclinic long waves, computed from (3.A.5). When $K \simeq 1$, all ratios are primarily dependent on the value of δ, the ratio of the upper to lower layer depths. If this is small, then barotropic energy will be mostly blocked and baroclinic energy transmitted. Of the total energy transmitted, most will be baroclinic, and of the total reflected, most will be barotropic. When K is small, the opposite is true; baroclinic energy is blocked and barotropic energy is transmitted.

Away from the limiting case of $K \simeq 1$, the behavior of the barrier model depends on the details of parameters and dynamics, so the specific predictions of the model may be misleading if applied to a physical situation. The main accomplishment of the barrier model is its illumination of the limiting case of low frequency motion, in which the scale difference between long and short Rossby waves leads to model behavior that is not sensitive to details. In this limit,

Table 3.A-1

Energy flux ratios for Rossby waves incident on lower layer barrier.

	Incident Barotropic Wave	Incident Baroclinic Wave
$\frac{\text{total transmitted}}{\text{incident}}$	$(1+\frac{K}{\delta})^{-1}$	$\frac{K}{\delta}(1+\frac{K}{\delta})^{-1}$
$\frac{\text{total reflected}}{\text{incident}}$	$\frac{K}{\delta}(1+\frac{K}{\delta})^{-1}$	$(1+\frac{K}{\delta})^{-1}$
$\frac{\text{transmitted baroclinic}}{\text{transmitted barotropic}}$	$\frac{K}{\delta}$	$\frac{K}{\delta}$
$\frac{\text{reflected baroclinic}}{\text{reflected barotropic}}$	$\frac{\delta}{K}$	$\frac{\delta}{K}$

the weak coupling of the layers with respect to short waves implies that the upper layer does not feel the presence of the ridge to the east of the ridge. In the previous chapter we saw that lateral friction of reasonable magnitudes does not substantially increase the coupling between layers, while bottom friction tends to decouple the layers. Hence, the omission of explicit friction in the barrier model seems unlikely to have seriously affected the low frequency limit.

B. Theory of flow over a sloping bottom

In this section we will consider the dynamic effects of a sloping bottom on the sorts of motion discussed in Chapter II. We will restrict our attention to the case of constant slope, with parallel isobaths running north-south. Two distinct types of analysis will be used. The first is the plane wave analysis of the type used by Rhines (1970), based on the approximations $h=1$ and $f=1$ except where differentiated. This leads to vorticity equations with constant coefficients. These admit plane wave solutions which we will later use for calculating the flow over more complicated topography. Although all the solutions take the form of plane waves, some of them (the lower layer long waves) are not really wavelike in their dynamics. This is made clear in the second type of analysis which begins with a careful scaling of the full vorticity equations. Consistent approximations and perturbation expansions are then found for various parts of the parameter space of interest. This illuminates the dynamics of the types of motion found in the simpler plane wave analysis, as well as showing the types of error that result from the approximations $h=1$ and $f=1$.

Consider a region of constant slope so that

$$h = 1 + S\gamma A x \qquad (3.B.1)$$

$$\gamma \equiv \frac{L}{H_{20}} \left| \frac{dH_2}{dx'} \right|$$

$$S \equiv \left(\frac{dH_2}{dx'} \right) \Big/ \left| \frac{dH_2}{dx'} \right| \qquad (3.B.1)$$

where H_2 and x' are dimensional. A very steep slope in the ocean might be $|dH_2/dx'| = .1$, a rise of 1 km in 10 km. A rather small value might be 10^{-3}, a rise of 1 km in 1000 km. For L = 10^6m (annual scale) and $H_2 \simeq 3500$ m, this range of slopes means a range of γ from 30 to .3. The same slopes with L = 10^5m (eddy scale) produce a range of γ from 3 to 3×10^{-2}. The parameter S takes the value +1 if the slope is down to the east and -1 if down to the west.

With h defined as in (3.B.1), the lower layer vorticity equation (2.A.19b), becomes

$$\begin{aligned} &-i\sigma h \nabla_s^2 p_2 - i\sigma\gamma S p_{2x} \\ &\quad + i\sigma\alpha^{-2} S A f^2 (p_2 - p_1) \\ &\quad + bh p_{2x} + f\gamma S A p_{2y} \\ &\qquad = -\delta \left(\frac{E_v f}{2} \right)^{1/2} \nabla_s^2 p_2 \\ &\qquad\quad + E_H A^{-3} \left(h \frac{\partial^4 p_2}{\partial x^4} + \gamma S A \frac{\partial^3 p_2}{\partial x^3} \right) \end{aligned} \qquad (3.B.2)$$

We will assume that the friction terms are small except possibly when A approaches the short wave scale.

The two terms in (3.B.2) involving γ are $-i\sigma\gamma S p_{2x}$ and $f\gamma S A p_{2y}$. The second term is the product of the geostrophic zonal velocity component and the slope, while the first term

is approximately the ageostrophic zonal velocity times the slope. The second term is always the most important for low frequency motion, and will usually be referred to simply as the slope term. The first term, referred to henceforth as the ageostrophic slope term, is $O(\sigma A^{-1})$ relative to the second term. Hence at low frequencies it will be negligible unless the zonal scale is very small.

1. Onset of the slope effects

The first questions to ask are, what is the smallest slope that significantly perturbs each of the free and forced motions of interest, and what is the nature of the perturbations? Let us begin with barotropic long waves.

The barotropic long wave balance is characterized by $p_1 \simeq p_2$ and $A = b/\sigma$. The ratio of slope to beta terms is then γ/σ, so slope will become important as this approaches O(1). At the annual scales, this occurs with a bottom slope of only 10^{-5}. At eddy scales, $\gamma/\sigma = 1$ for a slope of about $.5 \times 10^{-3}$, so again even the smallest slopes are important.

The baroclinic long wave balance is characterized by $p_1 \simeq -\delta^{-1} p_2$ and $A = b/\sigma\lambda^{-2}$. This gives a ratio of slope term to beta term of $\gamma/\sigma\lambda^{-2}$ which equals one at a slope of about 3×10^{-3} for annual scales and about 10^{-3} for eddy scales. Hence baroclinic long waves are less sensitive to slopes than are barotropic long waves, but still only a small slope is sufficient to alter the lower layer vorticity balance

Short waves at low frequencies have a scale $A = \sigma/b$, for which the ratio of slope to beta terms becomes unity at slopes of about -1 for annual scales and about .05 for eddy scales. Hence, short waves are quite insensitive to slopes. As we will see, however, this conclusion is not quite correct. Although a moderate slope has little effect on the scale of short wave motion, it has a considerable effect on the vertical mode structure of the waves. Indeed, a given slope produces exactly the same vertical mode structure for both long and short waves, as will be seen.

2. Plane wave solutions

Equations (2.A.19a) and (3.B.2) cannot be solved directly as they are. The main obstacles are the nonconstant coefficients h and f. If b and γA are small, then for x and y of O(1) the approximations $h \simeq 1$ and $f \simeq 1$ are appropriate; that is, the coefficients are locally constant. This permits plane wave solutions and the coupled differential equations are reduced to algebraic equations. The solutions obtained by this method are useful even when the approximation of constant coefficients is poor. Although quantitative accuracy is lost, qualitative information of the scales and dynamical balances is still present. In fact, the procedure of approximating constant coefficients, substitutiong plane wave solutions, and then solving the algebraic dispersion relations, is equivalent to performing a scale analysis.

With $f \to 1$, $h \to 1$, $E_V = E_H = 0$, and the ageostrophic slope term neglected, the vorticity equations (2.A.19a) and (3.B.2) can be written

$$\mathcal{L} p_1 - (p_2 - p_1) = -iG \qquad (3.B.3a)$$

$$\mathcal{L} p_2 + \delta (p_2 - p_1) + \alpha s \ell p_2 = 0 \qquad (3.B.3b)$$

where

$$\mathcal{L} \equiv (i\sigma x^{-2} A)^{-1} \left(-i\sigma \sigma_s^2 + b \frac{\partial}{\partial x} \right)$$

$$\alpha \equiv \frac{\gamma}{\sigma x^{-2}} \qquad (3.B.4)$$

A meridional dependence $e^{i\ell y}$ with $\ell = \pm 1$ has been assumed for p_1, p_2, and the forcing, G.

Now we can find the vertical structures of the modes of oscillation by setting $p_2 = R p_1$, where R is a constant for each mode, so that both layers have the same zonal as well as meridional and temporal variations. The operator $\mathcal{L}$ can then be eliminated from (3.B.3a,b). With $G = 0$ a quadratic equation for R results:

$$R^2 + R(\delta - 1 + \alpha s \ell) - \delta = 0 \qquad (3.B.5)$$

Hence R depends only on α, which is the ratio of the steepness of the slope to the strength of the coupling between layers, and on the product of the sign of the slope and the meridional wavenumber. These are externally imposed parameters in our problem, so the vertical mode structure expressed by R is independent of the zonal wavenumber. This convenient simplification results from our alignment of the y coordinate, for which the wavenumber is specified, parallel to the isobaths. Neglect of the ageostrophic slope term is also required. However, the restriction of the slope to east-west is not essential. If the coordinate axes were rotated along with the slope so that north were at an angle θ to the y axis, the only difference in (3.B.3) and (3.B.4) would be the replacement in the latter of $b\frac{\partial}{\partial x}$ by $b\cos\theta\frac{\partial}{\partial x} - bA\sin\theta\frac{\partial}{\partial y}$ in the operator $\mathcal{L}$. Since (3.B.5) does not involve $\mathcal{L}$, the values of R would be unaffected. Hence (3.B.5) is really the same as (2.8) in Rhines (1970), which was derived for the case of two-layer flow over a slope oriented north-south (with isobaths running east-west).

In the limit of no slope, $\alpha = 0$, we recover the barotropic and baroclinic modes of (2.B.1): $R_T = 1$, $R_c = -\delta$. For small slopes the perturbed values of R are

$$R_T \simeq 1 - \frac{\alpha s l}{1+\delta}$$

$$R_c \simeq -\delta\left(1 + \frac{\alpha s l}{1+\delta}\right) \qquad \text{(3.B.6)}$$

Note the dependence on the product $s\ell$, which is typical of the slope term. A wave with northward phase propagation on a slope down to the east is affected by slope in the same way as a wave with southward phase propagation on a slope down to the west: lower layer flow is induced in the opposite direction to the upper layer flow. Thus if $s\ell > 0$ then the barotropic mode is enhanced in the upper layer while the baroclinic mode is enhanced in the lower layer. The situation is reversed for $s\ell < 0$.

Equation (2.B.5) can, of course, be solved in general:

$$R_T = \frac{1}{2}\left\{1 - \delta - \alpha s\ell + \left[(1 - \delta - \alpha s\ell)^2 + 4\delta\right]^{1/2}\right\}$$

$$R_C = \frac{1}{2}\left\{1 - \delta - \alpha s\ell - \left[(1 - \delta - \alpha s\ell)^2 + 4\delta\right]^{1/2}\right\} \quad (3.B.7)$$

The variations of R_T and R_C with α for both cases $s\ell > 0$ and $s\ell < 0$ are plotted in Figure (3.B-1). The most important feature of (3.B.7) is that each depends monotonically on α. Thus in the limit of large α, the barotropic mode becomes confined to the upper layer for $s\ell > 0$ and the lower layer for $s\ell < 0$. The baroclinic mode becomes confined to the lower layer for $s\ell > 0$ and the upper layer for $s\ell < 0$. Of course, the designations "barotropic" and "baroclinic" are no longer entirely appropriate but are used as a convenient means of specifying the modes in which upper and lower layer

motions are in phase, and π radians out of phase, respectively. As we shall see, for large α the barotropic wave with $s\lambda > 0$ is dynamically similar to the baroclinic wave with $s\lambda < 0$, and both will be identified as "upper layer waves." The same is true for "lower layer waves."

The vertical mode structure derived above for two-layer stratification has a counterpart in a continuously stratified fluid. Suarez (1971) considered in detail the motions of a fluid with constant Brunt-Väisälä frequency (N) on a beta-plane over a sloping bottom. The vertical mode structure is found by solving a transcendental equation resulting from the bottom boundary condition. When $s\lambda > 0$ (in the notation of this thesis), all the modes go as cos m z. The lowest, or "zeroth" mode has no zero-crossing within the fluid. It has a maximum at the surface and corresponds to the 'barotropic' upper layer wave in the two-layer fluid. The first mode has one node within the fluid and corresponds to the 'baroclinic' lower layer wave. There is also an infinite set of higher modes that have no counterparts in a two-layer fluid. When $s\lambda < 0$, the lowest mode goes as cosh m z; it is bottom trapped, or decreases exponentially away from the bottom. This corresponds to the 'barotropic' lower layer wave. All the higher modes go as cos m z. The first has one zero-crossing and corresponds to the 'baroclinic' upper layer wave. The higher modes again have no two-layer counterparts. Note

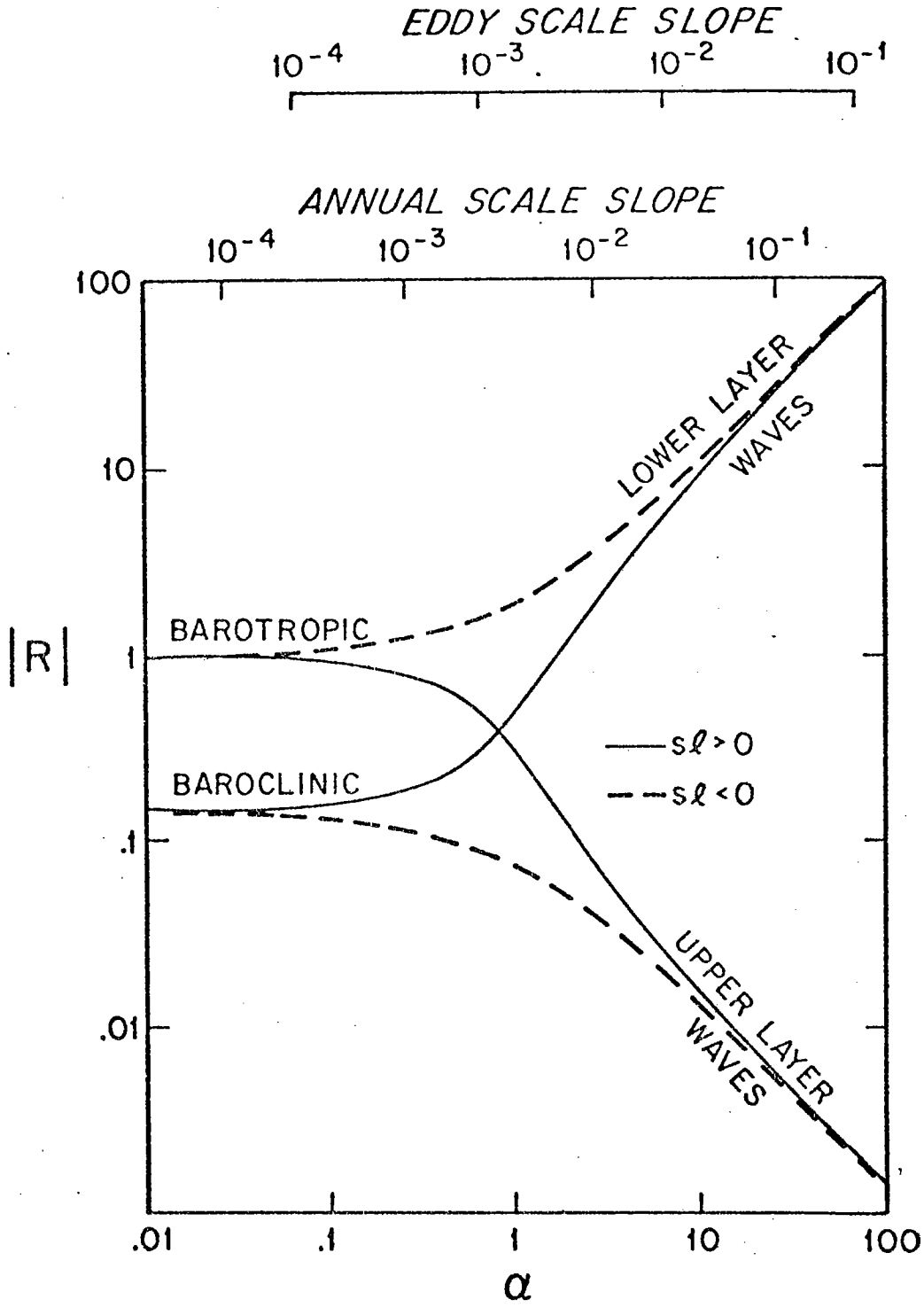

Figure 3.B-1. Vertical mode structure as a function of slope.

that the analogy between modes in the constant-N and two-layer cases must not be carried too far. With constant N the nodes move up or down depending on the slope and wave-number, with two layers the node is of course fixed. With large slopes the two-layer modes become almost entirely confined to the upper or lower layer; the constant-N modes are, with the single exception of the bottom-trapped wave, restricted by their sinusoidal form. There is no exponentially decaying "surface-trapped wave." Instead, the node simply shifts toward the bottom as the slope is increased.

Having found R we can now set $p_1 = e^{ikx} e^{ily}$, $p_2 = R e^{ikx} e^{ily}$. Substitution in either of (3.B.3a) or (3.B.3b) with $G = 0$ will yield a quadratic dispersion relation for k for each value of R. Since we are not using scale analysis here to eliminate terms, we set $A = 1$. The two equivalent dispersion relations are

$$k^2 + \frac{b}{\sigma} k + l^2 + \lambda^{-2}(1-R) = 0 \qquad \text{(3.B.8a)}$$

$$k^2 + \frac{b}{\sigma} k + l^2 + \lambda^{-2}\left[\delta(1-R^{-1}) + \alpha s l\right] = 0 \qquad \text{(3.B.8b)}$$

The roots of these equations as functions of α are shown in Figure (3.B-2). The vorticity balances leading to these waves will be considered shortly, but first let us find the response of (3.B.3) to forcing.

We will consider only zonally uniform forcing. Since the coefficients of (3.B.3) are constant, the response is also zonally uniform. Substituting $G = ie^{ily}$, $p_1 = p_{1F}e^{ily}$, $p_2 = p_{2F}e^{ily}$ in (3.B.3) gives simultaneous equations for p_{1F} and p_{2F}:

$$\begin{aligned} (l^2\lambda^2 + 1)p_{1F} - p_{2F} &= 1 \\ -\delta p_{1F} + (l^2\lambda^2 + \delta + \alpha s l)p_{2F} &= 0 \end{aligned} \qquad (3.B.9)$$

Solutions are shown in Figure (3.B-3). The main feature is the enormous reduction in response as the slope increases. Only a small zonal velocity perpendicular to a slope is sufficient to produce a vertical velocity at the bottom equal to the Ekman velocity imposed by G. Very little of the torque of the wind stress curl goes into accelerating the fluid, unlike the barotropic forced response (2.B.20).

Now let us consider the vorticity balances that control the various free and forced motions.

3. Vorticity balance

a. Long upper layer wave

We saw in the plane wave analysis (Fig. 3.B-2) that regardless of the slope there is a wave with scale $A_u = b/\sigma\lambda^2$.

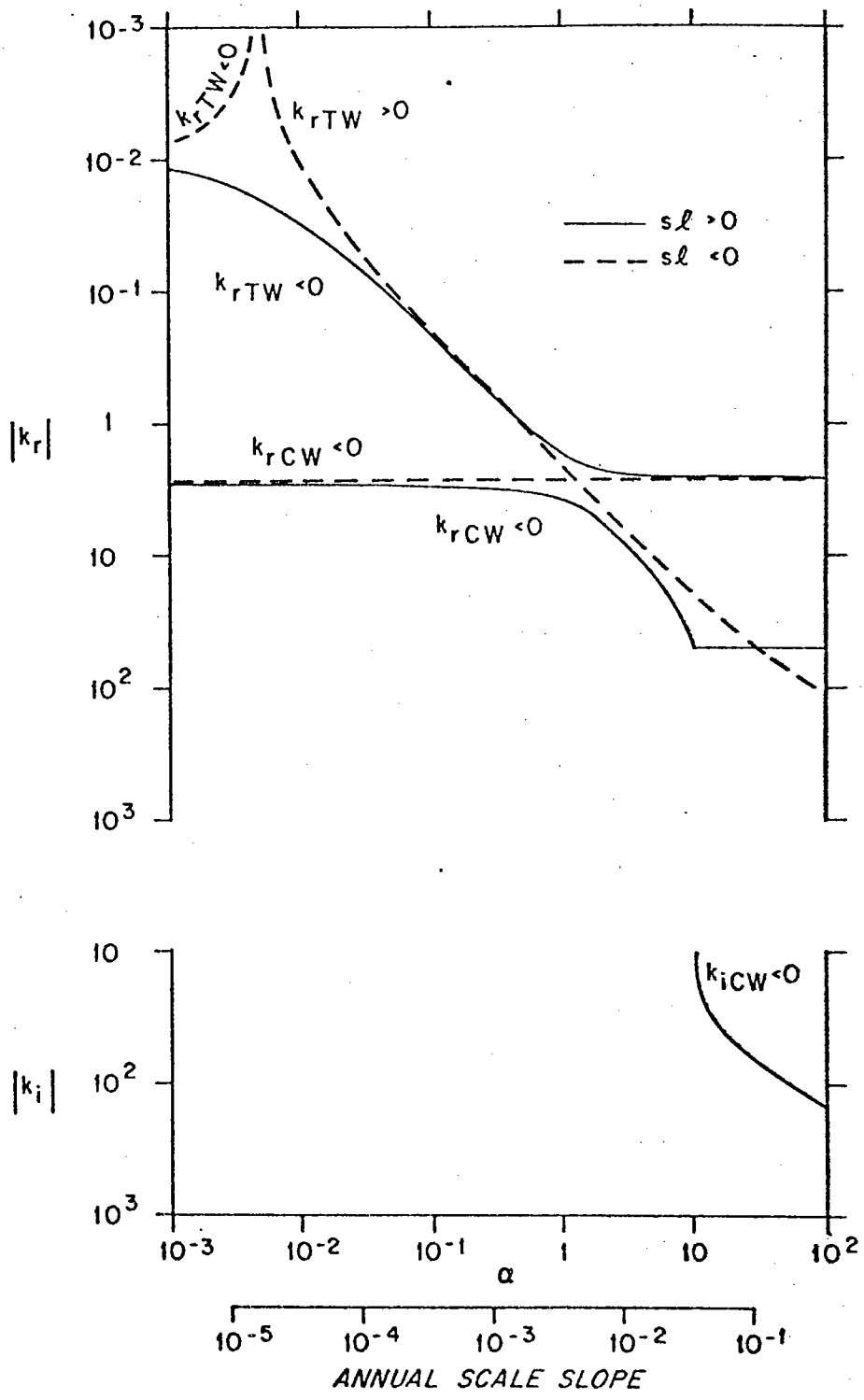

Figure 3.B-2a. Wavenumbers of long waves for annual scale. $k = k_r + i\,k_i$

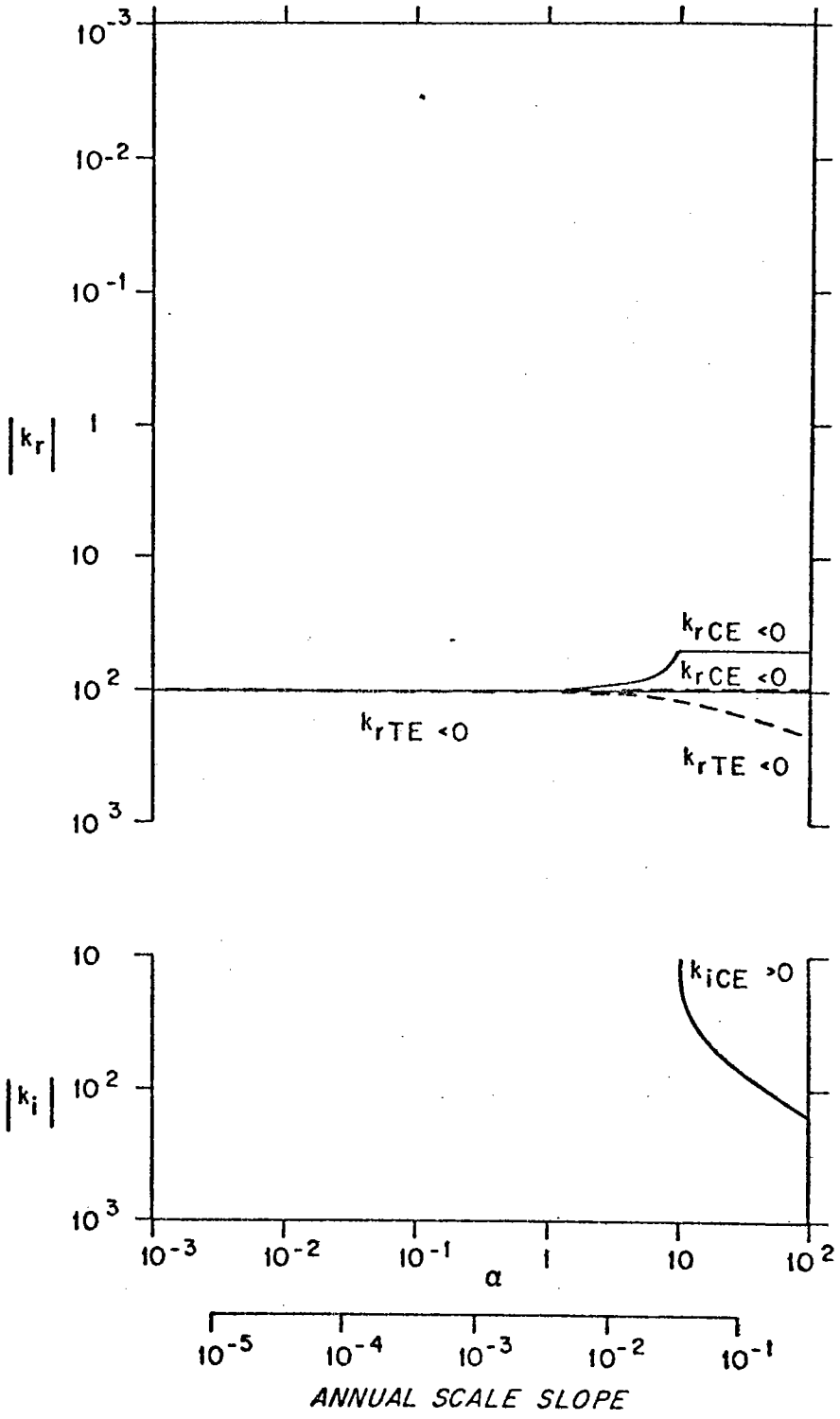

Figure 3.B-2b. Wavenumbers of short waves for annual scale.

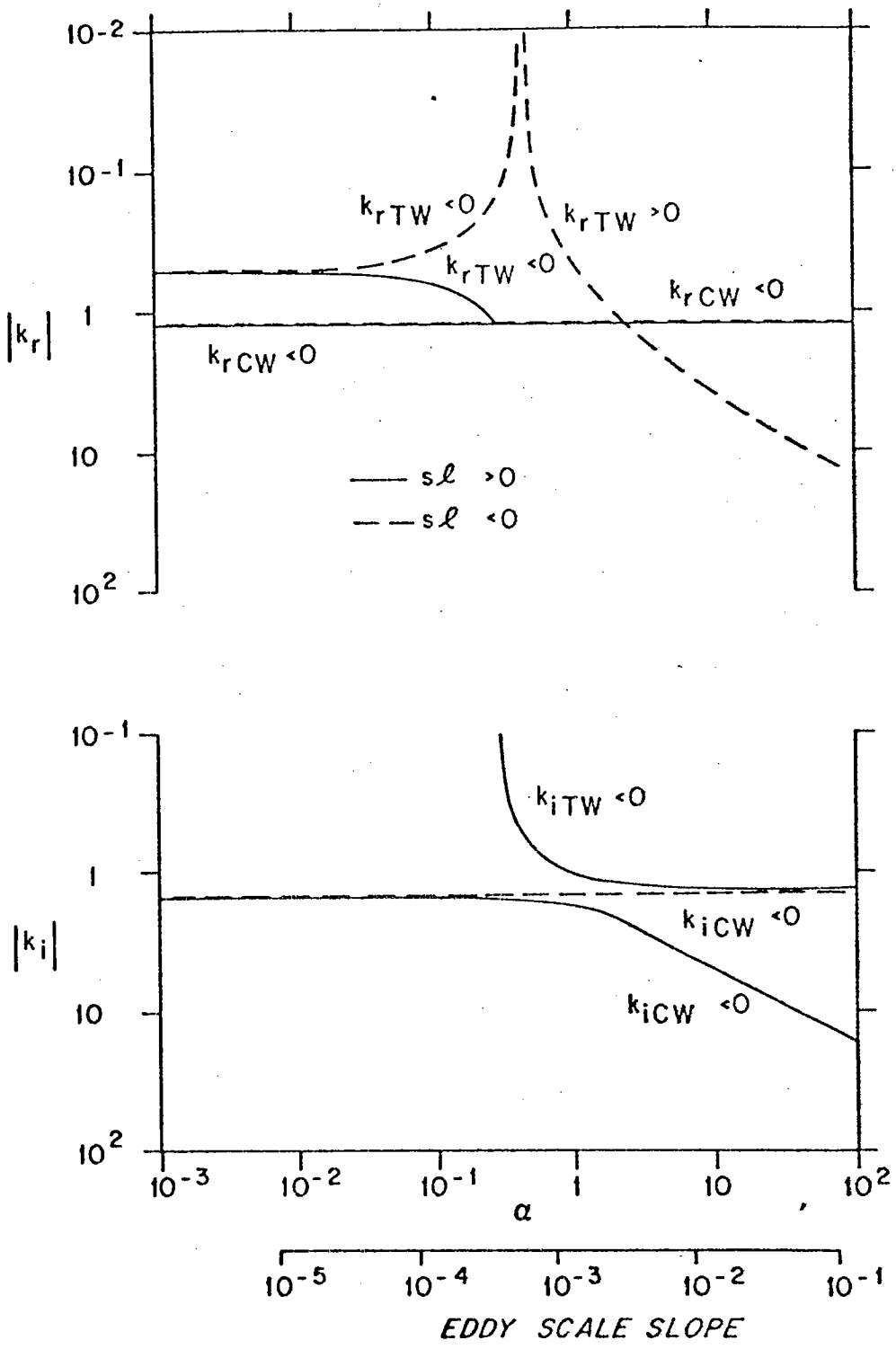

Figure 3.B-2c. Wavenumbers of long waves for eddy scale.

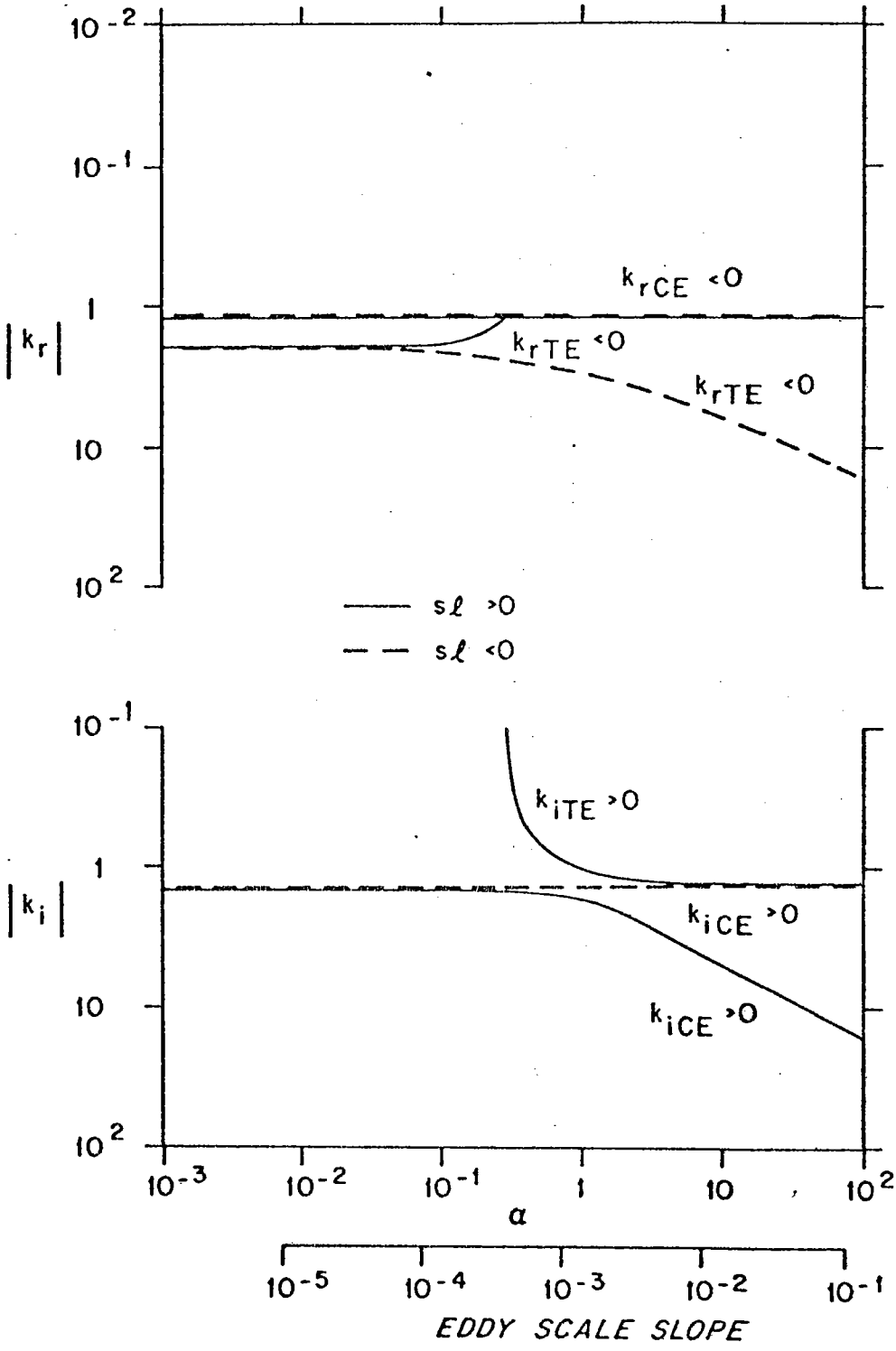

Figure 3.B-2d. Wavenumbers of short waves for eddy scale.

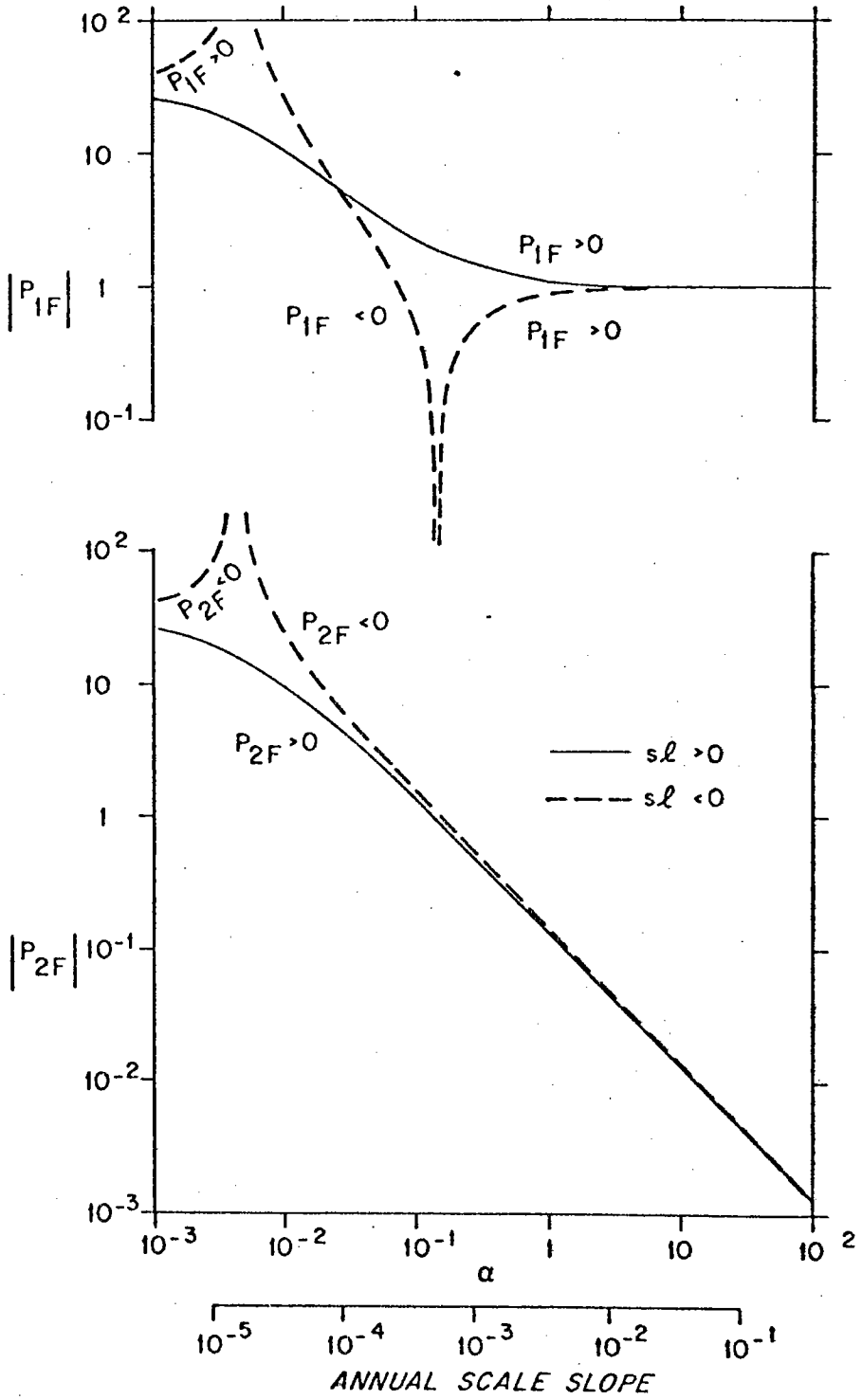

Figure 3.B-3a. Directly forced response, annual scale.

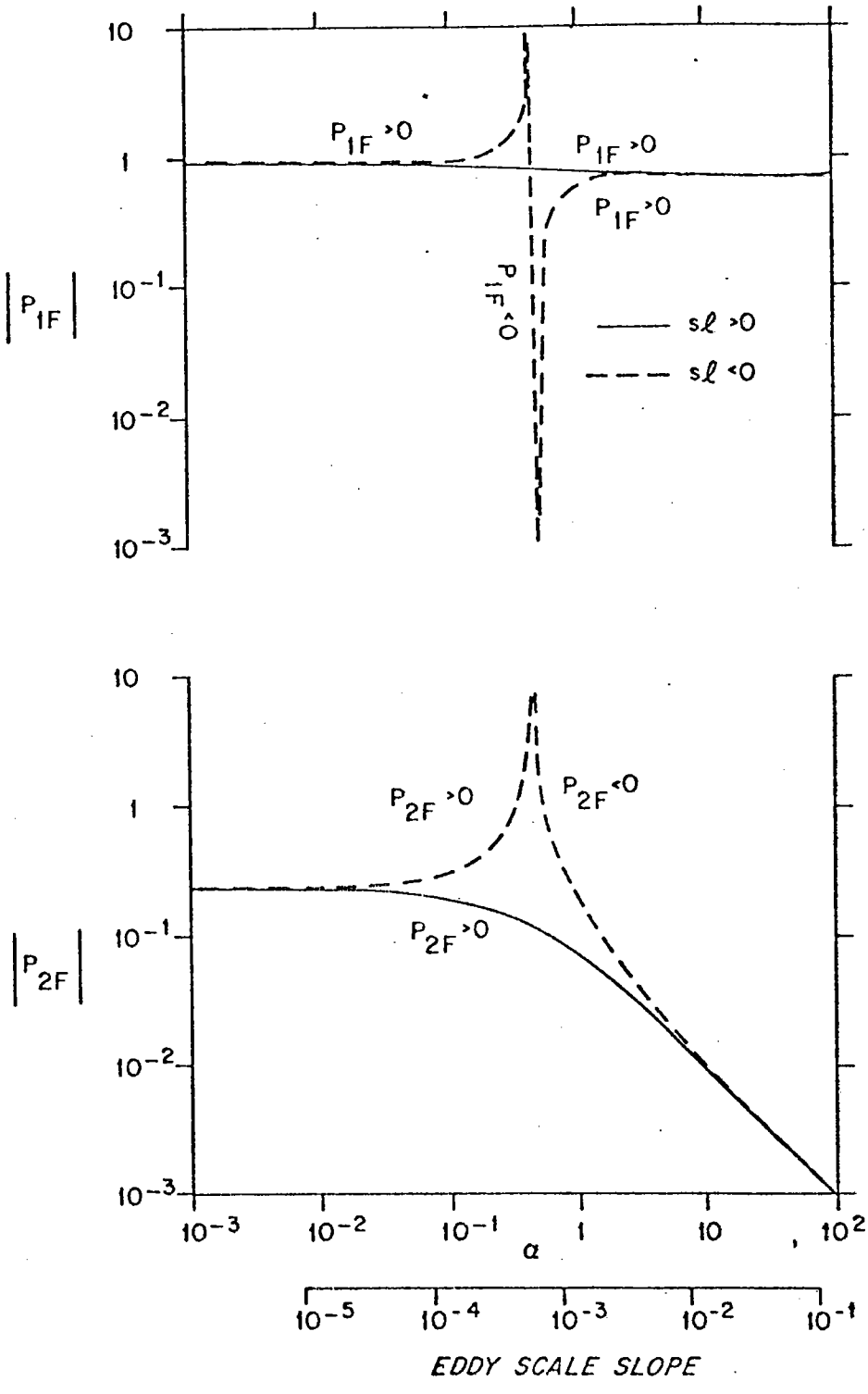

Figure 3.B-3b. Directly forced response, eddy scale.

Since this scale results from a balance between beta and vortex stretching in the upper layer, we will refer to it as the upper layer scale. The vorticity equations (2.A.19a) and (3.B.2) with $A = A_u$, $E_V = E_H = G = 0$, and the ageostrophic slope term omitted since $A_u \sigma << 1$, are

$$-i\left[\lambda^2 p_{1yy} + \left(\frac{\sigma}{b\lambda}\right)^2 p_{1xx}\right] - i f^2 (p_2 - p_1) + p_{1x} = 0 \tag{3.B.10a}$$

$$-ih\left[\lambda^2 p_{2yy} + \left(\frac{\sigma}{b\lambda}\right)^2 p_{2xx}\right] + i f^2 \delta (p_2 - p_1) + h p_{2x} + f s \alpha p_{2y} = 0 \tag{3.B.10b}$$

All the terms involving the slope parameter α are in the second equation. If $p_2 << p_1$, then these terms are unimportant for the system as a whole and the zonal scale of the motion is insensitive to the magnitude of the slope.

The first two terms in each equation, the relative vorticity terms, are both about .4 for eddy scales. Although they do not invalidate the $A = A_u$ scaling, they do dominate the dynamics by preventing the upper layer wave

from propagating zonally. At annual scales, on the other hand, these terms are very small ($O(10^{-2})$) and can be neglected leaving

$$-if^2(p_2-p_1)+p_{1x}=0 \qquad \text{(3.B.11a)}$$

$$if^2\delta(p_2-p_1)+hp_{2x}+f\alpha Sp_{2y}=0 \qquad \text{(3.B.11b)}$$

Although this system with its nonconstant coefficients is too difficult to solve in general, it is possible to final approximate solutions by expanding the dependent variables in powers of α if $\alpha<<1$ or in α^{-1} if $\alpha>>1$. In the first case we find modifications of the baroclinic long wave by small slopes, and in the second case we find the structure of the upper layer wave over steep slopes. In the second case the variation of $h=1+b\alpha Sx$ may be O(1); there is only a weak restriction that h must not get too small.

If $\alpha<<1$ we may assume a solution of (3.B.11) of the form

$$p_1 = \exp i\left[\phi^\circ(x,y) + \alpha\,\phi'(x,y) + \ldots\right]$$
$$p_2 = \left[p_2^\circ(\alpha x, y) + \alpha\, p_2'(\alpha x, y) + \ldots\right] p_1. \qquad \text{(3.B.12)}$$

Substitution in (3.B.11) yields to $O(\alpha)$:

$$O(\alpha^\circ): \quad -f^2(p_2^\circ - 1) + \phi_x^\circ = 0 \qquad \text{(3.B.13a)}$$

$$\delta f^2(p_2^\circ - 1) + h\, p_2^\circ\, \phi_x^\circ = 0 \qquad \text{(3.B.13b)}$$

$$O(\alpha'): \quad -f^2 p_2' + \phi_x' = 0 \qquad \text{(3.B.13c)}$$

$$h\left[-i\,p_{2\alpha x}^\circ + (p_2'\,\phi_x^\circ + p_2^\circ\,\phi_x')\right] + \delta f^2 p_2' + f s\, p_2^\circ\, \phi_y^\circ = 0 \qquad \text{(3.B.13d)}$$

The lowest order solution is

$$p_2^\circ = -\frac{\delta}{h}$$
$$\phi^\circ = -f^2 \int_{x_0}^{x} \left(1 + \frac{\delta}{h}\right) dx + g(y) \qquad \text{(3.B.14)}$$

This is just the ordinary baroclinic mode with the local value of the lower layer thickness determining the local ratio of upper to lower layer pressure. Explicit effects of slope are found in the $O(\alpha)$ terms:

$$p_2' = -(if^2)^{-1}(\delta+4)^{-1}\, s\, p_2^0\,(b - if\,\phi_y^0)$$

$$\phi' = f^2 \int_{x_0}^{x} p_2'\, dx. \qquad (3.B.15)$$

These $O(\alpha)$ corrections contain three parts.

First, if one sets $g(y) = ly$ (so that the lowest order meridional dependence is e^{ily}) and takes the lowest order terms in an expansion in b, the result is

$$p_2' \sim \frac{-\delta s l}{1+\delta} + \ldots \qquad (3.B.16a)$$

$$\phi' \sim \frac{-\delta s l}{1+\delta}(x - x_0) + \ldots \qquad (3.B.16b)$$

These are the $O(\alpha)$ corrections to the baroclinic plane wave. Equation (3.B.16a), which matches (3.B.6), gives the lower layer enhancement for $sl > 0$ and the reverse for $sl < 0$. Along with lower layer enhancement (diminution) goes an increase (decrease) in zonal wavenumber.

Second, there is a contribution to p_2' from the integral in ϕ_y^0:

$$p_2' \sim 2sb\,\frac{\delta}{4}\int_{x_0}^{x}\left(1+\frac{\delta}{4}\right) dx + \ldots \qquad (3.B.17)$$

This is due to the refraction of the wave by the variation in f. Refraction tilts the lines of constant phase relative

to the slope, adding a positive meridional component to the local wavenumber as the wave propagates west. The contribution of (3.B.17) is then just a correction to (3.B.16) due to the altered meridional wavenumber. It is the secularity of this term that limits the range of α and therefore of h over which the expansion is valid. The (3.B.17) correction and the variation of h are both $O(\alpha b x)$.

Third, there is an imaginary term in (3.B.15):

$$p_2' \sim \frac{-i s \delta b}{f^2 h (\delta + h)} + \dots$$
$$\phi' \sim -i s \delta b \int_{x_0}^{x} \frac{dx}{h (\delta + h)} + \dots \qquad (3.B.18)$$

This term describes the upslope decay of the upper layer pressure as the upper layer does work on the lower layer to increase the relative velocity of the latter, as required by (3.B.14). For a wave propagating downslope the process is reversed. The lower layer decelerates downslope as the upper layer accelerates.

If the slope is large, $\alpha >> 1$, a solution of the form

$$p_1 = \exp i\left[\phi^0(x,y) + \alpha^{-1}\phi'(x,y) + \dots\right]$$
$$p_2 = \left(\alpha^{-1} p_2' + \alpha^{-2} p_2^2 + \dots\right) p_1 \qquad (3.B.19)$$

is appropriate. Substitution in (3.B.11) gives, to $O(\alpha^{-1})$

$$\begin{aligned} O(\alpha^0): &\quad f^2 + \phi^0_x = 0 \\ O(\alpha^{-1}): &\quad -f^2 p_2' + \phi'_x = 0 \\ &\quad -\delta f^2 + fs\left(p_2' \phi^0_y - i p_{2y}'\right) = 0 \end{aligned} \tag{3.B.20}$$

The lowest order solution is a wave confined to the upper layer with phase

$$\phi^0 = -f^2 x + g(y) \tag{3.B.21}$$

The $O(\alpha^{-1})$ corrections are

$$p_2' = \frac{i\delta}{s} e^{-i\phi^0} \int f e^{i\phi^0} dy \tag{3.B.22a}$$

$$\phi' = f^2 \int p_2' dx \tag{3.B.22b}$$

The integrals are difficult to evaluate exactly so we will let $g(y) = \ell y$, expand in b, and neglect $O(b^2)$ to get

$$p_2' = \frac{\delta}{s\ell}\left(f + \frac{2bx}{\ell} + \frac{bi}{\ell}\right) + O(b^2) \tag{3.B.23a}$$

$$\phi' = \frac{\delta}{s\ell}\left(fx + \frac{b}{\ell}(x^2 - x_0^2) + \frac{ibx}{\ell}\right) + O(b^2) \tag{3.B.23b}$$

The first term in (3.B.23a) is, except for the factor of f, the same as the lower layer pressure found in the plane wave analysis for large α. Note the usual dependence on the sign of $s\ell$; upper and lower layers are in phase if $s\ell > 0$, opposed if $s\ell < 0$. The second term is the correction to the first due to the alteration of the local meridional wavenumber by diffraction. The third term is imaginary, hence $\pi/2$ out of phase with the other terms, and comes from the factor of f inside the integral in (3.B.22a). It produces an imaginary contribution to ϕ' which gives growing behavior upslope and decaying behavior downslope. This is the opposite of the behavior in the small α expansion. Here, p_2' is independent of h; instead of a decrease in p_1 and an increase in p_2 as h decreases, p_2 stays the same and p_1 increases. Energy is transferred from the lower to the upper layer.

b. Long lower layer waves

The upper layer waves we have been considering are so called because their zonal scale is determined by the upper layer vorticity balance and is independent of the slope. In contrast, there is a set of motions for which the zonal scale is determined by the lower layer vorticity balance and for which the slope is critical. For small slopes these motions are essentially barotropic and for large slopes they are highly concentrated in the lower layer. For convenience they may all be referred to as lower layer waves.

For very small slopes, $\gamma \ll \sigma$, the barotropic long wave scale $A_{TW} \equiv b/\sigma$ is appropriate and the effect of slope is small and uninteresting. However, when $\gamma \gtrsim \sigma$, a new and important scale becomes dominant. This scale is $A_G = b/\gamma$ and results from a balance between beta and slope terms. In the low frequency limit, lower layer flow in quasi-steady along geostrophic contours (hence the subscript G) defined by constant f/h if the slope is large or $f/(h+\delta)$ if the slope is small. As slope increases, A_G decreases until $A_G \simeq A_{TE} \equiv \sigma/b$, the short wave scale. For still larger slopes, both the long waves and the short waves are replaced by motions with a characteristic scale $A_S \equiv (\sigma/\gamma)^{1/2}$

For our present investigation the most important part of this progression of scales is that of the geostrophic contour scale, A_G. With $A = A_G$ and $E_H = E_V = G = 0$, (2.A.19a) and (3.B.2) become

$$-i\left(\frac{\sigma}{\gamma} p_{1yy} + \frac{\sigma\gamma}{b^2} p_{1xx}\right) - i f^2 \alpha^{-1}(p_2 - p_1) + p_{1x} = 0 \qquad (3.B.24a)$$

$$-ih\left(\frac{\sigma}{\gamma} p_{2yy} + \frac{\sigma\gamma}{b^2} p_{2xx}\right) - is\sigma\frac{\gamma}{b} p_{2x} + i\delta\alpha^{-1} f^2 (p_2 - p_1) + h p_{2x} + f s p_{2y} = 0 \qquad (3.B.24b)$$

This scale is appropriate so long as both of the relative vorticity terms are less than unity. For eddy scales this requires slopes between 3×10^{-3} and 5×10^{-4}, so the

A_G scale prevails only over a narrow range of small slopes. Even there it is evident that the relative vorticity terms are not generally negligible. For annual scales on the other hand, the range of slopes for which A_G prevails is wide: from 10^{-6} to over 10^{-1}.

Over most of this range both relative vorticity terms are small. Since $b < 1$, the ageostrophic slope term is smaller than the p_{xx} vorticity term and will therefore be neglected. Then (3.B.24a,b) reduce to

$$-i\alpha^{-1} f^2 (p_2 - p_1) + p_{1x} = 0 \qquad \text{(3.B.25a)}$$

$$i\delta\alpha^{-1} f^2 (p_2 - p_1) + h p_{2x} + fs p_{2y} = 0 \qquad \text{(3.B.25b)}$$

These are the same, except for the scaling, as the upper layer wave equations (3.B.11a,b). The difference in scaling emphasizes the dynamical differences between the two types of motion so long as α is either large or small. When $\alpha \approx 1$ the two sets of equations are identical and the distinction between upper layer waves and lower layer waves is lost.

As in the case of the upper layer waves, (3.B.25a,b) are not easily solvable as they stand. If the coefficients $h = 1 + sbx$ and $f = 1 + by$ are approximated by constants, the results are essentially those of the earlier plane wave analysis. Note that the variation of both coefficients is

$O(b)$, so if the finite variation of one is taken into account, that of the other must be included as well. The effects of the variable coefficients can be calculated in the limiting cases of small and large α by using α and α^{-1}, respectively, as expansion parameters.

When $\alpha << 1$ (the slope is small), solutions to (3.B.25) can be sought in the form

$$p_2 = \exp i\left[\phi^\circ(x,y) + \alpha\,\phi'(x,y) + \ldots\right]$$
$$p_1 = \left[p_1^\circ(x,y) + \alpha\, p_1'(x,y) + \ldots\right] p_2 \qquad \text{(3.B.26)}$$

Substitution in (3.B.25) gives the immediate result

$$p_1^\circ = 1 \qquad \text{(3.B.27)}$$

and the sequence of equations

$$(\delta+h)\,\phi^\circ_x + fs\,\phi^\circ_y = 0 \qquad \text{(3.B.28a)}$$

$$f^2 p_1' + \phi^\circ_x = 0 \qquad \text{(3.B.28b)}$$

$$(\delta+h)\,\phi'_x + fs\,\phi'_y + \delta\left(p_1'\phi^\circ_x - i\,p_{1x}'\right) = 0 \qquad \text{(3.B.28c)}$$

The lowest order equations, (3.B.27) and (3.B.28), specify that the lowest order pressure is independent of depth and constant

along geostrophic contours based on the total depth, that is contours of constant $f/(\delta+h)$. Since this barotropic motion has a component perpendicular to the slope, there is a vertical velocity at the bottom which decreases linearly to zero at the surface. The vertical velocity moves the interface, producing slopes and therefore thermal wind. This $O(\alpha)$ shear produced by the $O(1)$ barotropic flow is specified in (3.B.28b). As we have seen, the shear can augment flow in either the upper layer or the lower, depending on the product of the signs of the slope and the meridional phase propagation. If upper layer flow is enhanced, lower layer flow is reduced, and therefore the effect of the slope on the vertically integrated vorticity balance is also reduced. Then, instead of adhering strictly to geostrophic contours, the flow is along lines a bit closer to latitude lines. If it is the lower layer flow that is enhanced, the integrated effect of the slope is strengthened. Then the flow must follow lines more nearly parallel to the geostrophic contours of the lower layer alone, lines of constant f/h. These effects are described by (3.B.28c)

Equations (3.B.28a-c) can be solved exactly. It is helpful to replace the coordinates (x, y) by new coordinates (ζ, ξ) defined by

$$\zeta = x \tag{3.B.29a}$$

$$\xi = \frac{f}{b(\delta+h)} \tag{3.B.29b}$$

Let $\phi^\circ = \ell y$ and $h = 1$ at $x = 0$, so the lowest order pressure goes as $e^{i\ell y}$ at $x = 0$. With this initial condition the solutions of (3.B.30a,b) and (3.B.28b) are

$$\phi^\circ = \ell\left[\xi(\delta+1) - b^{-1}\right] = \frac{\ell}{b}\left[f\,\frac{\delta+1}{\delta+h} - 1\right] \tag{3.B.31a}$$

$$\phi' = \frac{\delta\ell s}{4b}(\delta+1)(\delta+h)^{-4}\left[2\xi^{-1}i - \ell(\delta+1)\right] = \frac{\delta\ell s}{4b}(\delta+1)(\delta+h)^{-4}\left[2\frac{b}{f}(\delta+h)i - \ell(\delta+1)\right] \tag{3.B.31b}$$

$$p_1' = \frac{\ell s}{b}(\delta+1)(\delta+h)^{-3}\xi^{-1} = \frac{\ell s}{f}(\delta+1)(\delta+h)^{-2} \tag{3.B.31c}$$

The solution can more easily be visualized if the phases are expressed locally as linear functions of x and y, so the solution takes a local $e^{i\ell y}e^{ikx}$ form:

$$\phi^\circ \simeq \phi^\circ(x_0,y_0) + \frac{\ell(\delta+1)}{\delta+h}(y-y_0) - \frac{\ell s f(\delta+1)}{(\delta+h)^2}(x-x_0) \tag{3.B.32a}$$

$$\phi' \simeq \phi'(x_0,y_0) + \delta\ell s^2(\delta+1)^2(\delta+h)^{-5}(x-x_0) - \frac{ib\delta\ell s}{2f^2}(\delta+1)(\delta+h)^{-4}\cdot \left[3sf(x-x_0) + (\delta+h)(y-y_0)\right] \tag{3.B.32b}$$

where h and f are to be evaluated at (x_0, y_0). The results of our earlier plane wave analysis can be obtained from these expressions by setting $b = 0$ so that $h = f = 1$. Note that this eliminates the imaginary part of ϕ', which is $O(b)$. This term is required only when the finite variations of f and h cause finite variations in the ratio of p_1 to p_2. The primary effect of the finite variation of f and h is geometric rather than dynamic. That is, the flow is quasi-steady in either case, but the streamlines are parallel if $h = f = 1$, and have slopes that decrease towards the equator if h and f vary. This variation of slope of the geostrophic contours produces a convergence of contours in the upslope direction and a consequent alteration of meridional scale.

When $\alpha >> 1$ (the slope is large) all $O(1)$ flow in the lower layer wave mode is in the lower layer, and solutions to (3.B.25) can be found in the form

$$p_2 = \exp i\left(\phi^\circ(x,y) + \alpha^{-1}\phi'(x,y) + \ldots\right)$$

$$p_1 = \left(\alpha^{-1}p_1'(x,y) + \alpha^{-2}p_1^2(x,y) + \ldots\right)p_2 \qquad \text{(3.B.33)}$$

Substitution in (3.B.25) gives

$$h\phi^\circ_x + fs\phi^\circ_y = 0 \qquad \text{(3.B.34a)}$$

$$p_{1x}' + i\phi_x^0 p_1' - if^2 = 0 \qquad (3.B.34b)$$

$$h\phi_x' + fs\phi_y' + \delta f^2 = 0 \qquad (3.B.34c)$$

The first equation states that the lowest order flow is along the geostrophic contours of the lower layer, contours of constant f/h. In the second equation, an upper layer meridional flow of $O(\alpha^{-1})$ is needed to balance the upper layer stretching due to the $O(1)$ lower layer flow. In the third equation, the stretching term in the lower layer due to the $O(1)$ lower layer flow produces $O(\alpha^{-1})$ flow across geostrophic contours.

Equations (3.B.34) are similar to (3.B.28) and can also be simplified by a change of coordinates. Here, however, define

$$\zeta = x$$
$$\xi = \frac{f}{bh} \qquad (3.B.35)$$

so that ξ now labels geostrophic contours of the lower layer. Then (3.B.34a,c) become

$$\phi_\xi^0 = 0 \qquad (3.B.36a)$$

$$\phi_\xi' = -\delta(bh\xi)^2 \qquad (3.B.36b)$$

Again requiring $\phi^0 = \ell y$ and $h = 1$ at $x = 0$ leads to the results

$$\phi^0 = \ell\left(\xi - b^{-1}\right) = \frac{\ell}{b}\left(\frac{f}{h} - 1\right) \tag{3.B.37a}$$

$$\phi' = -\frac{\delta b}{2s}\xi^2 h^2 = -\frac{\delta}{2sb} f^2 \tag{3.B.37b}$$

$$p_1' = i f^2 e^{\frac{-i\ell f}{bh}} \int e^{\frac{i\ell f}{bh}} dx \tag{3.B.37c}$$

For small b the leading behavior of this last expression is

$$p_1' \simeq \frac{-h^2 f}{\ell s}\left[1 - 2i\frac{bh}{\ell f} + O(b^2)\right] \tag{3.B.38}$$

The effects of finite variation of f and h here are essentially the same as in the solution for small α. Again the major effect is to make the geostrophic contours converge upslope. A minor difference between the small and large α cases is that for large α the phase correction, ϕ', is real and p_1' is complex, while the reverse is true for small α.

As the slope increases and the scale of lower layer motion decreases, the relative vorticity term grows until it can no longer be neglected. Simultaneously the layers become

increasingly decoupled, so let us consider the case $\alpha^{-1} \ll \gamma\sigma/b^2 \ll 1$. In this limit the coupling between layers is negligible, so we need work only with an equation for the lower layer pressure. Deviations from simple flow along geostrophic contours are caused by the p_{xx} relative vorticity term which is of order $\varepsilon \equiv \gamma\sigma/b^2$, a small parameter in powers of which the solution can be expanded. Since we are now concerned with rather small zonal scales, bottom friction may be significant and will be included in the dynamics. Likewise, the ageostrophic slope term must now be included.

Under these conditions and with $A = A_G$ and $E_H = G = 0$, (3.B.2) becomes approximately

$$p_{2x} + \frac{f}{h} S p_{2y} + \varepsilon \left[\left(-i + F_B \frac{f^{1/2}}{h} \right) p_{2xx} - i \frac{bS}{h} p_{2x} \right] = 0 \qquad (3.B.39)$$

where $F_B \equiv \frac{\delta}{\sigma} \left(\frac{E_V}{2} \right)^{1/2}$ is a bottom friction parameter. If a solution of the form

$$p_2 = \exp i \left(\phi^0 + \varepsilon \phi' + \ldots \right) \qquad (3.B.40)$$

is substituted we see that to lowest order the pressure is constant along geostrophic contours. As in the expansion in α^{-1} , the coordinate change (3.B.35) is helpful and leads to (3.B.36a) for ϕ^0 . If we again pick (3.B.37) as the lowest

order solution and substitute it in the $O(\varepsilon)$ balance of (3.B.39), we find

$$\phi'_\xi = \ell s^2 b^2 \xi \left[h^{-2}(i - \ell\xi) + i F_B b^{1/2} \xi^{1/2} h^{-5/2} (2i - \ell\xi) \right] \qquad (3.B.41)$$

The effect of the ageostrophic slope term in this equation is solely to reduce by half the first of the four terms on the right hand side. This imaginary part of ϕ'_ξ leads to growth of p_2 to the west along geostrophic contours if $\ell > 0$ and to the east if $\ell < 0$. The function of this term is to produce a contribution to u_2 that cancels the ageostrophic $O(\varepsilon)$ contribution from ϕ°. The result is that in spite of the substantial ageostrophy of u_2, in the absence of friction p_2 and u_2 are exactly $\pi/2$ radians out of phase to $O(\varepsilon)$, so energy flux must arise from higher order corrections. The imaginary term in (3.B.41) due to friction always leads to decay of p_2 to the west, consistent with the westward component of group velocity of the wave.

Integration of (3.B.41) gives

$$\phi' = -s\ell f h^{-2}\left(i - \frac{\ell f}{hb}\right) + \frac{2}{3} F_B \ell s f^{3/2} h^{-3}\left(2 + \frac{i\ell f}{hb}\right) \qquad (3.B.42)$$

Differentiating to find the $O(\varepsilon)$ correction to the local zonal wavenumber gives

$$\frac{\partial \phi'}{\partial x} = s^2 l f h^{-3} \left[(2ib - 3lfh^{-1}) - 4F_B f^{1/2} h^{-1} (b + \tfrac{1}{3} i l f h^{-1}) \right] \tag{3.13.43}$$

The first real term, due to the p_{xx} vorticity term, is always positive, so the zonal scale is decreased if $ls > 0$ and increased if $ls < 0$. Lines of constant phase are rotated counterclockwise from geostrophic contours if $l > 0$, clockwise if $l < 0$.

c. Large slopes and short waves

As the slope increases, we have seen that the p_{xx} relative vorticity term gains importance; but it is this term that is also crucial in short wave dynamics. Therefore, it is appropriate to consider short waves and steep topography together.

Until the topography gets very steep, that is, until A_α approaches A_{TW} , the only effect of slope on annual short wave dynamics is to change the vertical mode structure. As we have seen in the plane wave analysis, the vertical mode structure depends only on the slope, and not on whether the motion consists of short or of long waves. The reason slopes have little effect on short wave scales and dynamics is that

the flow in short waves is predominantly meridional, along the slope; it is only the component of flow normal to the slope that produces vorticity changes.

With $G=0$ and $A=A_{TW}$, (3.B.2) becomes approximately

$$\begin{aligned}&\left(-ih+F_B f^{1/2}\right)p_{2xx}\\&+i\delta\alpha^{-1}\varepsilon f^2(p_2-p_1)\\&+(h-i\varepsilon bs)p_{2x}+f\varepsilon s p_{2y}\\&=F_H\left(h p_{2xxxx}+\varepsilon bs p_{2xxx}\right)\end{aligned}\qquad(3.B.44)$$

where $F_H \equiv b^2 E_H/\sigma^3$ is the horizontal friction parameter and $h=1+\varepsilon bsx$. Let us immediately take the limit of large α so that the lower layer can be considered independent of the upper. With this simplification the equation is still too complicated to solve. In particular, the variation of bottom friction with latitude due to the factor of $f^{1/2}$ adds greatly to the difficulty. To make the problem tractable, let us neglect lateral friction entirely and restrict bottom friction to be of $O(\varepsilon)$. We are left with

$$\begin{aligned}&\left(1+i F_B \frac{f^{1/2}}{h}\right)p_{2xx}\\&+(i+b\varepsilon s)p_{2x}+i\varepsilon s\frac{f}{h}p_{2y}=0.\end{aligned}\qquad(3.B.45)$$

A solution of the form

$$p_2 = exp\ i\left(\phi^0 + \varepsilon\phi' + \ldots\right) \tag{3.B.46}$$

can be found with

$$\phi^0 = -x + \ell y \tag{3.B.47a}$$

$$\phi'_x = s\ell\frac{f}{h} + i\left(bs + \frac{F_B}{\varepsilon}\frac{f^{1/2}}{h}\right) \tag{3.B.47b}$$

To lowest order we find, of course, a plane short Rossby wave unaffected by slope. At $O(\varepsilon)$ there are three corrections to the local zonal wavenumber. The first term in (3.B.47b) is due to the slope term and shortens the zonal wavelength if $s\ell > 0$, lengthens it if $s\ell < 0$. The second term comes from the ageostrophic slope term and produces an upslope growth in amplitude such that the product of h and the amplitude is constant to $O(\varepsilon)$. The third term represents the decay to the east produced by bottom friction.

When the slope is so large that $\varepsilon > 1$, a new scale dominates for both long and short waves. A balance between the P_{xx} vorticity term and the slope term leads to the scale $A_s = (\sigma/\gamma)^{1/2}$. With this scale and with $G = 0$,

(3.B.2) is approximately

$$-ih\,p_{2xx} - is(\sigma\gamma)^{1/2}\,p_{2x} + \varepsilon^{-1/2}h\,p_{2x} + fs\,p_{2y} + i\alpha^{-1}\delta f^2(p_2 - p_1) = -\sigma^{-1}\left(\frac{E_v f}{2}\right)^{1/2}\delta\,p_{2xx} + \gamma\sigma^{-2}E_H(h\,p_{2xxx})_x \qquad (3.B.48)$$

with $h = 1 + (\sigma\gamma)^{1/2}\,sx$. If all but the two principle terms are small then the lowest order balance is

$$-ih\,p_{2xx} + fs\,p_{2y} = 0 \qquad (3.B.49)$$

With $h \simeq 1$ and $f \simeq 1$ this has plane wave solutions $p_2 \simeq e^{ikx}e^{ily}$. Note that there are two values of k for each l ; long and short waves concentrated in the lower layer now have the same lowest order balance. Both zonal wavenumbers are imaginary if $ls > 0$, one root giving decay to the west, one decay to the east. If $ls < 0$, both roots are real and the behavior is oscillatory. The other terms in (3.B.48) will of course modify the behavior but the sign of ls remains the most important qualitative factor. Its effect is clearly seen in the plane wave analysis in Figure 3.B-2.

At the large, slow scale of the annual oscillation the A_s scale does not enter until the slope reaches about .13. Since the A_s scale is so small, we may expect lateral friction to be important. Neither the ageostrophic slope term nor the beta term can be neglected, and the scale of variation

of h is comparable to A_S . Under these conditions the plane wave analysis is highly inaccurate and a more complete analysis would be difficult. Fortunately, the major topographic features of the oceans have average slopes smaller than .1, so the A_S scale is not relevant to the large scale aspects of annual oscillations in the oceans.

For smaller meridional scales of motion a smaller slope is required to bring in the A_S scale. The minimum slope occurs at $\varepsilon = 1$; at eddy scales this implies a slope of about 3×10^{-3} , or $\gamma = 10^{-1}$. In this case the plane wave analysis is quite good, since $(\sigma\gamma)^{1/2} \simeq .04$. As the slope increases, the importance of the beta term diminishes while that of the ageostrophic slope term increases. When the slope is .1 both are of O(.2).

d. Forced motion over a slope

We will restrict our attention to zonally uniform forcing and to large scale annual motions. Then the only zonal scale is that of the topography, so if the relative change in lower layer depth, δh , is $O(1)$ then it is appropriate to set $A = \gamma^{-1}$. In the plane wave analysis, with $h = 1$ and $f = 1$, the absence of a zonal scale in the forcing immediately implied that the response was also zonally independent and the value of A arbitrary. Here, however, we must consider the possibility that the zonal variation of the coefficient $h = 1 + S\alpha$ may result in zonal variations in the response.

With friction and the ageostrophic slope term neglected and with $G = e^{ily}$, (2.A.19a) and (3.B.2) become

$$-i\sigma(\gamma^2 p_{1xx} + p_{1yy}) + i\sigma\lambda^{-2}f^2(p_1 - p_2) + b\gamma p_{1x} = \gamma e^{ily} \tag{3.B.50a}$$

$$-i\sigma h(\gamma^2 p_{2xx} + p_{2yy}) - i\sigma\lambda^{-2}f^2\delta(p_1 - p_2) + b\gamma h p_{2x} + \gamma f s p_{2y} = 0 \tag{3.B.50b}$$

Unless $p_1 \simeq p_2$, the vortex stretching terms are much larger than the p_{yy} vorticity terms so the latter can be neglected. Then the only term with coefficients varying in x involve differentiation with respect to x, so zonally independent solutions may be found:

$$p_2 \simeq \delta(s\gamma)^{-1}\int f^{-1}e^{ily}\,dy \tag{3.B.51a}$$

$$p_1 \simeq p_2 + (i\sigma\lambda^{-2}f^2)^{-1}e^{ily} \tag{3.B.51b}$$

In the upper layer, the torque applied by the forcing is balanced by vortex stretching. In the lower layer, stretching is balanced by zonal motion up or down the slope. In other words, fluid columns in the lower layer do not change their length but just slide up and down the slope as the

interface is moved up and down. The steeper the slope, the less the columns have to move to conserve their length. As we see in Fig. 2.B.3a for $\alpha > 1$ the lower layer flow is relatively small, so the geostrophic shear associated with the interface displacement results in an upper layer flow that is insensitive to the slope. For $\alpha < 1$, the lower layer flow becomes comparable to the upper layer flow, and the same geostrophic shear may result in any of a range of upper layer responses depending on the magnitude of the slope and the sign of $s\ell$. If $s\ell < 0$ and $\alpha = \delta + \ell^2\lambda^2$, the upper layer pressure response vanishes entirely, although there is still an Ekman transport in the upper layer, of course. For very small values of α, say $\alpha < .05$, the response becomes largely barotropic, with $p_1 \simeq p_2$. Then the p_{yy} term can no longer be neglected and (3.B.51) is invalid. However, the slope is so small that δh is small for any reasonable topographic feature, and the limit $h \to 1$ used in computing Fig. 2.B.3 is valid.

4. Summary

The vorticity equations in terms of pressure for two-layer flow over a bottom with constant slope in the zonal direction are too complicated to solve in general. In particular, they have coefficients h and f that vary in the

zonal and meridional directions. If the ranges of variation of these coefficients are not too large, the approximation $h = f = 1$ is appropriate. The simplified equations then have free plane wave solutions regardless of the magnitude of the slope. The vertical modal structure and wavenumbers of these solutions are easily found, especially if friction is neglected. They are shown in Figures 2.B.1,2. Similarly, the response to zonally uniform forcing can be found in a simple form, shown in Figure 3.B.3.

Although the vorticity equations with nonconstant coefficients cannot be solved in general, it is possible to find approximate solutions over substantial parts of the parameter range of interest by expanding the solutions and equations in powers of various small parameters. These solutions illuminate the dynamics of the flow by showing which terms in the vorticity equations control the response. They also indicate the quantity and quality of error involved in the simpler plane wave theory.

The conclusion reached by comparing the plane wave theory with the perturbation expansion solutions is that the former accurately determines the scales and general characteristics of the motion even when the actual variations of h and f are $O(1)$. Some significant qualitative features, such as the refraction of baroclinic or upper

layer waves, are lost in the plane wave description. However, this is a small price to pay for the simplicity of the description. It is this simplicity that will allow us in the next section to calculate analytically some effects of topographic features on annual oscillations.

It is perhaps worth noting that the approximation $h = 1$ corresponds to a physically consistent, if unrealizable, model. The model has a flat bottom, so layer depths are constant, but the bottom is porous and acts as a source or sink of lower layer fluid. The strength of the source is proportional to the zonal component of lower layer velocity.

Before proceeding to the calculation of flows over complete topographic features, let us briefly review the characteristics of flow over a constant zonal slope.

The vertical modal structure depends only on the parameters α, δ, and $s\ell$, and is the same for short and long waves. As α increases, the barotropic mode becomes enhanced in the upper (lower) layer if $s\ell > 0$ $(s\ell < 0)$, and the baroclinic mode does the opposite. For $\alpha >> 1$ one mode is almost entirely confined to the upper layer and the second is nearly confined to the lower layer.

The baroclinic long wave for small α and the upper layer long wave for large α are characterized by a balance between upper layer vortex stretching and beta. The slope has little influence other than determining the ratio of the pressures in the two layers.

The barotropic long wave for small α and the lower layer long wave for large α are characterized by a balance between beta and slope terms. The flow is not really wavelike in its dynamics, but is quasi-steady along the appropriate geostrophic contours.

Short waves are characterized by a balance between beta and p_{xx} vorticity change terms. Except for the determination of the vertical structure, slope has little effect until it is so large that the lower layer wave scale approaches the short wave scale. Then the two types of wave become increasingly similar, eventually being distinguished only by the direction of the group velocity if $s\ell < 0$ or by the direction of decay if $s\ell > 0$.

The directly forced response to zonally independent forcing is itself independent of longitude. As long as there is a reasonable slope, larger than about one part in ten thousand, the vertical velocity is constant below the Ekman layer. The response then consists of a lower layer zonal motion sufficient to make the bottom vertical velocity equal to the Ekman pumping, and a vertical motion

of the interface that is also the same as the Ekman pumping. The known lower layer motion and interface slope allow calculation of the geostrophic upper layer motion.

C. Two-dimensional topography

In this section we will use the results of the last section and of Chapter II to improve our model of the response of the mid-latitude ocean to seasonal wind variations. We are concerned not so much with the details of the response as with the major integrated features that determine the western boundary transport. Some questions of interest are: (1) What effect does a slope at the eastern boundary have on the quasi-steady Sverdrup response and on the baroclinic wave generated at the eastern boundary? (2) Is the highly idealized barrier model of Section III-A useful in predicting the effect of a more realistic ridge? (3) What is the effect of a lower, broader ridge such as the Mid-Atlantic Ridge?

1. Method

Topography that varies only in the zonal direction can be modeled as a series of segments each with constant slope. In the region over each segment the flow consists of a directly forced part plus four free waves, as discussed in the previous section. The amplitude of each of the four waves in each region is determined so as to satisfy matching conditions at each junction between regions. There are four matching conditions at each junction; both velocity components must be continuous in each layer. In addition there may be either rigid wall or radiation boundary

conditions to the east and west of the topographic feature.

The procedure of matching solutions at the junctions requires that all the solutions have the same meridional dependence. Therefore we are restricted to use of the plane wave theory obtained by approximating $h = f = 1$. Determination of the complete flow over the topography then requires only the solution of a system of linear algebraic equations in the free wave amplitudes. The solution is easily found for any numerical example with the aid of a computer.

The geostrophic approximation for the velocities is consistent with the plane wave theory, so matching the velocities is equivalent to matching the pressure and its zonal derivative. For any component of the motion, the amplitude of the zonal derivative goes inversely as the zonal scale. The phase of the zonal derivative depends on whether the motion is a propagating wave, a damped wave, or a purely decaying motion. As was shown in the previous section, the plane wave model yields the correct scales and general character of motion even when the actual changes in h and f are substantial. Therefore this model can be expected to give a reasonable indication of the effect of rather large topography even though it is inadequate in its details.

The plane wave analysis as given here neglects friction entirely. However, we know that friction is important for the short waves. Their group velocity is so slow that a small amount of friction will dissipate them within a few wavelengths. A model that depends critically on information carried many short wavelengths by the short waves is therefore unrealistic. The inclusion of either bottom or lateral friction in the plane wave model would result in a considerable increase in complexity, so instead we may use the simple, if unrealistic, Rayleigh friction that was introduced in Section 3.A in the context of the thin barrier model. This form of dissipation has little effect other than to make all the free waves decay. Equation (3.B.4) becomes

$$\mathcal{L} \equiv \left(i\sigma \alpha^{-2} A \right)^{-1} \left(-i\sigma_d \nabla_s^2 + b \frac{\partial}{\partial x} \right) \qquad (3.C.1)$$

and the dispersion relations (3.B.8) become

$$k^2 + \frac{b}{\sigma_d} k + l^2 + \frac{\sigma}{\sigma_d} \alpha^{-2} (1-R) = 0 \qquad (3.C.2a)$$

$$k^2 + \frac{b}{\sigma_d} k + l^2 + \frac{\sigma}{\sigma_d} \alpha^{-2} \left[\delta (1-R^{-1}) + \alpha s l \right] = 0 \qquad (3.C.2b)$$

where

$$\sigma_d \equiv \sigma(1 - id) \qquad (3.C.3)$$

as before.

Calculations of flow over topography were made with d = 0, .1, and .5. Differences among the three cases were at most a few percent in all of the eastern boundary slope calculations, so only the results with d = 0 will be presented. In a few of the ridge calculations dissipation had a moderate but significant effect, so some calculations with d = .5 will be presented for comparison with those with d = 0.

The unimportance of dissipation in most of the calculations is due to the decrease in amplitude of the short waves with increasing width of topography. When the slopes are gentle, the long waves in adjacent regions have comparable scales so only small amplitudes of short waves are needed to match v at the junction. For most of the calculations to be presented, the short wave amplitudes are one to two orders of magnitude smaller than the long wave amplitudes. On the other hand, when slopes are short and steep so that short wave amplitudes are comparable to long wave amplitudes, then the waves are not greatly dissipated within the width of the slope.

2. Eastern boundary

It was shown in Chapter II that the response of the ocean interior to zonally uniform forcing can be calculated as the sum of a directly forced solution and two waves generated at the eastern boundary. Furthermore, we have seen that the presence of a sloping bottom profoundly alters both the directly forced solution and the free waves. The question naturally arises, then, whether the presence of a sloping region at the eastern boundary might significantly affect the response of the ocean interior to large scale annual forcing.

To address this question, consider an ocean basin divided into two regions; a semi-infinite flat bottom region to the west, and a strip with constant bottom slope at the eastern boundary (Figure 3.C.1). The height of the topography as a fraction of the lower layer thickness in the flat region is Δh, and the nondimensional width of the topography is X. Then $\gamma = \Delta h / X$ and α is determined by (3.B.4). For the annual scale motion in which we are interested, $\sigma \lambda^{-2} = 1$ so $\alpha = \gamma$. Since the slope at the eastern boundary is up to the east, the parameter S takes the value -1.

Let superscript S denote variables in the slope region. Absence of a superscript denotes variables in the flat region. Both regions experience the same zonally uniform

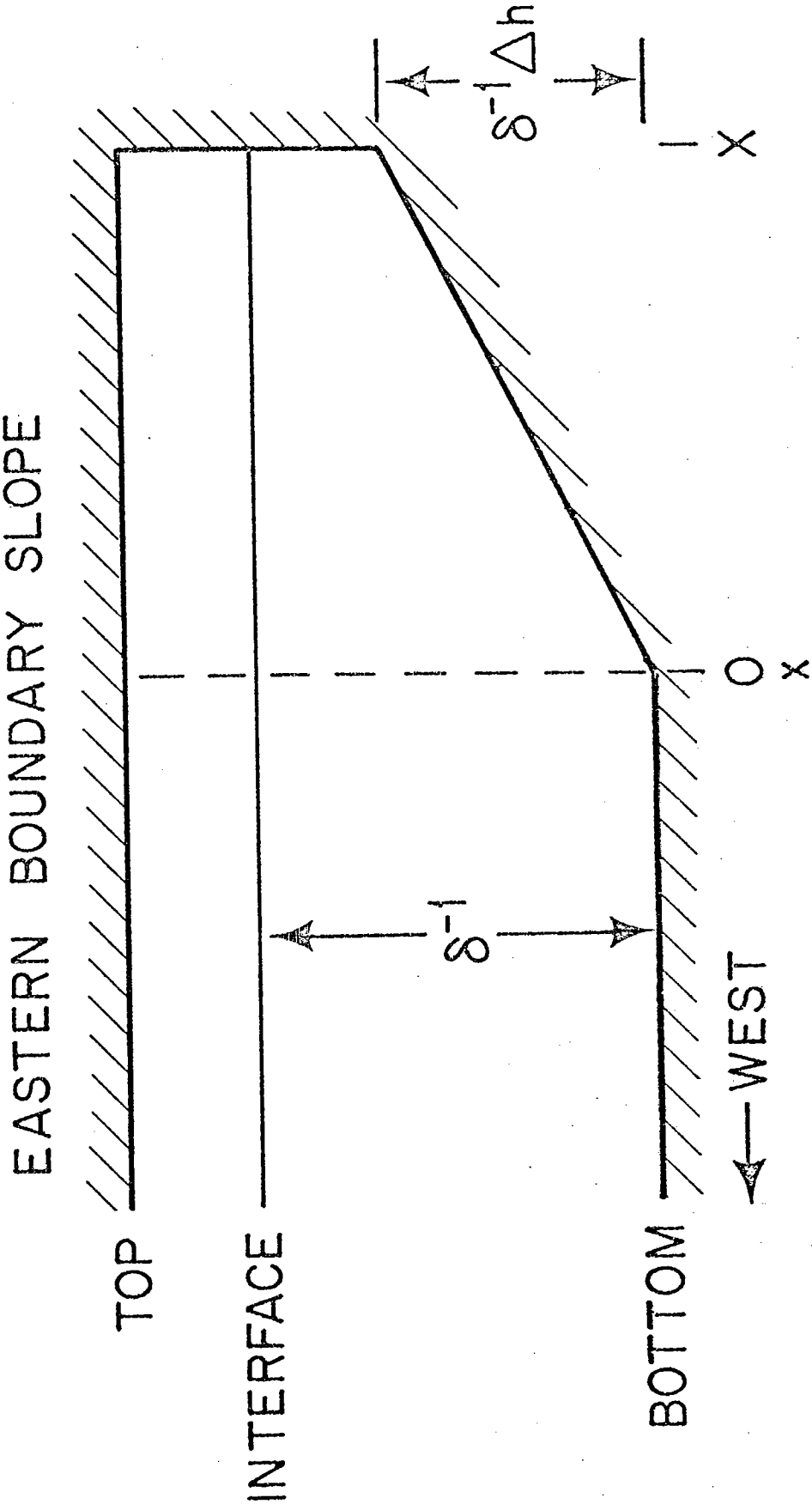

Figure 3.C-1. Eastern boundary slope model.

forcing, $G = e^{ily}$, so the response will also be proportional to e^{ily}. The motion in the slope region consists of the directly forced motion in each layer with amplitudes p^s_{1F} and p^s_{2F} determined by (3.B.9), and four free waves with complex amplitudes p^s_{TW}, p^s_{TE}, p^s_{cW}, and p^s_{cE}. In the flat region the directly forced motion has amplitudes p_{1F} and p_{2F} from (3.B.9) with $\alpha = 0$. There are two free waves, with amplitudes p_{TW} and p_{cW} since the radiation condition in the west eliminates the two waves with eastward group velocity. The vertical structures and zonal wavenumbers of all the waves are determined by (3.B.5) and (3.B.8) with $\alpha = 0$ for the flat region.

The conditions of no flow into the boundary and continuity of velocity at the junction lead to six simultaneous linear equations for the six unknown complex wave amplitudes. In matrix form these become

$$A_{ij} p_j = F_i \qquad (3.C.4)$$

The elements of these matrices are given in Table 3.C-1.

The solution of (3.C.4) in terms of the six pressure amplitudes in p_j is not immediately informative, so we will use it to calculate two indices of the overall effect of the topography. Let the solution of (3.C.4) for the case of zero slope in both regions be denoted by the

Table 3.C-1a

Elements of the matrix A_{ij} where $\chi_{MD} \equiv \exp(ik_{MD}X)$

j \ i	1	2	3	4	5	6
1	1	1	1	1	-1	-1
2	R_T^S	R_T^S	R_C^S	R_C^S	$-R_T$	$-R_C$
3	k_{TW}^S	k_{TE}^S	k_{CW}^S	k_{CE}^S	$-k_{TW}$	$-k_{CW}$
4	$R_T^S k_{TW}^S$	$R_T^S k_{TE}^S$	$R_C^S k_{CW}^S$	$R_C^S k_{CE}^S$	$-R_T k_{TW}$	$-k_C k_{CW}$
5	χ_{TW}^S	χ_{TE}^S	χ_{CW}^S	χ_{CR}^S	0	0
6	$R_T^S \chi_{TW}^S$	$R_T^S \chi_{TE}^S$	$R_C^S \chi_{CW}^S$	$R_C^S \chi_{CR}^S$	0	0

Table 3.C-1b

Elements of the column vectors P_j and F_j

j	P_j	F_j
1	P^S_{TW}	$-P^S_{1F} + P_{1F}$
2	P^S_{TE}	$-P^S_{2F} + P_{2F}$
3	P^S_{CW}	0
4	P^S_{CE}	0
5	P_{TW}	$-P^S_{1F}$
6	P_{CW}	$-P^S_{2F}$

superscript H. Then the ratio of the interior baroclinic wave amplitude with a slope at the eastern boundary to that in the absence of a slope is

$$I_{sc} \equiv \rho_{cw} / \rho_{cw}^{H} \qquad (3.C.5)$$

The ratio of the total barotropic response with a slope to the approximate Sverdrup balance that occurs without topography is

$$I_{ST} \equiv \frac{1 + \frac{\rho_{TW}}{\rho_{FT}} e^{-i k_{TW} x_I}}{1 - e^{-i k_{TW} x_I}} \qquad (3.C.6)$$

where x_I is the distance from the eastern boundary at which the ratio is evaluated. We will take $x_I = 4$, so as to measure the effect of the eastern boundary slope 4000 km west of the boundary.

Equation (3.C.4) was solved, and the indices I_{SC} and I_{ST} were calculated, for numerical examples with Δh = .1, .5, and 1.0 ; with slope widths X = .05, .1, .2, .4, .8, and 1.6; and with meridional wave number ℓ = 1 and -1. The results are given in Table 3.C-2 and Figure 3.C-2.

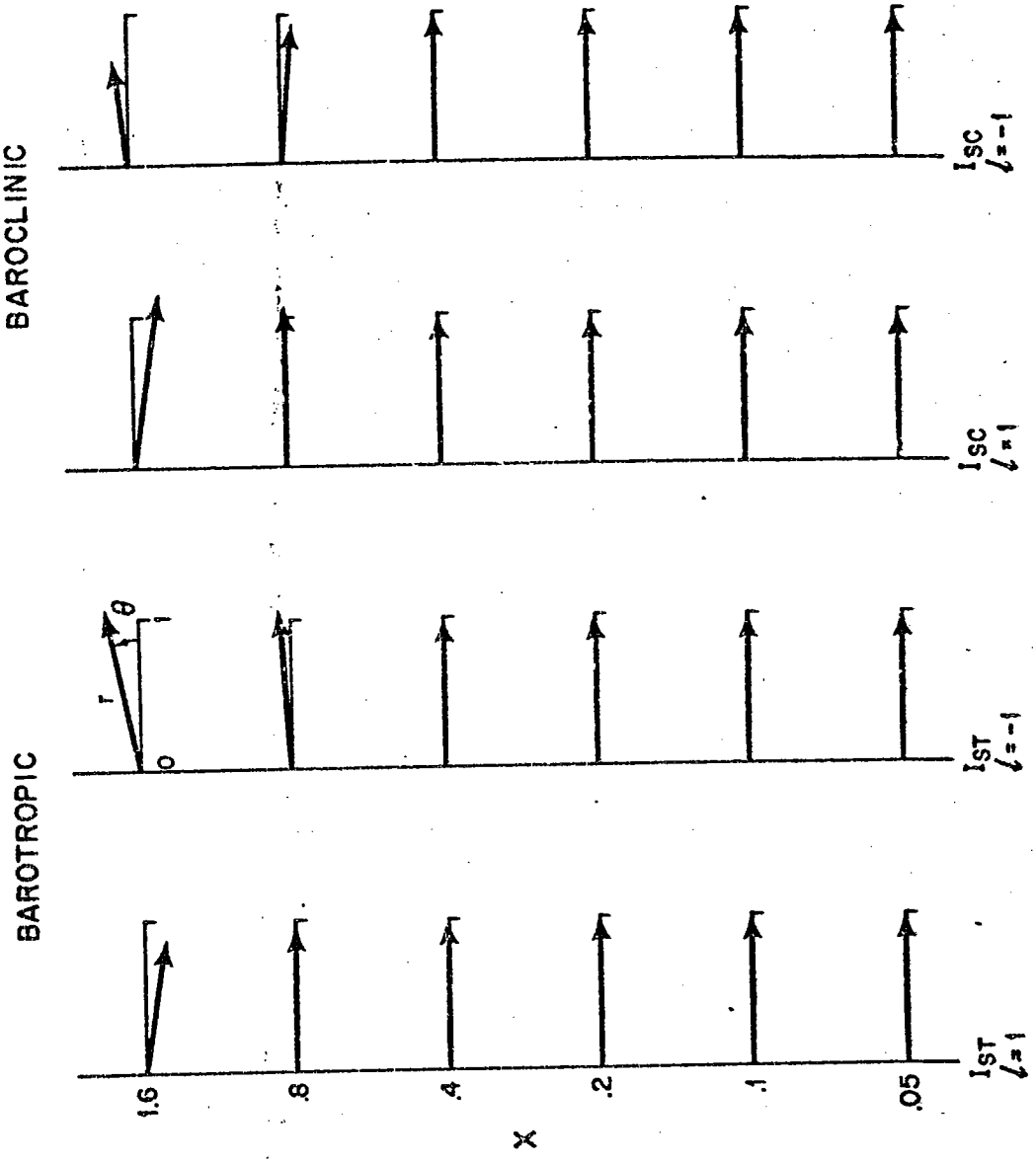

Figure 3.C-2a. Effect of eastern boundary slope with $\Delta h = .5$ (Table 3.C-2b). Complex polar notation, $re^{i\theta}$.

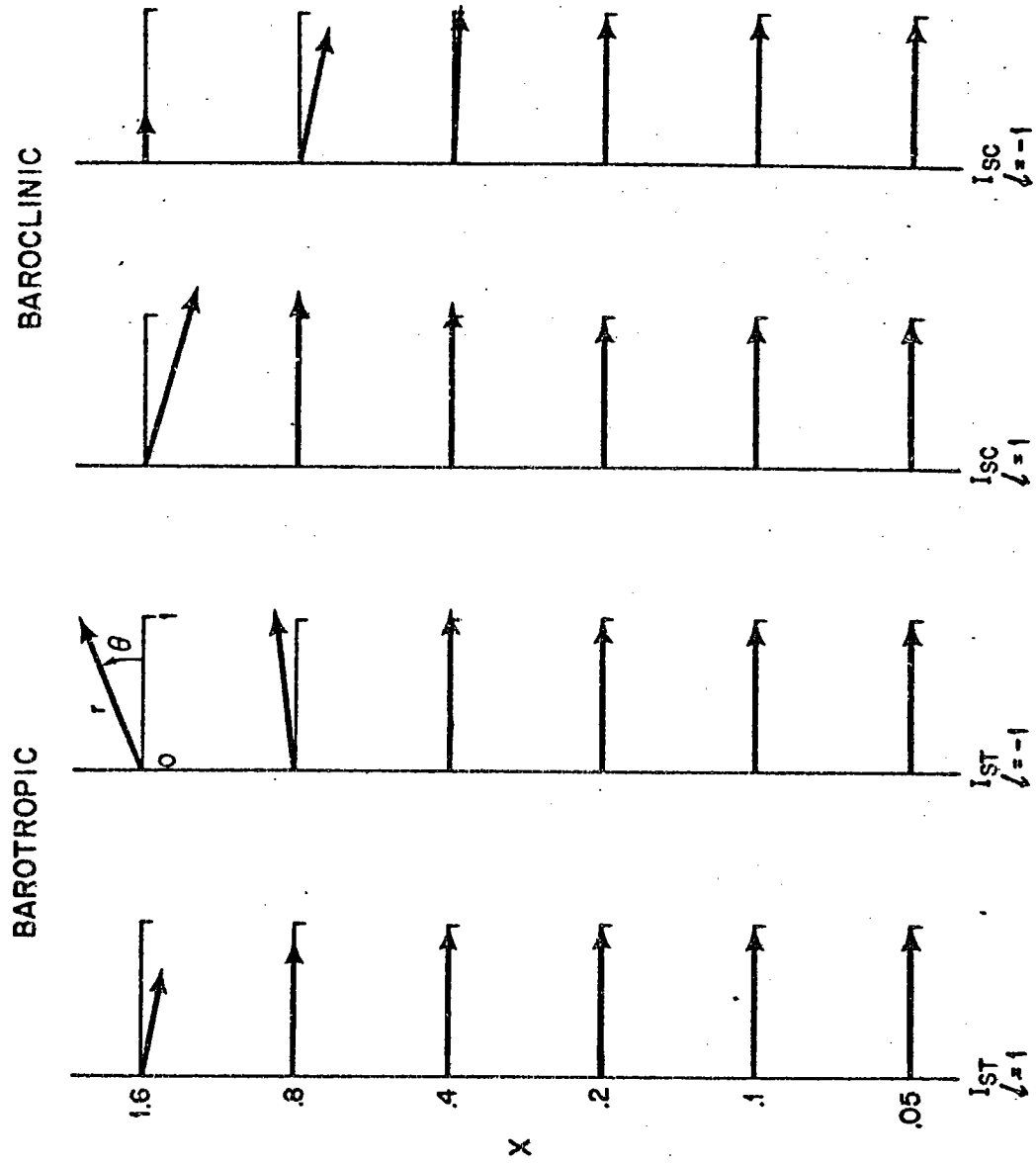

Figure 3.C-2b. Effect of eastern boundary slope with $\Delta h = 1$ (Table 3.C-2c).

Table 3.C-2a

Effect of eastern boundary slope with $\Delta h = .1$. For each value of X, the first row is for $\ell = 1$ and the second is for $\ell = -1$. The indices I_{ST} and I_{SC} are given in complex polar form $re^{i\theta}$ with θ in radians.

	I_{ST}		I_{SC}		$\left\|\frac{dH_2}{dx'}\right\|$	
X	r	θ	r	θ	$\times 10^2$	α
.05	1.000	.00	1.000	.00	.7	2.0
	1.000	-.00	1.000	-.00		
.1	1.000	.00	1.000	.00	.35	1.0
	1.000	-.00	1.000	-.00		
.2	.999	-.00	1.000	.00	.175	.5
	1.001	.00	1.000	-.00		
.4	.996	-.00	1.003	.00	.0875	.25
	1.004	.00	.997	-.01		
.8	.988	-.01	1.019	.01	.0438	.125
	1.012	.01	.982	-.01		
1.6	.976	-.03	1.044	-.03	.0219	.0625
	1.021	.04	.951	.03		

Table 3.C-2b

Effect of eastern boundary slope with $\Delta h = .5$.

	I_{ST}		I_{SC}		$\left\|\frac{dH_2}{dx'}\right\|$	
X	r	θ	r	θ	$\times 10^2$	α
.05	1.000	.00	1.000	.00	3.5	10
	1.000	-.00	1.000	-.00		
.1	.999	.00	1.001	.00	1.75	5
	1.001	.00	1.000	-.00		
.2	.995	.00	1.004	.01	.875	2.5
	1.005	.00	.997	-.01		
.4	.984	.00	1.019	.02	.4375	1.25
	1.015	.01	.994	-.02		
.8	.938	-.01	1.091	.01	.022	.625
	1.046	.05	.919	-.08		
1.6	.856	-.15	1.172	-.16	.011	.312
	1.080	.19	.713	.13		

Table 3.C-2c

Effect of eastern boundary slope with $\Delta h = 1.0$.

	I_{ST}		I_{SC}		$\left\|\frac{dH_2}{dx'}\right\|$	
X	r	θ	r	θ	$\times 10^2$	α
.05	1.000	.00	1.000	.00	7	20
	1.000	.00	1.001	-.00		
.1	.999	.00	1.002	.00	3.5	10
	1.002	.00	1.003	-.00		
.2	.994	.00	1.009	.01	1.75	5
	1.007	.01	1.006	-.01		
.4	.970	.01	1.043	.02	.875	2.5
	1.026	.02	.995	-.06		
.8	.888	.00	1.162	-.01	.4375	1.25
	1.063	.11	.912	-.22		
1.6	.693	-.19	1.234	-.29	.2188	.625
	1.070	.39	.362	-.03		

The most obvious conclusion to be drawn from these results is that a slope at the eastern boundary has little effect on the response of the ocean basin to annual forcing. A slope of 400 km width or less has no appreciable effect in this model. The effect of the 800 km slope is under 10% with $\Delta h = .5$ and under 20% with $\Delta h = 1$. The widest slope has a major effect on both the barotropic and the baroclinic modes with $\Delta h = 1$, but its effect is under 20% when $\Delta h = .5$. The maximum phase change of the barotropic response is .4 radians, or less than one month.

There are two reasons for the unimportance of the eastern boundary slope. First, near the eastern boundary the ocean's response to annual forcing is a Sverdrup balance confined to the upper layer. With no flow in the lower layer, the topography has no effect. Second, a slope at the eastern boundary bends the geostrophic contours to the south but does not close them. Any zonal flow in the interior implies a flow across geostrophic contours somewhere in order to complete the gyre. This requires a supply of vorticity, which in the case of the Sverdrup balance is the windstress curl. There is no additional net source of vorticity in the eastern boundary slope. The vorticity supplied by downslope flow in one place must be removed by equal upslope flow somewhere else. This means, however, that there can be a transfer of potential vorticity from one

latitude to another, and it is this that produces what small deviations from Sverdrup balance there are.

The barotropic flow is increased $(|I_{ST}|>1)$ and the baroclinic wave is decreased $(|I_{Sc}|<1)$ when $\ell<0$. The reverse is true for $\ell>0$. This is consistent with the character of the directly forced motion over the slope. Since $S<0$ for the eastern boundary slope, the case $\ell<0$ involves a directly forced motion (Figure 2.B.3a) that is 'barotropic' in the sense that the upper and lower layers move in phase. Similarly, in the case of $\ell>0$, the directly forced motion is 'baroclinic' in the sense that the layers are π radians out of phase.

The phase of the index I_{ST} is generally negative for $\ell>0$ and positive for $\ell<0$, so the barotropic response is shifted to the north in both cases. The reason is simple. The barotropic response is largely due to the integral of the forcing along each geostrophic contour. Since the slope bends the contours to the south, the flow at a given latitude in the interior responds to an average of the forcing at that latitude and at latitudes to the south. In a barotropic model this phase shift (and slight reduction of amplitude) due to the crossing of latitude lines by geostrophic contours would be the only effect of the slope and would be exactly the same for $\ell=1$ as for $\ell=-1$. Baroclinicity disrupts the symmetry and adds new effects but the essential mechanism remains.

3. Ridge

The thin barrier model developed in the first section of this chapter represents topography that is extreme in at least two senses; it is infinitely steep, and it completely blocks the lower layer. The first condition can be relaxed by putting a region of constant slope on each side of the barrier, which then rises from the crest of a triangular ridge. The second condition can be relaxed by removing the barrier and leaving the triangular ridge. These configurations, shown in Figure 3.C-3, will be called the ridge-barrier and ridge models, respectively.

There are four regions of constant slope in each model, and four free wave amplitudes to be determined in each region. Application of the radiation condition in each of the two flat regions removes four of the waves from consideration, leaving twelve amplitudes still to be computed. There are two conditions on the velocity in each layer at each of the three junctions, for a total of twelve conditions. On both models both components of the velocity are continuous in each layer at $x = \pm X$ and in the upper layer at $x = 0$. In the ridge model the lower layer velocity is also continuous at $x = 0$. In the ridge-barrier model the zonal component of velocity is zero at $x = 0+$ and at $x = 0-$. The meridional component is unconstrained.

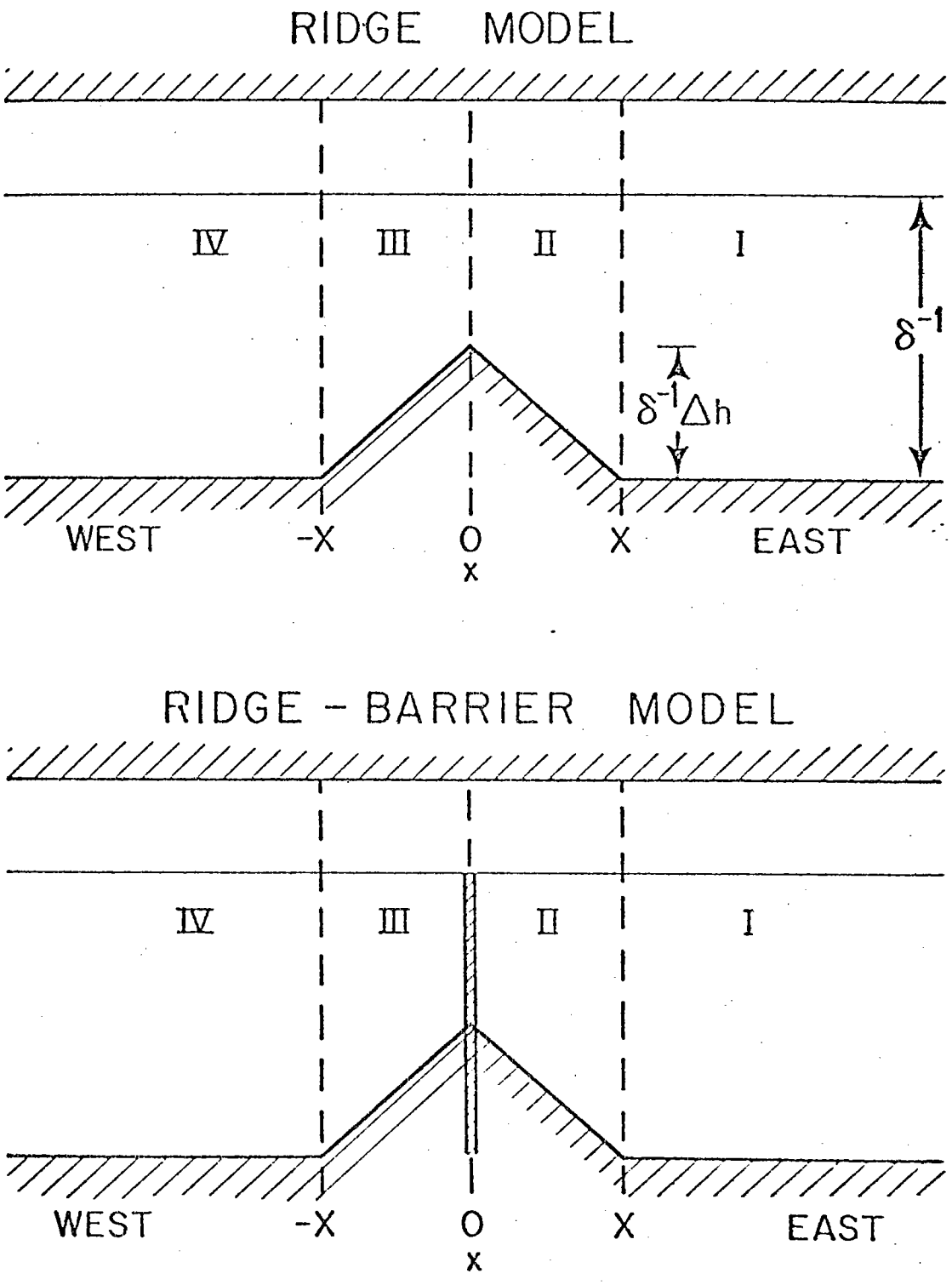

Figure 3.C-3. Ridge and ridge-barrier models.

In order to determine the effect of the ridge and the ridge-barrier on annual oscillations, three sets of calculations are made. First, zonally uniform forcing ($G = e^{il\gamma}$) is applied and there are no free waves incident on the topography. Second, forcing is zero but there is a long barotropic wave of unit amplitude incident from the east. Third, forcing is again zero but there is a long baroclinic wave of unit amplitude incident from the east. As usual, all motions have $e^{il\gamma}$ meridional dependence and l takes the values 1 and -1. The effect of topography in a basin with an eastern boundary will be found by combining the results of the first two sets of calculations: the response to direct forcing and to an incident barotropic wave.

The amplitudes of the free waves are determined by the same linear equation (3.C.4) as in the eastern boundary slope calculation with the elements of A_{ij} for the ridge model given in Tables 3.C-3a. For the ridge-barrier model all but two of the rows of A_{ij} are the same as in the ridge model. The two rows that differ are given in Table 3.C-3.B. The right hand side of (3.C.4) for each of the three sets of calculations is given in Table 3.C-3c. The elements of P_i along with the notation used in these tables are given in Table 3.C-3d.

Solutions of (3.C.4) were calculated for ridge half-widths X = .05, .1, .2, .4, .8, and 1.6, with topographic heights αh = .1, .5, and 1. Tables 3.C-4 through 3.C -9

and Figure 3.C-4 give the results in terms of the wave energy fluxes, radiating away from the topography. The energy fluxes are defined so as to make the flux of a barotropic wave of unit amplitude equal to one:

$$E_T = |p_T|^2$$

$$E_c = |p_c|^2 \delta K \qquad (3.C.7)$$

where K is defined by (3.A.6). (The difference between E_c as defined here and in the barrier calculation is due to a difference in the normalization of the mode amplitude.) In the first set of calculations, where the motion is due to forcing, the wave amplitudes have been normalized by the amplitude of the barotropic directly forced motion over the flat regions. For the second and third sets of calculations, with incident barotropic and baroclinic waves of unit amplitude, the amplitudes and phases of the transmitted waves are given in Tables 3.C.10,11; an incident barotropic wave $e^{ik_{TW}x}$ will produce a transmitted barotropic wave $T_T e^{ik_{TW}x}$ to the west of the topography, and similarly for the baroclinic wave. The values of T_T and T_c are independent of the sign of ℓ, whereas all the other reflected and scattered wave amplitudes (and energy fluxes) depend on the sign of ℓ.

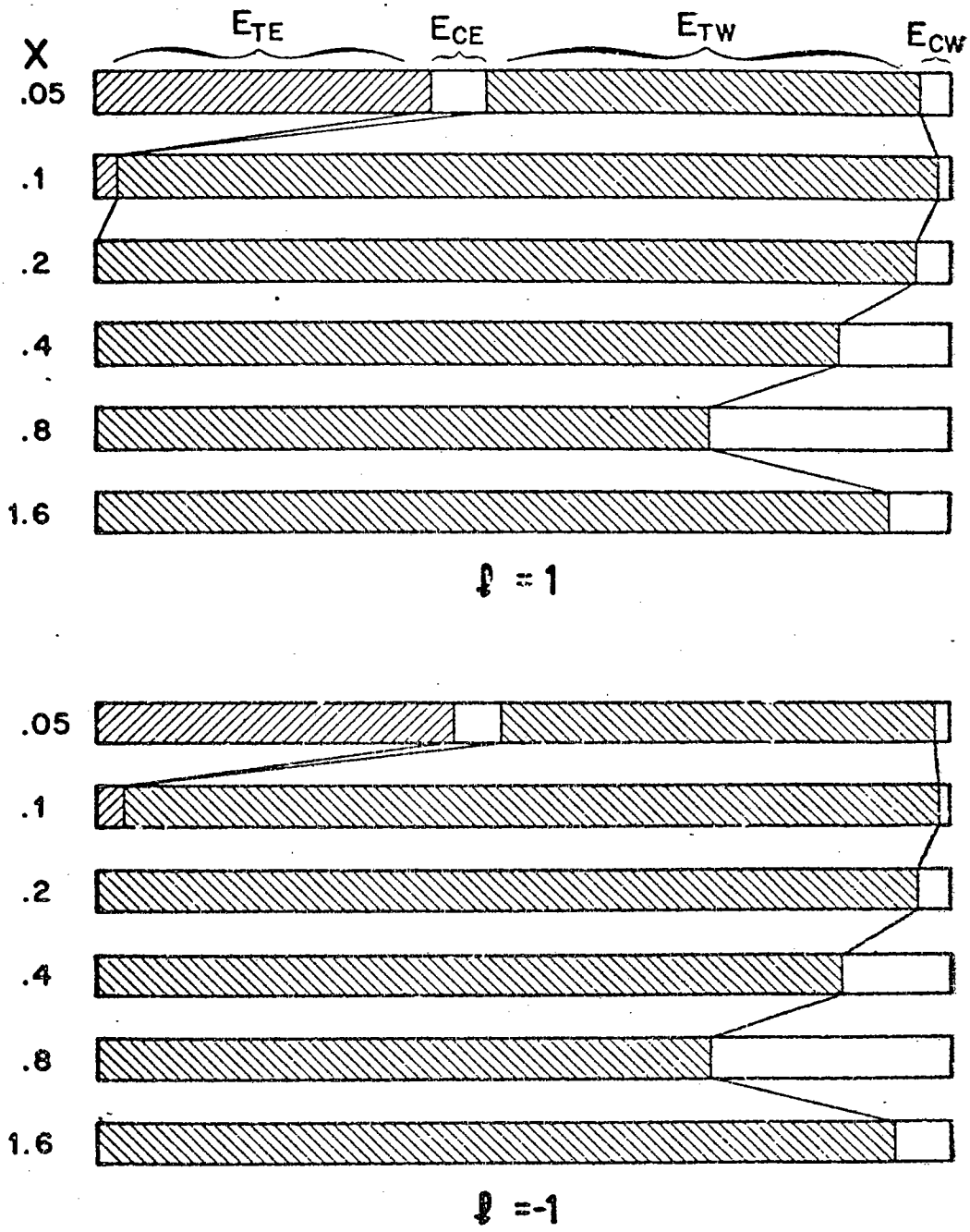

Figure 3.C-4a. Ridge model, wave energy fluxes due to incident barotropic wave, $\Delta h = .5$ (Table 3.C-6b).

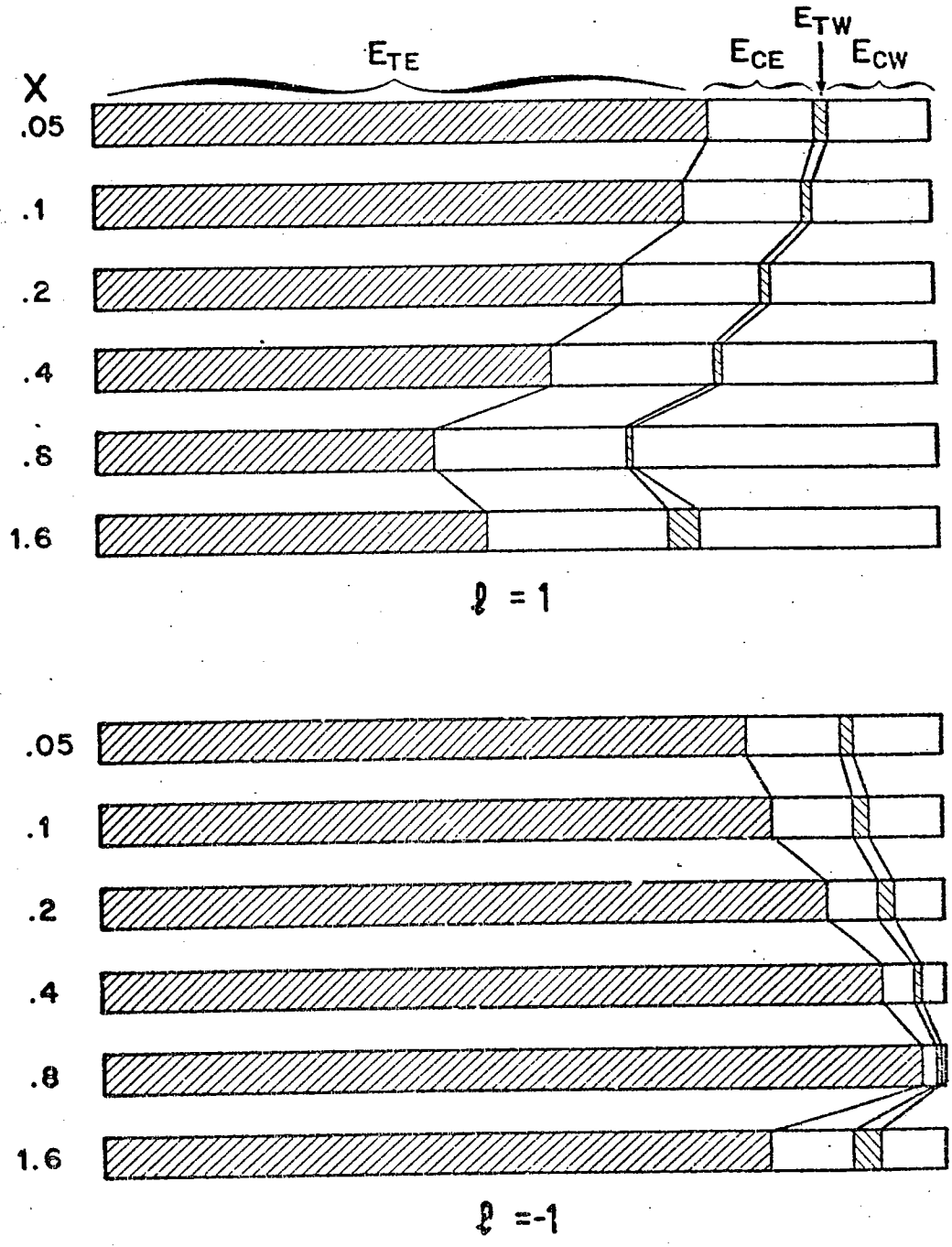

Figure 3.C-4b. Ridge-barrier model, wave energy fluxes due to incident barotropic wave, $\Delta h = 5$ (Table 3.C-7b).

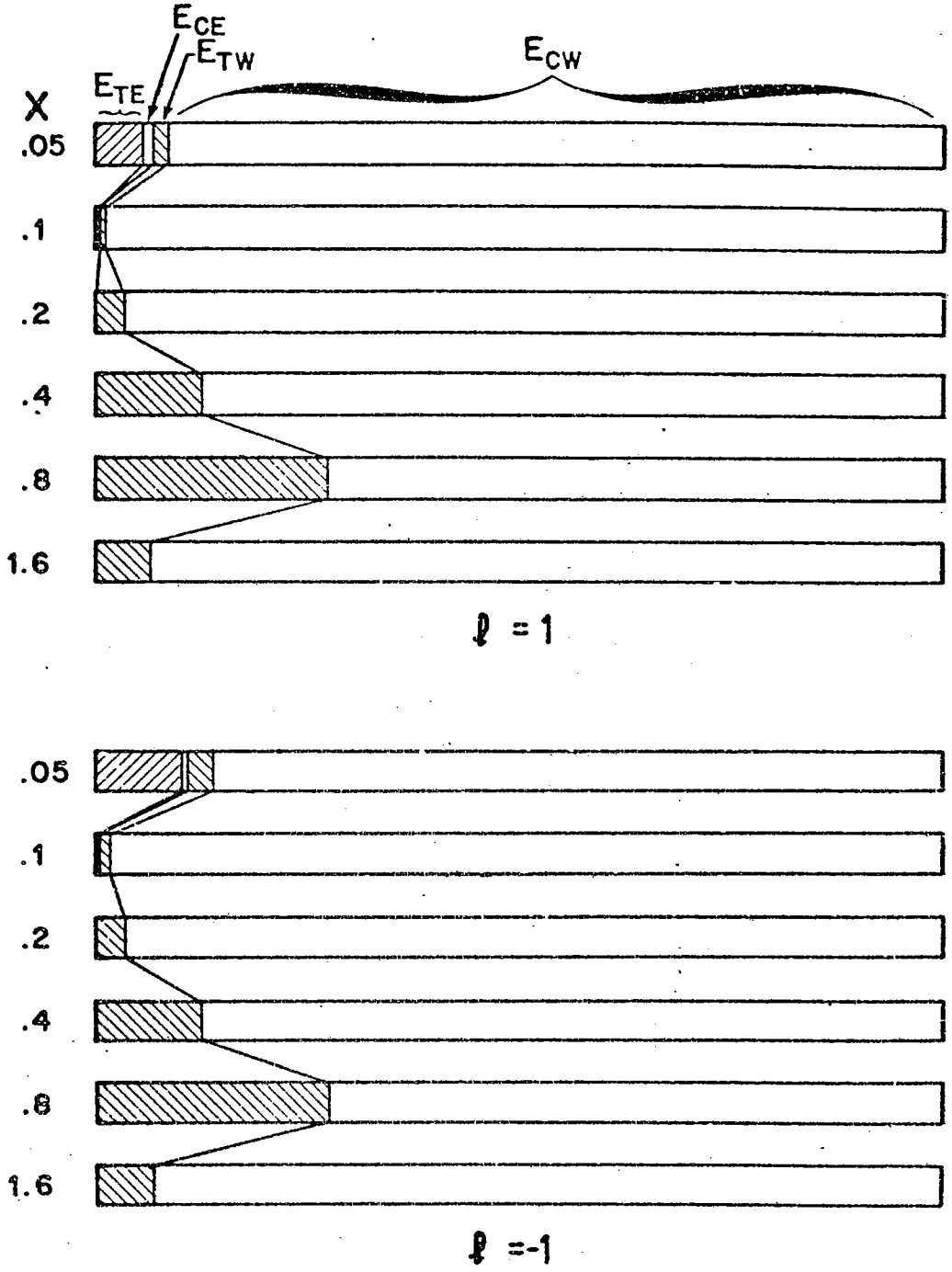

Figure 3.C-4c. Ridge model, wave energy fluxes due to incident baroclinic wave, $\Delta h = .5$ (Table 3.C-8b).

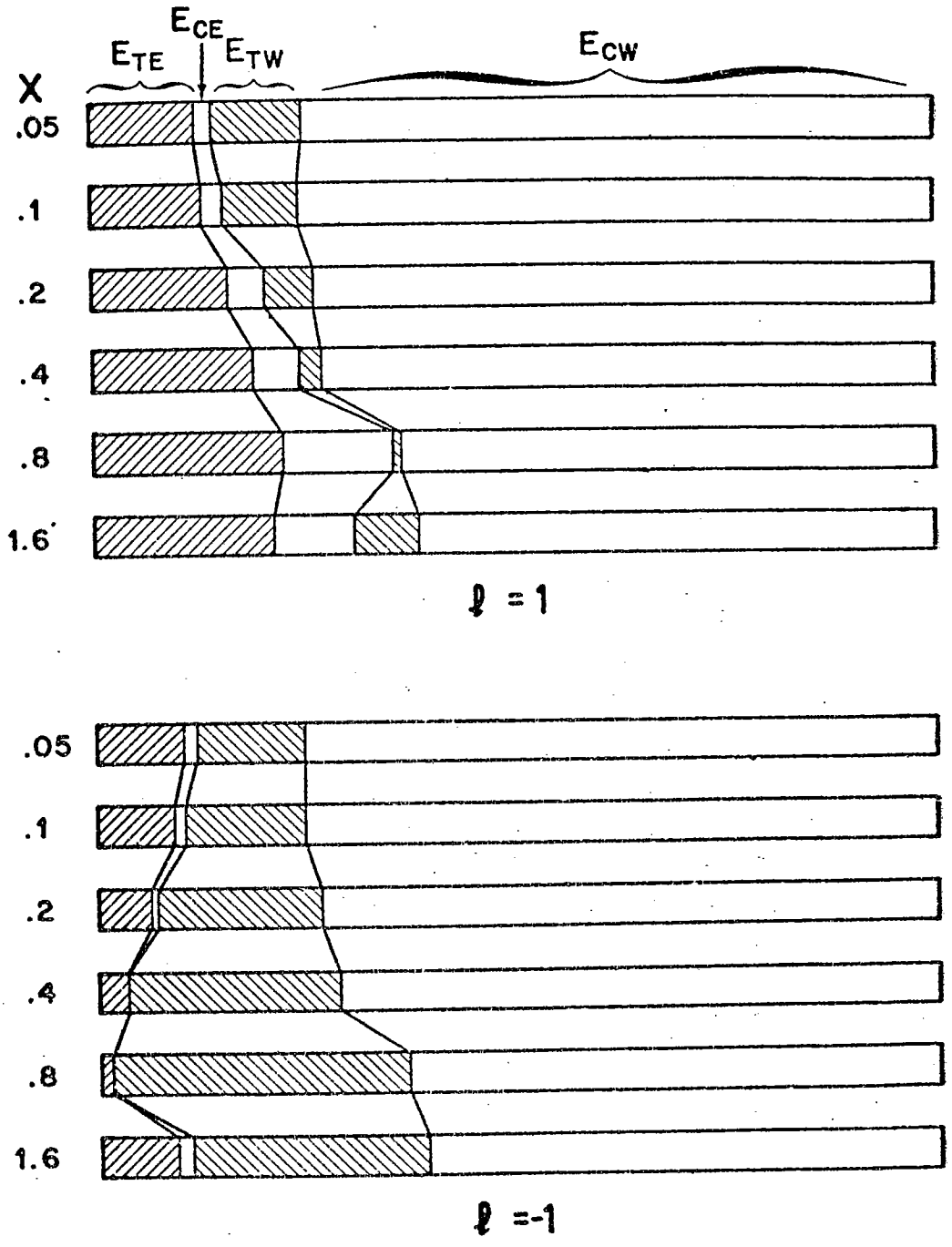

Figure 3.C-4d. Ridge-barrier model, wave energy fluxes due to incident baroclinic wave, $\Delta h = .5$ (Table 3.C-9b).

Table 3.C-3a

Elements of the matrix A_{ij} for the ridge model. Each term has the subscript j equal to its column number; the subscripts are omitted for compactness. For example, $A_{45} = -R_5 k_5 \chi_5$. The subscript identifies the region, mode, and type of wave, as given in Table 3.C-3d.

i \ j	1	2	3	4	5	6
1	χ	χ	$-\chi$	$-\chi$	$-\chi$	$-\chi$
2	$R\chi$	$R\chi$	$-R\chi$	$-R\chi$	$-R\chi$	$-R\chi$
3	$k\chi$	$k\chi$	$-k\chi$	$-k\chi$	$-k\chi$	$-k\chi$
4	$Rk\chi$	$Rk\chi$	$-Rk\chi$	$-Rk\chi$	$-Rk\chi$	$-Rk\chi$
5	0	0	1	1	1	1
6	0	0	R	R	R	R
7	0	0	k	k	k	k
8	0	0	Rk	Rk	Rk	Rk
9	0	0	0	0	0	0
10	0	0	0	0	0	0
11	0	0	0	0	0	0
12	0	0	0	0	0	0

Table 3.C-3a (Contd)

i \ j	7	8	9	10	11	12
1	0	0	0	0	0	0
2	0	0	0	0	0	0
3	0	0	0	0	0	0
4	0	0	0	0	0	0
5	-1	-1	-1	-1	0	0
6	-R	-R	-R	-R	0	0
7	-k	-k	-k	-k	0	0
8	-Rk	-Rk	-Rk	-Rk	0	0
9	χ	χ	χ	χ	χ	χ
10	$R\chi$	$R\chi$	$R\chi$	$R\chi$	$-R\chi$	$-R\chi$
11	$k\chi$	$k\chi$	$k\chi$	$k\chi$	$-k\chi$	$-k\chi$
12	$Rk\chi$	$Rk\chi$	$Rk\chi$	$Rk\chi$	$-Rk\chi$	$-Rk\chi$

Table 3.C-3b

Elements of rows 6 and 8 of A_{ij} for the ridge-barrier model. All other rows are the same as in Table 3.C-3a.

i \ j	1	2	3	4	5	6
6	O	O	R	R	R	R
8	O	O	O	O	O	O

i \ j	7	8	9	10	11	12
6	O	O	O	O	O	O
8	R	R	R	R	O	O

Table 3.C-3c

Right hand sides of 3.C.4 for ridge and ridge-barrier models: elements of F_j^F, F_j^T, F_j^C corresponding to direct forcing, incoming barotropic wave, and incoming baroclinic wave, respectively.

j	F_j^F	F_j^T	F_j^C
1	$-P_{F1}^{I}+P_{F1}^{II}$	$-\chi_{TW}$	$-\chi_{CW}$
2	$-P_{F2}^{I}+P_{F2}^{II}$	$-R_T\chi_{TW}$	$-R_C\chi_{CW}$
3	0	$-k_{TW}\chi_{TW}$	$-k_{CW}\chi_{CW}$
4	0	$-R_T k_{TW}\chi_{TW}$	$-R_C k_{CW}\chi_{CW}$
5	$-P_{F1}^{II}+P_{F1}^{III}$	0	0
6	$-P_{F2}^{II}+P_{F2}^{III}$	0	0
7	0	0	0
8	0	0	0
9	$-P_{F1}^{III}+P_{F1}^{IV}$	0	0
10	$-P_{F2}^{III}+P_{F2}^{IV}$	0	0
11	0	0	0
12	0	0	0

Table 3.C-3d

Elements of P_j for ridge and ridge-barrier models, along with interpretation of R_j, k_j, and χ_j in previous tables. For example, $k3 = k_{TW}^{II}$ refers to the wavenumber of the 'barotropic' long wave in region II.

j	P_j	R_j	k_j	χ_j
1	P_{TE}^{I}	R_T	k_{TE}	$\exp(ik_{TE}\ X)$
2	P_{CE}^{I}	R_C	k_{CE}	$\exp(ik_{CE}\ X)$
3	P_{TW}^{II}	R_T^{II}	k_{TW}^{II}	$\exp(ik_{TW}^{II}\ X)$
4	P_{TE}^{II}	R_T^{II}	k_{TE}^{II}	$\exp(ik_{TE}^{II}\ X)$
5	P_{CW}^{II}	R_C^{II}	k_{CW}^{II}	$\exp(ik_{CW}^{II}\ X)$
6	P_{CE}^{II}	R_C^{II}	k_{CE}^{II}	$\exp(ik_{CE}^{II}\ X)$
7	P_{TW}^{III}	R_T^{III}	k_{TW}^{III}	$\exp(-ik_{TW}^{III}\ X)$
8	P_{TE}^{III}	R_T^{III}	k_{TE}^{III}	$\exp(-ik_{TE}^{III}\ X)$
9	P_{CW}^{III}	R_C^{III}	k_{CW}^{III}	$\exp(-ik_{CW}^{III}\ X)$
10	P_{CE}^{III}	R_C^{III}	k_{CE}^{III}	$\exp(-ik_{CE}^{III}\ X)$
11	P_{TW}^{IV}	R_T	k_{TW}	$\exp(-ik_{TW}\ X)$
12	P_{CW}^{IV}	R_C	k_{CW}	$\exp(-ik_{CW}\ X)$

Table 3.C-4a

Ridge model, wave energy fluxes due to direct forcing, $\Delta h = .1$.

X	E_{TE}	E_{CE}	E_{TW}	E_{CW}
.05	.002	.000	.000	.000
	.002	.000	.000	.000
.1	.002	.000	.000	.000
	.002	.000	.000	.000
.2	.001	.000	.000	.002
	.001	.000	.000	.002
.4	.000	.000	.000	.006
	.000	.000	.000	.006
.8	.000	.000	.000	.013
	.000	.000	.000	.013
1.6	.000	.000	.000	.003
	.000	.000	.000	.003

Table 3.C-4b

Ridge model, wave energy fluxes due to direct forcing, $\Delta h = .5$.

X	E_{TE}	E_{CE}	E_{TW}	E_{CW}
.05	.396	.062	.171	.030
	.424	.051	.171	.015
.1	.033	.005	.056	.013
	.037	.003	.056	.011
.2	.003	.001	.027	.035
	.004	.001	.027	.034
.4	.005	.000	.020	.125
	.005	.000	.020	.125
.8	.000	.000	.026	.275
	.000	.000	.022	.279
1.6	.000	.000	.009	.065
	.000	.000	.007	.067

Table 3.C-4c

Ridge model, wave energy fluxes due to direct forcing, $\Delta h = 1$.

X	E_{TE}	E_{CE}	E_{TW}	E_{CW}
.05	.719	.114	.560	.091
	.780	.089	.559	.058
.1	.516	.096	1.045	.128
	.606	.058	1.044	.077
.2	.064	.012	.375	.071
	.087	.002	.374	.059
.4	.002	.003	.259	.300
	.008	.002	.254	.300
.8	.000	.002	.267	.718
	.005	.000	.249	.732
1.6	.000	.000	.086	.283
	.000	.000	.073	.296

Table 3.C-5a

Ridge-barrier model, wave energy fluxes due to forcing, $\Delta h = .1$.

X	E_{TE}	E_{CE}	E_{TW}	E_{CW}
.05	.741	.117	.749	.118
	.757	.110	.749	.109
.1	.736	.119	.751	.121
	.765	.107	.751	.105
.2	.728	.122	.752	.126
	.774	.103	.752	.100
.4	.702	.133	.754	.141
	.796	.093	.753	.088
.8	.681	.141	.758	.154
	.815	.085	.755	.078
1.6	.713	.127	.750	.132
	.777	.103	.743	.099

Table 3.C-5b

Ridge-barrier model, wave energy fluxes due to forcing, $\Delta h = .5$.

X	E_{TE}	E_{CE}	E_{TW}	E_{CW}
.05	.728	.122	.749	.126
	.767	.106	.749	.103
.1	.701	.133	.754	.142
	.795	.094	.753	.088
.2	.624	.162	.772	.190
	.857	.066	.769	.056
.4	.540	.190	.818	.250
	.923	.036	.812	.027
.8	.400	.226	.885	.360
	.975	.012	.871	.008
1.6	.459	.213	.679	.273
	.799	.098	.652	.076

Table 3.C-5c

Ridge-barrier model, wave energy fluxes due to forcing, $\Delta h = 1$.

X	E_{TE}	E_{CE}	E_{TW}	E_{CW}
.05	.738	.117	.767	.122
	.789	.096	.766	.093
.1	.706	.131	.783	.141
	.819	.083	.781	.077
.2	.601	.170	.826	.205
	.873	.059	.823	.049
.4	.387	.233	.998	.363
	.968	.015	.988	.009
.8	.146	.239	1.172	.579
	.949	.026	1.149	.011
1.6	.118	.224	.549	.552
	.770	.113	.515	.045

Table 3.C-6a

Ridge model, wave energy fluxes due to incident barotropic wave, $\Delta h = .1$.

X	E_{TE}	E_{CE}	E_{TW}	E_{CW}
.05	.002	.000	.997	.000
	.002	.000	.997	.000
.1	.002	.000	.997	.000
	.002	.000	.997	.000
.2	.001	.000	.997	.002
	.001	.000	.997	.002
.4	.000	.000	.994	.006
	.000	.000	.994	.006
.8	.000	.000	.987	.013
	.000	.000	.987	.013
1.6	.000	.000	.997	.003
	.000	.000	.997	.003

Table 3.C-6b

Ridge model, wave energy fluxes due to incident barotropic wave, $\Delta h = .5$.

X	E_{TE}	E_{CE}	E_{TW}	E_{CW}
.05	.399	.063	.508	.030
	.426	.051	.508	.015
.1	.033	.005	.949	.013
	.037	.003	.949	.011
.2	.003	.001	.961	.035
	.004	.000	.961	.034
.4	.004	.000	.870	.125
	.005	.000	.870	.125
.8	.000	.000	.721	.278
	.000	.000	.721	.278
1.6	.000	.000	.933	.067
	.000	.000	.933	.067

Table 3.C-6c

Ridge model, wave energy fluxes due to incident barotropic wave, $\Delta h = 1$.

X	E_{TE}	E_{CE}	E_{TW}	E_{CW}
.05	.725	.115	.068	.092
	.784	.089	.068	.058
.1	.520	.097	.254	.129
	.609	.059	.254	.078
.2	.065	.012	.852	.071
	.088	.002	.852	.059
.4	.002	.003	.690	.303
	.008	.002	.690	.299
.8	.000	.002	.267	.731
	.005	.000	.267	.728
1.6	.000	.000	.713	.287
	.000	.000	.713	.287

Table 3.C-7a

Ridge-barrier model, wave energy fluxes due to incident barotropic wave, $\Delta h = .1$.

X	E_{TE}	E_{CE}	E_{TW}	E_{CW}
.05	.746	.118	.017	.119
	.762	.111	.017	.110
.1	.741	.120	.017	.122
	.770	.107	.017	.105
.2	.733	.123	.017	.127
	.779	.103	.017	.100
.4	.708	.134	.017	.142
	.801	.094	.017	.088
.8	.686	.142	.016	.155
	.820	.086	.016	.078
1.6	.720	.129	.018	.134
	.780	.103	.018	.099

Table 3.C-7b

Ridge-barrier model, wave energy fluxes due to incident barotropic wave, $\Delta h = .5$.

X	E_{TE}	E_{CE}	E_{TW}	E_{CW}
.05	.733	.123	.017	.126
	.772	.106	.017	.104
.1	.706	.134	.017	.143
	.800	.094	.017	.089
.2	.630	.163	.015	.192
	.861	.067	.015	.057
.4	.546	.192	.010	.252
	.927	.036	.010	.027
.8	.406	.229	.004	.361
	.976	.012	.004	.008
1.6	.469	.217	.034	.280
	.794	.097	.034	.075

Table 3.C-7c

Ridge-barrier model wave energy fluxes due to incident barotropic wave, $\Delta h = 1$.

X	E_{TE}	E_{CE}	E_{TW}	E_{CW}
.05	.743	.119	.015	.123
	.794	.097	.015	.094
.1	.711	.132	.014	.142
	.824	.084	.014	.078
.2	.607	.172	.014	.207
	.877	.060	.014	.050
.4	.392	.235	.006	.337
	.970	.015	.006	.010
.8	.150	.244	.017	.590
	.946	.026	.017	.011
1.6	.122	.232	.084	.562
	.759	.111	.084	.046

Table 3.C-8a

Ridge model, wave energy fluxes due to incident baroclinic wave, $\Delta h = .1$.

X	E_{TE}	E_{CE}	E_{TW}	E_{CW}
.05	.000	.000	.000	.999
	.000	.000	.000	.999
.1	.000	.000	.000	.999
	.000	.000	.000	.999
.2	.000	.000	.002	.998
	.000	.000	.002	.998
.4	.000	.000	.006	.994
	.000	.000	.006	.994
.8	.000	.000	.013	.987
	.000	.000	.013	.987
1.6	.000	.000	.003	.997
	.000	.000	.003	.997

Table 3.C-8b

Ridge model, wave energy fluxes due to incident baroclinic wave, $\Delta h = .5$.

X	E_{TE}	E_{CE}	E_{TW}	E_{CW}
.05	.063	.010	.015	.912
	.051	.006	.003	.912
.1	.005	.001	.011	.984
	.003	.000	.013	.984
.2	.001	.001	.034	.964
	.001	.000	.035	.964
.4	.000	.000	.125	.875
	.000	.000	.125	.875
.8	.000	.000	.278	.722
	.000	.000	.278	.722
1.6	.000	.000	.067	.933
	.000	.000	.067	.933

Table 3.C-8c

Ridge model, wave energy fluxes due to incident baroclinic wave, $\Delta h = 1$.

X	E_{TE}	E_{CE}	E_{TW}	E_{CW}
.05	.115	.018	.058	.808
	.089	.010	.092	.808
.1	.097	.019	.078	.807
	.059	.006	.129	.807
.2	.012	.002	.059	.927
	.002	.000	.071	.927
.4	.003	.003	.299	.694
	.002	.000	.304	.694
.8	.002	.002	.728	.269
	.000	.000	.731	.269
1.6	.000	.000	.287	.713
	.000	.000	.287	.713

Table 3.C-9a

Ridge-barrier model, wave energy fluxes due to incident baroclinic wave, $\Delta h = .1$.

X	E_{TE}	E_{CE}	E_{TW}	E_{CW}
.05	.118	.019	.110	.754
	.111	.016	.119	.754
.1	.120	.019	.105	.756
	.107	.015	.122	.756
.2	.123	.021	.100	.756
	.103	.014	.127	.756
.4	.134	.025	.088	.753
	.094	.011	.142	.753
.8	.142	.029	.078	.750
	.086	.009	.155	.750
1.6	.129	.023	.099	.749
	.103	.014	.134	.749

Table 3.C-9b

Ridge-barrier model, wave energy fluxes due to incident baroclinic wave, $\Delta h = .5$.

X	E_{TE}	E_{CE}	E_{TW}	E_{CW}
.05	.123	.021	.104	.753
	.106	.015	.126	.753
.1	.134	.026	.089	.752
	.094	.011	.143	.752
.2	.162	.043	.057	.737
	.067	.005	.192	.737
.4	.192	.069	.027	.711
	.036	.001	.252	.711
.8	.229	.136	.008	.627
	.012	.000	.361	.627
1.6	.217	.097	.075	.610
	.097	.013	.280	.610

Table 3.C-9c

Ridge-barrier model, wave energy fluxes due to incident baroclinic wave, $\Delta h = 1$.

X	E_{TE}	E_{CE}	E_{TW}	E_{CW}
.05	.119	.019	.094	.768
	.097	.012	.123	.768
.1	.132	.025	.078	.765
	.084	.009	.142	.765
.2	.172	.047	.050	.730
	.060	.004	.207	.730
.4	.236	.136	.010	.618
	.015	.000	.367	.618
.8	.244	.363	.011	.382
	.026	.001	.590	.382
1.6	.232	.415	.046	.307
	.111	.019	.562	.307

Table 3.C-10a

Ridge model, transmitted wave amplitudes T_T and T_C in complex polar form $re^{i\theta}$, with d = 0.

	T_T		T_C		
X	r	θ	r	θ	Δh
.05	.999	.02	1.000	.00	.1
	.712	.36	.955	.03	.5
	.261	.26	.899	-.02	1
.1	.998	.01	.999	.00	.1
	.974	.24	.992	.01	.5
	.504	1.37	.898	.01	1
.2	.998	.01	.999	-.00	.1
	.951	.16	.982	-.03	.5
	.923	.64	.963	-.10	1
.4	.997	.01	.997	-.00	.1
	.933	.13	.935	-.07	.5
	.831	.53	.833	-.26	1
.8	.994	.00	.994	.00	.1
	.849	.03	.849	-.00	.5
	.517	.22	.518	-.09	1
1.6	.999	-.00	.999	.00	.1
	.967	-.09	.966	.10	.5
	.844	-.27	.844	.34	1

Table 3.C-10b

Ridge model transmitted wave amplitude with d = .5.

	T_T		T_C		
X	r	θ	r	θ	Δh
.05	.986	.01	.998	.00	.1
	.706	.21	.955	.01	.5
	.353	.27	.909	-.01	1
.1	.994	.01	.999	.00	.1
	.853	.21	.975	-.00	.5
	.476	.62	.924	-.03	1
.2	.997	.01	.999	-.00	.1
	.919	.15	.975	-.03	.5
	.718	.58	.942	-.11	1
.4	.996	.00	.997	-.00	.1
	.905	.12	.934	-.07	.5
	.721	.51	.839	-.26	1

Table 3.C-11a

Ridge barrier model transmitted wave amplitude with d = 0.

X	T_T r	T_T θ	T_C r	T_C θ	Δh
.05	.131	.01	.868	-.00	.1
	.132	.08	.868	-.01	.5
	.122	.11	.877	-.02	1
.1	.130	.01	.869	-.00	.1
	.130	.11	.867	-.02	.5
	.120	.34	.875	-.06	1
.2	.130	.00	.869	-.00	.1
	.122	.19	.858	-.03	.5
	.119	.68	.854	-.11	1
.4	.129	.01	.868	-.00	.1
	.099	.30	.843	-.05	.5
	.075	1.53	.786	-.17	1
.8	.127	-.01	.866	-.00	.1
	.066	-.45	.792	-.04	.5
	.129	-2.21	.618	-.23	1
1.6	.133	-.01	.869	.00	.1
	.186	-.20	.781	.08	.5
	.290	-.35	.554	.29	1

Table 3.C-11b

Ridge-barrier model, transmitted wave amplitudes with d = .5.

	T_T		T_C		
X	r	θ	r	θ	Δh
.05	.131	.03	.870	-.00	.1
	.129	.09	.871	-.01	.5
	.126	.16	.874	-.02	1
.1	.131	.03	.869	-.00	.1
	.129	.14	.867	-.02	.5
	.122	.34	.873	-.05	1
.2	.130	.03	.869	-.00	.1
	.122	.22	.861	-.03	.5
	.114	.68	.858	-.10	1
.4	.129	.03	.868	-.01	.1
	.096	.31	.842	-.06	.5
	.080	1.52	.805	-.19	1

A general characteristic of all of the results is that the lowest topography has almost no effect. The ridge model produces little scattering while the ridge-barrier model acts like the thin barrier model. By way of comparison, $T_T = .132$ and $T_c = .868$ for the barrier model, virtually identical with values for the ridge-barrier model with $\Delta h = .1$.

Effects of the higher topography are significant. In the ridge model the greatest effect comes from the narrow ridges. In the most extreme case of $\Delta h = 1$ and $X = .05$ the ridge behaves much like the barrier in spite of the fact that the ridge model does not directly block flow in the lower layer across the crest of the ridge. Note that as the ridge width is decreased, more and more energy is found in short waves and the flow is increasingly blocked. In the ridge-barrier model, narrow slopes have little effect, indicating that the essential behavior of a narrow, high ridge is adequately modeled by the simple barrier model. As the slopes widen, however, some new effects are found. Both the phases and the amplitudes of T_T, and to a lesser extent T_c, are altered in a somewhat irregular manner. Since the calculations with dissipation show the same behavior, we may conclude that it is due to the interaction of the topographic and long wave scales and does not depend critically on the short waves. The phase of T_T is generally positive; the barotropic wave is delayed slightly by the ridge or ridge-barrier.

For $X \gtrsim .2$ the short wave fluxes are small. At each junction between regions of different slope the long waves available on either side of the junction have comparable scales, so only small amounts of short waves are needed to match both velocity components. The junction is then just a place where a motion that is composed of one pair of vertical modes on one side is translated into a different linear combination of a different pair of vertical modes on the other side. Each mode then propagates at its characteristic speed to the next junction where the resulting motion is again translated into still another pair of waves. It is the difference in phase speeds of the various waves that accounts for the scattering of energy by the topography. For example, suppose a barotropic wave is incident on a ridge. At the east side of the ridge the motion in the upper layer will produce an upper layer wave traveling across the ridge with the baroclinic long wave phase speed. The lower layer motion will be a quasi-steady flow along geostrophic contours. At the west side of the ridge, the upper layer motion will arrive after some delay due to the finite phase speed of the wave, but the lower layer will experience no significant net phase change (so long as the basin has the same depth on either side of the ridge). Hence the upper and lower layers are out of phase at the west side of the ridge and will therefore produce both barotropic and baroclinic long waves in the western flat part of the basin.

An example of this type of flow is shown in Figure 3.C-5, which is a contour map of the pressure in each layer when a barotropic wave is incident on a ridge with $X=.8$ and $\Delta h=.5$. In this case $\alpha=.625$ so the modes over the slopes are not heavily concentrated in either layer. Nevertheless, the baroclinic wave aspect of the upper layer flow is clear, as is the domination of the lower layer by geostrophic contours.

Rhines (1969a) calculated the effect of a triangular ridge on incident Rossby waves in a homogeneous fluid. Applying his calculations to the examples of interest here, we find that the effect of a narrow ridge is similar in the homogeneous and two-layer cases. For example, with $X=.05$ and $\Delta h=.5$ the homogeneous energy transmission coefficient is .527. With two layers, E_{TW} is .508 and E_{CW} is .015 or .03 depending on ℓ, so the same amount of energy, most of it barotropic, is transmitted as in the homogeneous case. With $X=.1$ and $\Delta h=.5$, the homogeneous transmission coefficient is .955. Just as in the two-layer case, there is little reflection unless the ridge is so steep that the zonal scale of flow along geostrophic contours over the slope approaches the short wave scale.

As the ridge width increases beyond 400 km or so, scattering of barotropic incident energy into baroclinic long waves occurs in the two-layer model, but not, of course, in

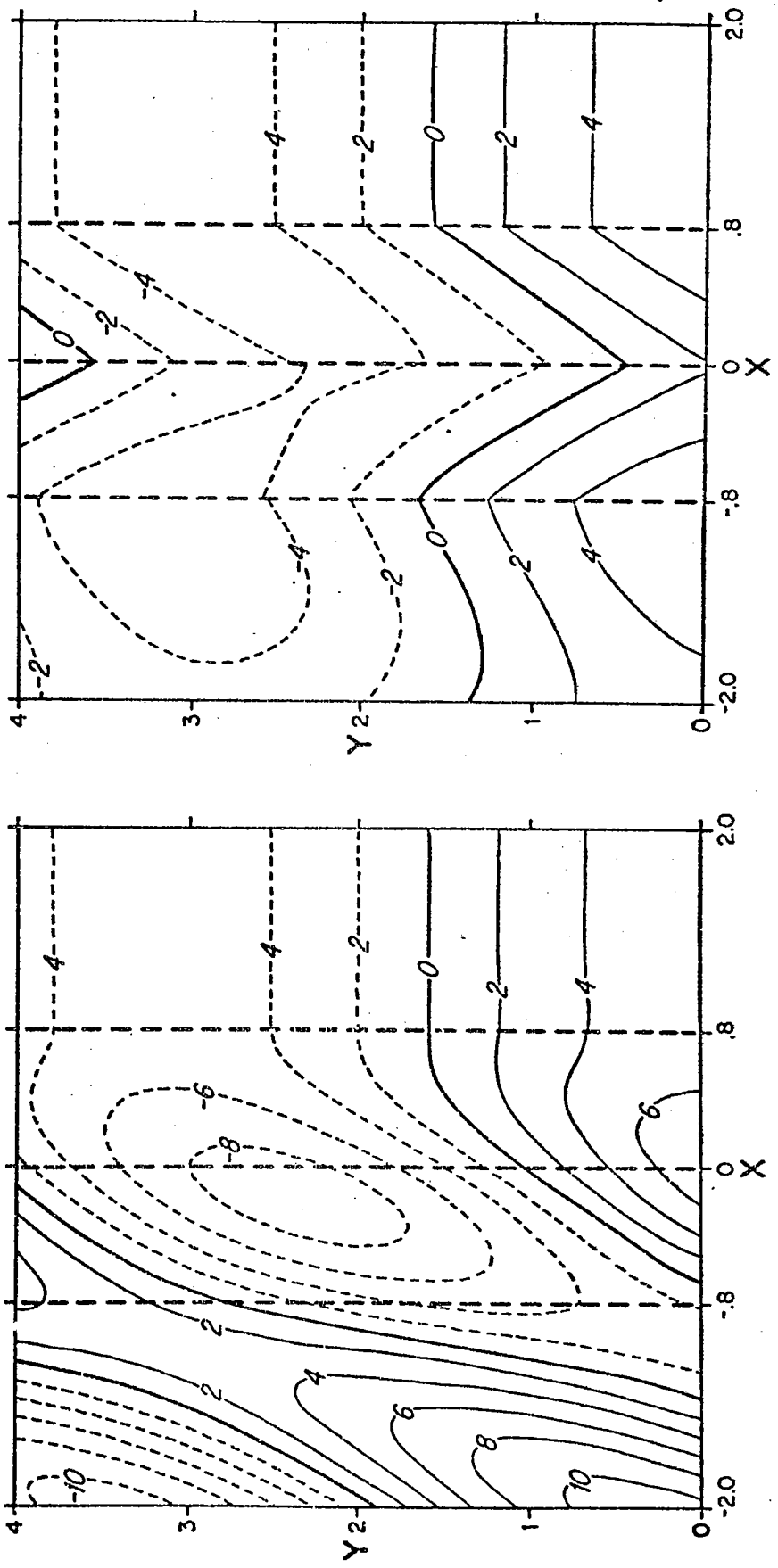

Figure 3.C-5a. Pressure in each layer due to barotropic wave incident on a ridge with X = .8, Δh = .5, ℓ = 1. Upper layer pressure on the left, lower layer on the right.

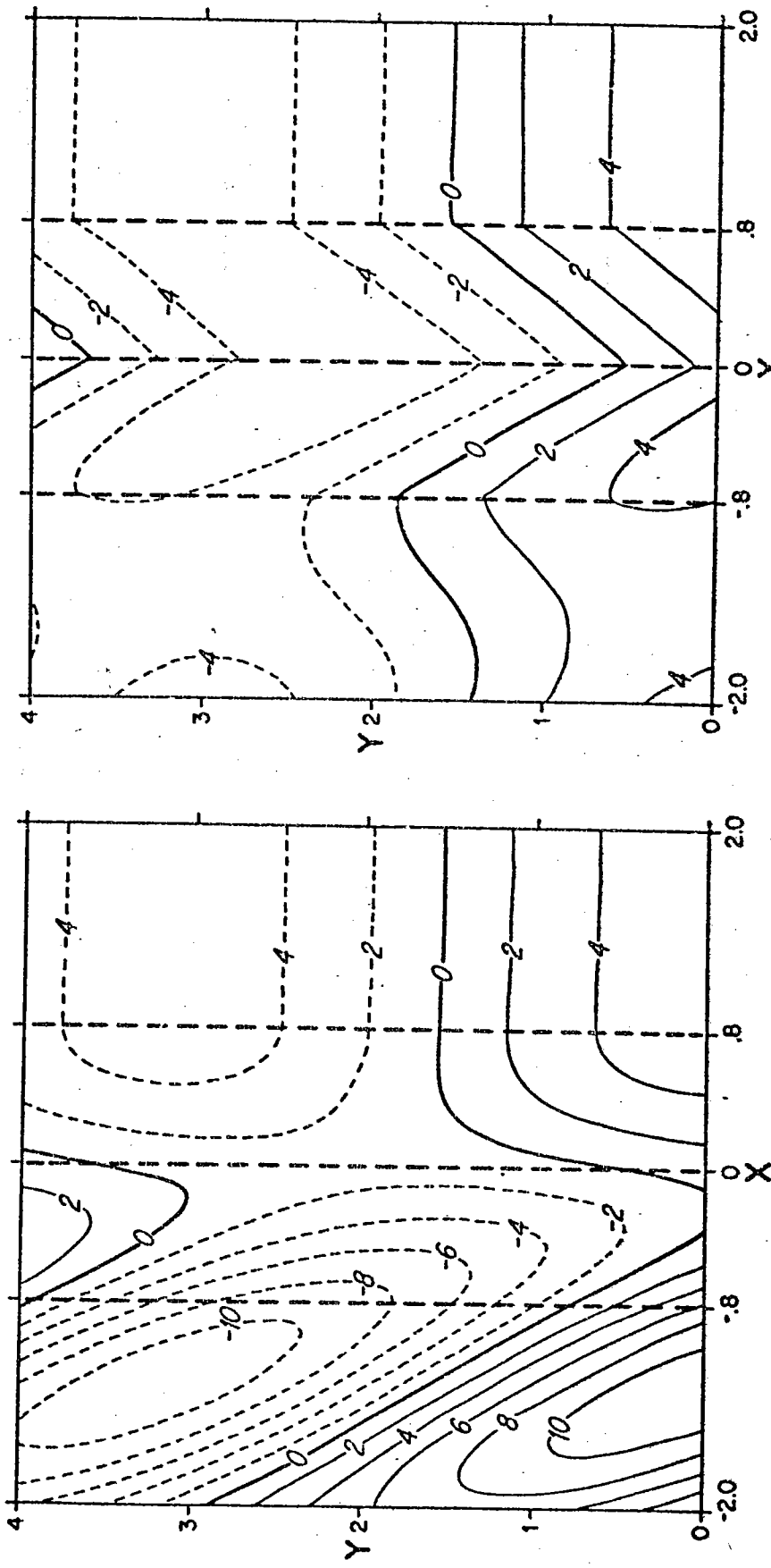

Figure 3.C-5b. Pressure in each layer due to barotropic wave incident on a ridge with X = .8, Δh = .5, ℓ = -1. Upper layer pressure on the left, lower layer on the right.

the homogeneous model. This scattering was studied by Hall (1976). In the examples he considered, Hall stated that the scattering was most efficient when the ridge width was comparable to the Rossby radius. However, in the present calculations we find that the scattering is greatest when the ridge width is comparable to a baroclinic long wavelength. Although the Rossby radius and the baroclinic wavelength are comparable in some parameter ranges, in the case of annual oscillations the baroclinic wavelength is around 2000 km at 20°N, while the Rossby radius is around 60 km.

A comparison of Tables 3.C-4-5 with 3.C-6,7 shows that the energy fluxes due to forcing are, with the exception of E_{TW}, almost identical to those due to an incident barotropic wave. This suggests that where both types of motion are present, as in the quasi-steady Sverdrup balance, the waves may tend to cancel each other. This is indeed the case.

To measure the net effect of the topography on annual oscillations in a basin with an eastern boundary we will define two indices. Suppose the topography is centered a distance $\alpha_I/2$ from the eastern boundary and we wish to measure the effect of topography at a distance $\alpha_I=4$ from the eastern boundary. Let p_{RTW} be the amplitude of the barotropic long wave due to forcing over the topography. In the notation of Table 3.C.3, $p_{RTW} = p^F_{(11)}/p_{TF}$ with $p^F_{(11)}$ calculated using the first of the three vectors F_j. Then an index of the effect of the topography on the barotropic motion in the basin is

$$I_{RT} \equiv \frac{1 - T_T e^{-ik_{TW}x_I} + \rho_{RTW} e^{-ik_{TW}x_I/2}}{1 - e^{-ik_{TW}x_I}} \qquad (3.C.8)$$

The denominator is the quasi-steady Sverdrup response that would exist in the absence of topography. The numerator is the sum of the directly forced response, the transmitted portion of the barotropic wave from the eastern boundary, and the barotropic long wave generated by forcing over the topography. The barotropic wave due to scattering of the baroclinic wave from the eastern boundary has been omitted for simplicity.

In addition to measuring the effect of the topography on the barotropic flow in the western part of the basin, we wish to measure its effect on the upper layer zonal velocity at the crest of the ridge or ridge-barrier. As in the case of the index I_{RT} we will consider the directly forced flow and the barotropic wave from the eastern boundary but will neglect the baroclinic wave from the eastern boundary. The upper layer pressure $p_1^R(0)$ at the crest of the ridge or ridge-barrier is then

$$p_1^R(0) = \frac{p_{1F}^{II}}{p_{TF}} + \frac{1}{p_{TF}} \sum_{j=3}^{6} p_j^F - \sum_{j=3}^{6} p_j^T e^{-ik_{TW}\frac{x_I}{2}} \qquad (3.C.9)$$

where superscripts F and T denote the amplitudes due to forcing and to an incident barotropic wave, respectively. In the absence of topography the upper layer pressure would be

$$p_1^H(0) = \frac{p_{CF}}{p_{TF}} + 1 - e^{-ik_{TW}x_I/2} \qquad (3.C.10)$$

The desired index of topographic effect is then

$$I_{RU} \equiv \frac{p_1^R(0)}{p_1^H(0)} \qquad (3.C.11)$$

Both indices can be computed for the barrier model as well. The barotropic index is again defined by (3.C.8) and has a numerical value of $I_{RT}^{(B)} = .571\, e^{.128i}$. The barotropic response is delayed slightly and reduced almost by half. Using (3.A.2), (3.A.5a), and (3.A.7) we find that the index corresponding to I_{RU} is

$$I_{RU}^{(B)} = 1 + \frac{p_2(0)}{p_1(0)} \frac{(1-K)}{(\delta+K)} \qquad (3.C.12)$$

where

$$p_1(0) = \left(1 - e^{-ik_{TW}x_I/2} + \delta^{-1}\frac{p_{CF}}{p_{TF}}\right)\left(1+\delta^{-1}\right)^{-1} \qquad (3.C.13a)$$

$$p_2(0) = \left(1 - e^{-ik_{TW}x_I/2} - \frac{p_{CF}}{p_{TF}}\right)\left(1+\delta^{-1}\right)^{-1} \qquad (3.C.13b)$$

Substituting the numerical values for the usual example of large scale annual oscillations yields $I_{RU}^{(B)} = 1.018\, e^{-.03i}$. Upper layer flow over the barrier is very slightly increased in amplitude and advanced in phase.

Amplitudes and phases of I_{RT} and I_{RU} for the ridge and ridge-barrier models are given in Tables 3.C-12 through 15 and Figure 3.C-6. Again we see that slopes with $\Delta h = .1$ have no appreciable effect.

With narrow slopes the ridge-barrier model acts like the thin barrier, and with steep narrow slopes the ridge model also has similar behavior, although it is unable to block the lower layer completely and is therefore less effective in reducing the barotropic flow. Both models tend to reduce the Sverdrup flow and shift the phase to the north. The reason for the phase shift is the same as in the case of the eastern boundary slope. Geostrophic contours are bowed to the south over the ridge, so the Sverdrup flow at a given latitude is due in part to forcing at a more southerly latitude with its consequent difference in phase. This averaging of the forcing over a band of latitudes reduces the amplitude of the response as well. Another process that reduces the amplitude is the scattering mechanism mentioned earlier. The ridge-barrier model adds these processes to the lower layer blockage so as to reduce the barotropic flow even more than does the thin barrier.

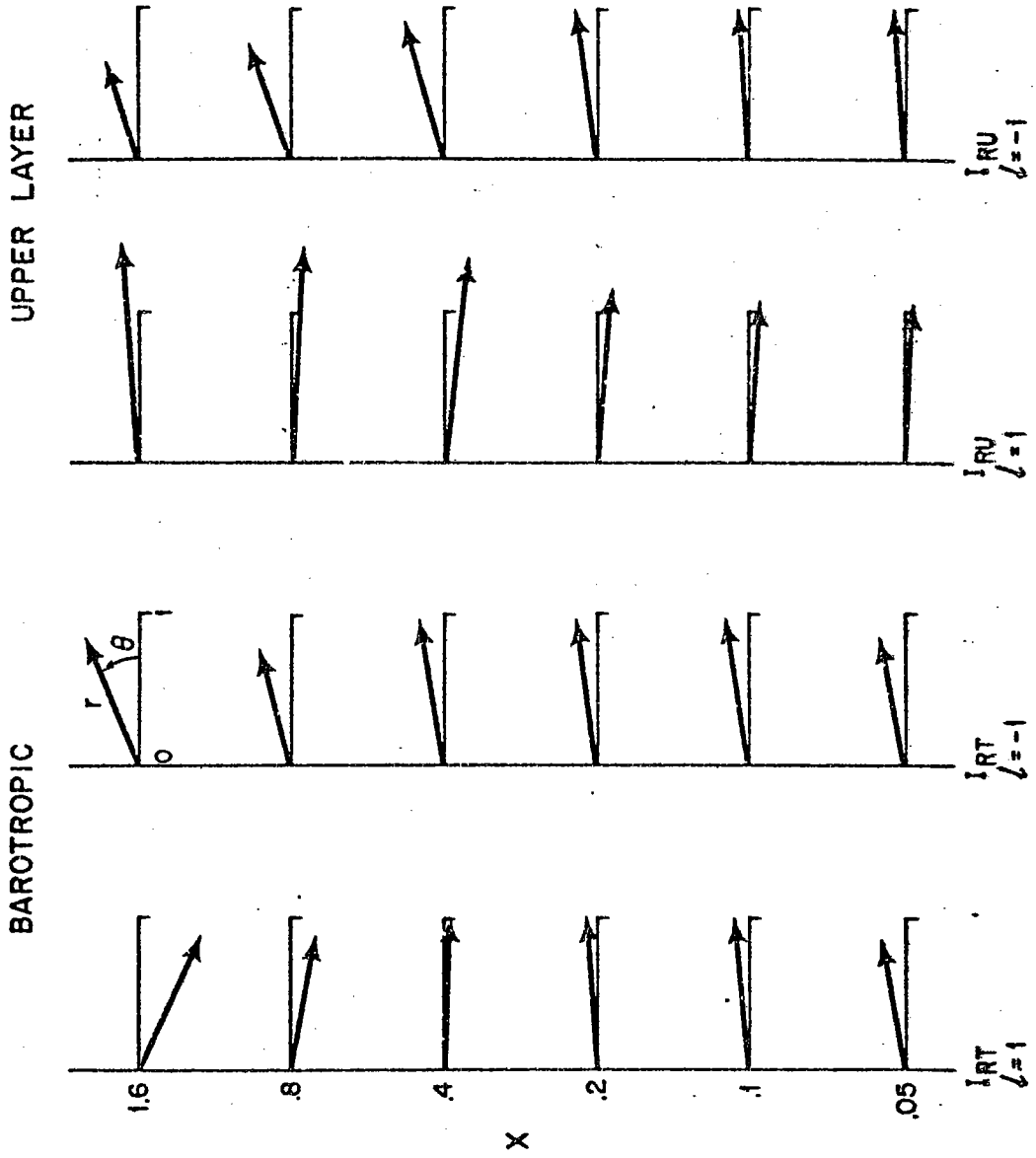

Figure 3.C-6a. Ridge model, I_{RT} and I_{RU} with $\Delta h = .5$ (Table 3.C-12b). Complex polar notation, $re^{i\theta}$.

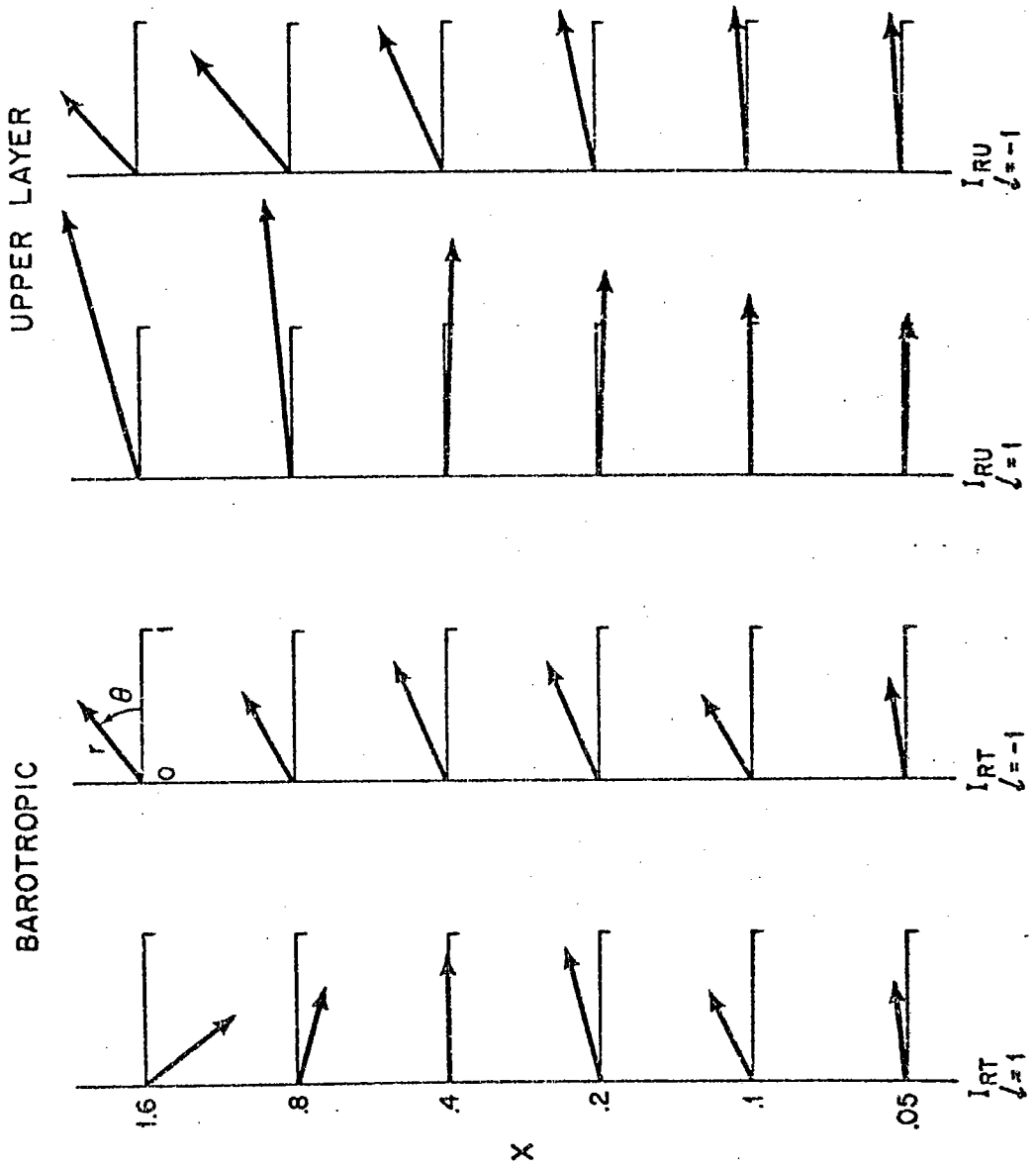

Figure 3.C-6b. Ridge model, I_{RT} and I_{RU} with $\Delta h = 1$ (Table 3.C-12c).

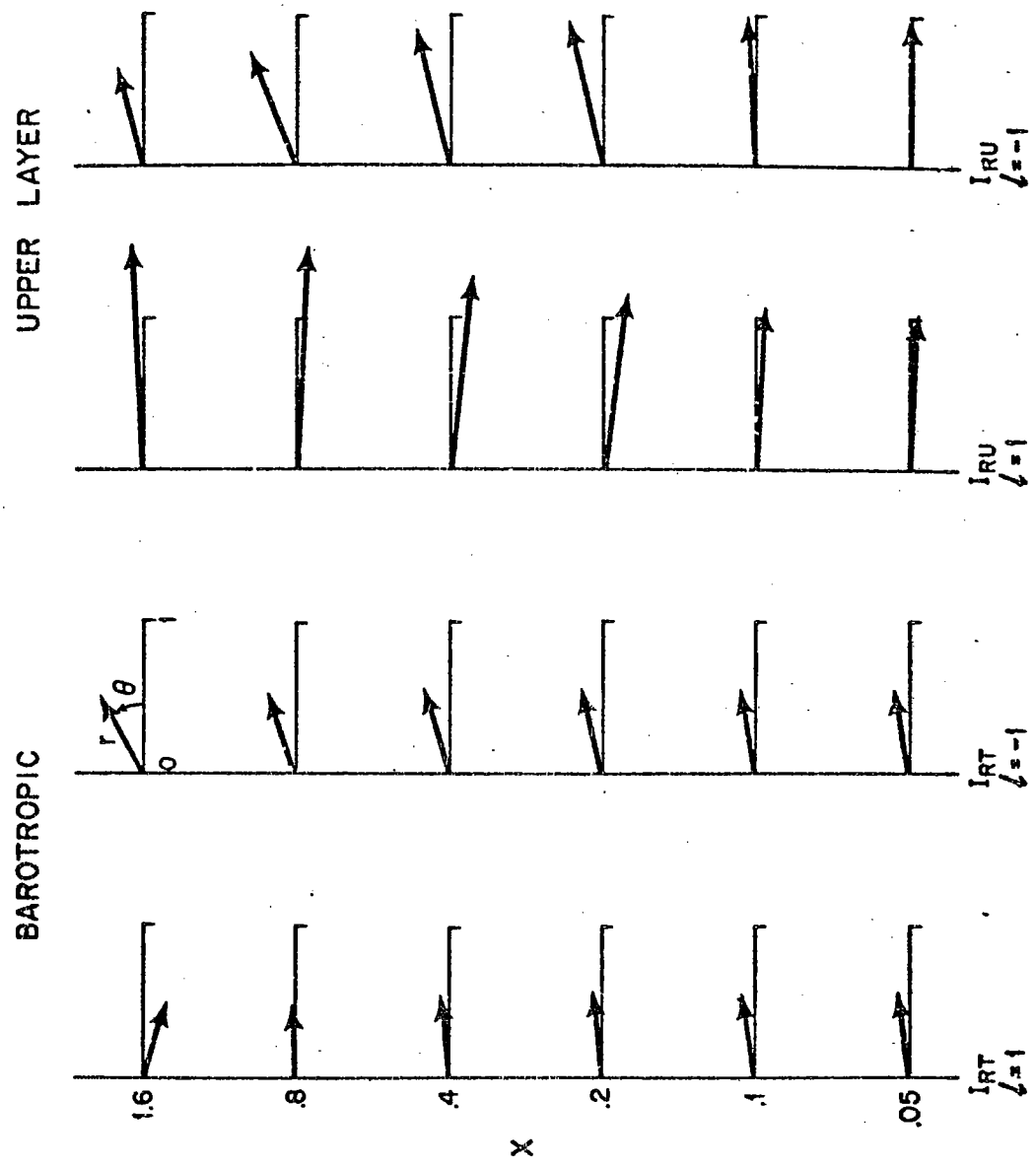

Figure 3.C-6c. Ridge-barrier model, I_{RT} and I_{RU} with $\Delta h = .5$ (Table 3.C-14b).

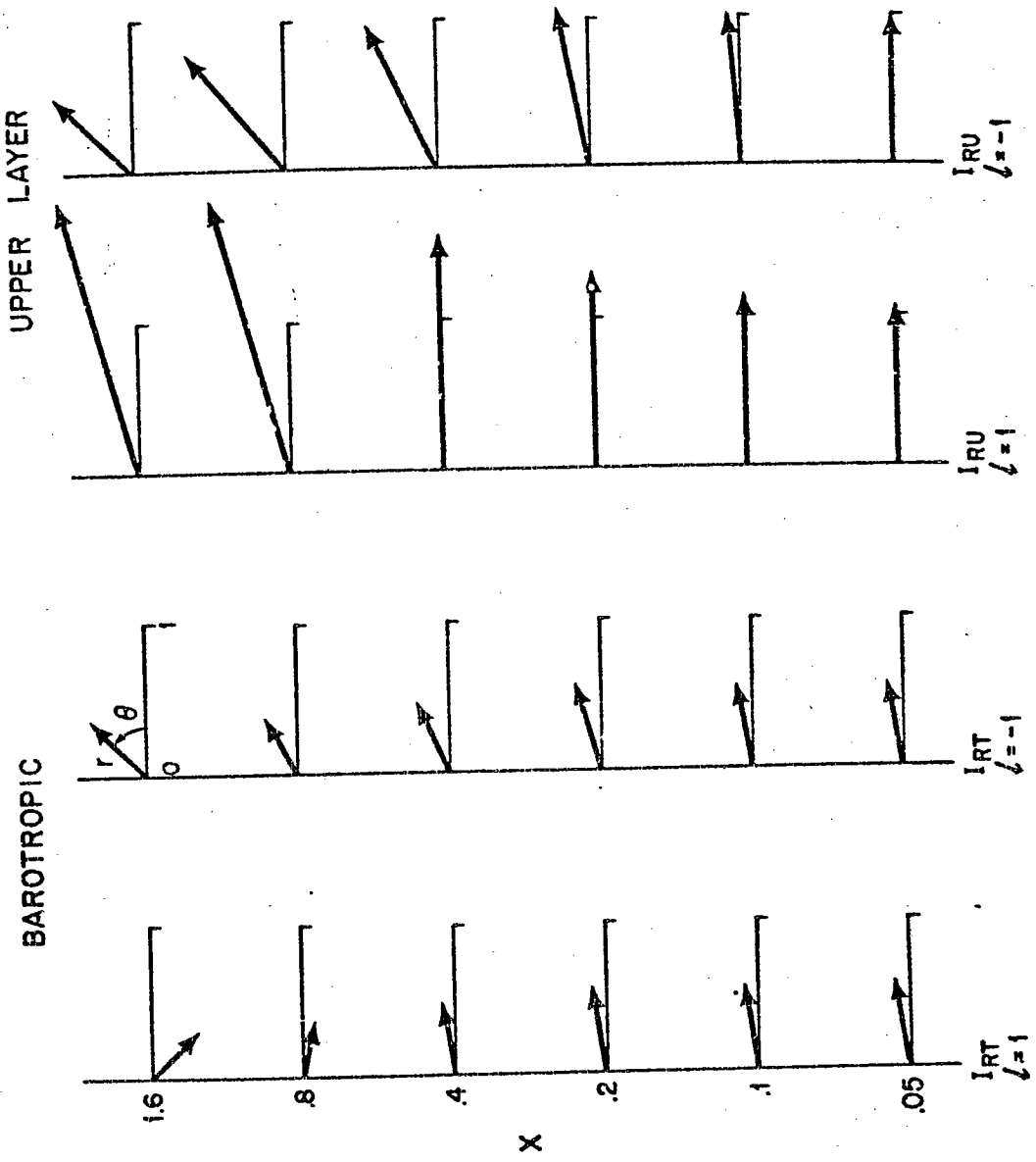

Figure 3.C-6d. Ridge-barrier model, I_{RT} and I_{RU} with $\Delta h = 1$ (Table 3.C-14c).

Table 3.C-12a

Ridge model, $\Delta h = .1$, $d = 0$.

	I_{RT}		I_{RU}	
X	r	θ	r	θ
.05	1.001	.01	.998	-.02
	1.001	.01	1.004	.02
.1	1.000	.00	1.007	-.02
	1.000	.01	.996	.02
.2	.999	-.01	1.019	-.03
	.999	.01	.988	.03
.4	.997	-.02	1.041	-.04
	.998	.02	.967	.05
.8	.995	-.04	1.085	-.04
	.995	.04	.927	.05
1.6	.997	-.08	1.090	-.01
	.996	.08	.916	.02

Table 3.C-12b

Ridge model, $\Delta h = .5$, $d = 0$.

	I_{RT}		I_{RU}	
X	r	θ	r	θ
.05	.867	.17	1.041	-.05
	.865	.19	1.012	.08
.1	.993	.10	1.070	-.08
	.993	.15	.994	.08
.2	.984	.04	1.145	-.09
	.986	.13	1.007	.12
.4	.944	-.03	1.263	-.12
	.950	.16	.936	.27
.8	.889	-.18	1.465	-.06
	.895	.23	.809	.36
1.6	.922	-.44	1.465	.07
	.909	.37	.685	.30

Table 3.C-12c

Ridge model, $\Delta h = 1$, $d = 0$.

	I_{RT}		I_{RU}	
X	r	θ	r	θ
.05	.631	.14	1.067	-.02
	.632	.17	1.05	.07
.1	.662	.47	1.195	-.00
	.655	.53	1.107	.08
.2	.910	.25	1.331	-.04
	.916	.38	1.117	.21
.4	.815	.10	1.542	-.03
	.847	.40	1.068	.40
.8	.618	-.27	1.855	.10
	.663	.51	1.023	.67
1.6	.729	-.92	1.846	.27
	.665	.69	.726	.76

Table 3.C-13a

Ridge model, $\Delta h = .1$, $d = .5$.

	I_{RT}		I_{RU}	
X	r	θ	r	θ
.05	.994	.01	1.005	-.01
	.994	.01	.998	.01
.1	.998	-.00	1.009	-.02
	.998	.01	.996	.02
.2	.998	-.01	1.020	-.03
	.998	.01	.987	.03
.4	.997	-.02	1.044	-.04
	.997	.02	.966	.05

Table 3.C-13b

Ridge model, $\Delta h = .5$, $d = .5$.

	I_{RT}		I_{RU}	
X	r	θ	r	θ
.05	.862	.11	1.051	-.04
	.861	.13	1.008	.05
.1	.932	.09	1.085	-.06
	.931	.13	1.015	.09
.2	.953	.03	1.151	-.09
	.955	.12	1.000	.15
.4	.931	-.03	1.281	-.10
	.937	.16	.950	.27

Table 3.C-13c

Ridge model, $\Delta h = 1$, $d = .5$.

	I_{RT}		I_{RU}	
X	r	θ	r	θ
.05	.681	.14	1.080	-.02
	.680	.17	1.035	.06
.1	.727	.23	1.164	-.02
	.725	.29	1.068	.12
.2	.819	.20	1.314	-.03
	.824	.33	1.094	.23
.4	.767	.09	1.552	-.00
	.798	.38	1.105	.42

Table 3.C-14a

Ridge-barrier model, $\Delta h = .1$, $d = 0$.

	I_{RT}		I_{RU}	
X	r	θ	r	θ
.05	.571	.14	1.019	.04
	.572	.14	1.011	.01
.1	.570	.13	1.026	.04
	.571	.15	1.004	.01
.2	.570	.13	1.034	-.04
	.571	.15	.993	.00
.4	.567	.12	1.061	-.06
	.572	.16	.975	.02
.8	.563	.10	1.101	-.06
	.573	.18	.933	.03
1.6	.563	.05	1.105	-.03
	.577	.22	.924	-.01

Table 3.C-14b

Ridge-barrier model, $\Delta h = .5$, $d = 0$.

	I_{RT}		I_{RU}	
X	r	θ	r	θ
.05	.571	.14	1.063	-.03
	.568	.16	1.013	-.00
.1	.566	.14	1.079	-.06
	.569	.17	1.011	.04
.2	.555	.12	1.156	-.11
	.567	.21	.985	.13
.4	.533	.10	1.285	-.10
	.554	.26	.936	.23
.8	.485	.04	1.471	-.06
	.537	.34	.804	.38
1.6	.509	-.33	1.490	.05
	.571	.51	.667	.26

Table 3.C-14c

Ridge-barrier model, $\Delta h = 1$, $d = 0$.

	I_{RT}		I_{RU}	
X	r	θ	r	θ
.05	.565	.14	1.069	-.01
	.561	.16	.998	.03
.1	.558	.15	1.176	.01
	.548	.20	1.016	.08
.2	.534	.17	1.318	-.02
	.538	.28	1.067	.20
.4	.457	.13	1.562	-.02
	.499	.40	1.055	.43
.8	.342	-.21	1.877	.11
	.422	.53	.992	.67
1.6	.412	-.78	1.868	.27
	.486	.79	.702	.76

Table 3.C-15a

Ridge-barrier model, $\Delta h = .1$, $d = .5$.

	I_{RT}		I_{RU}	
X	r	θ	r	θ
.05	.573	.14	1.032	-.02
	.573	.14	1.021	-.01
.1	.573	.14	1.036	-.03
	.578	.15	1.017	-.00
.2	.572	.13	1.048	-.04
	.574	.15	1.008	.01
.4	.570	.12	1.072	-.05
	.574	.16	.987	.03

Table 3.C-15b

Ridge-barrier model, $\Delta h = .5$, $d = .5$.

	I_{RT}		I_{RU}	
X	r	θ	r	θ
.05	.571	.14	1.064	-.03
	.570	.16	1.021	.02
.1	.569	.14	1.104	-.05
	.570	.17	1.013	.05
.2	.559	.13	1.173	-.08
	.567	.21	.994	.12
.4	.533	.10	1.304	-.09
	.556	.26	.941	.24

Table 3.C-15c

Ridge-barrier model, $\Delta h = 1$, $d = .5$.

	I_{RT}		I_{RU}	
X	r	θ	r	θ
.05	.567	.15	1.079	-.01
	.567	.17	1.033	.04
.1	.558	.15	1.158	-.01
	.558	.20	1.045	.10
.2	.533	.16	1.307	-.02
	.541	.27	1.065	.21
.4	.461	.14	1.550	.01
	.499	.00	1.077	.42

The upper layer response as indicated by I_{RU} is almost identical in the ridge and ridge-barrier models. In general $|I_{RU}|$ is smaller for $\ell = -1$ than for $\ell = 1$, and when the slope is moderate $|I_{RU}| < 1$ for $\ell = -1$. This can be explained in terms of the scattering mechanism. Since short waves are of little importance over the ridge (unless the ridge is very narrow), the flow at the crest of the ridge is controlled by conditions to the east. Since $s = 1$ for the eastern slope, $\ell = 1$ implies that the upper layer wave is 'barotropic' and the lower layer wave is 'baroclinic.' The barotropic part of the motion in the flat region to the east excites these two waves such that their upper layer motions are 180° out of phase but their lower layer motions are in phase (see Figure 3.C-7). West of the junction the relative phases of the two modes will change due to their differing phase speeds. Since the upper layer components were initially opposite in phase, any change in relative phase must increase the net upper layer flow while reducing the lower layer flow. When $\ell = -1$ the reverse occurs: upper layer flow is reduced and lower layer flow is increased.

The phase of I_{RU} shows two tendencies: the average of the phases for $\ell = 1$ and for $\ell = -1$ is positive, so there is a general time lag introduced by the topography; and the phase for $\ell = -1$ is greater than that for $\ell = 1$. The first tendency is due to the finite westward phase speed of the

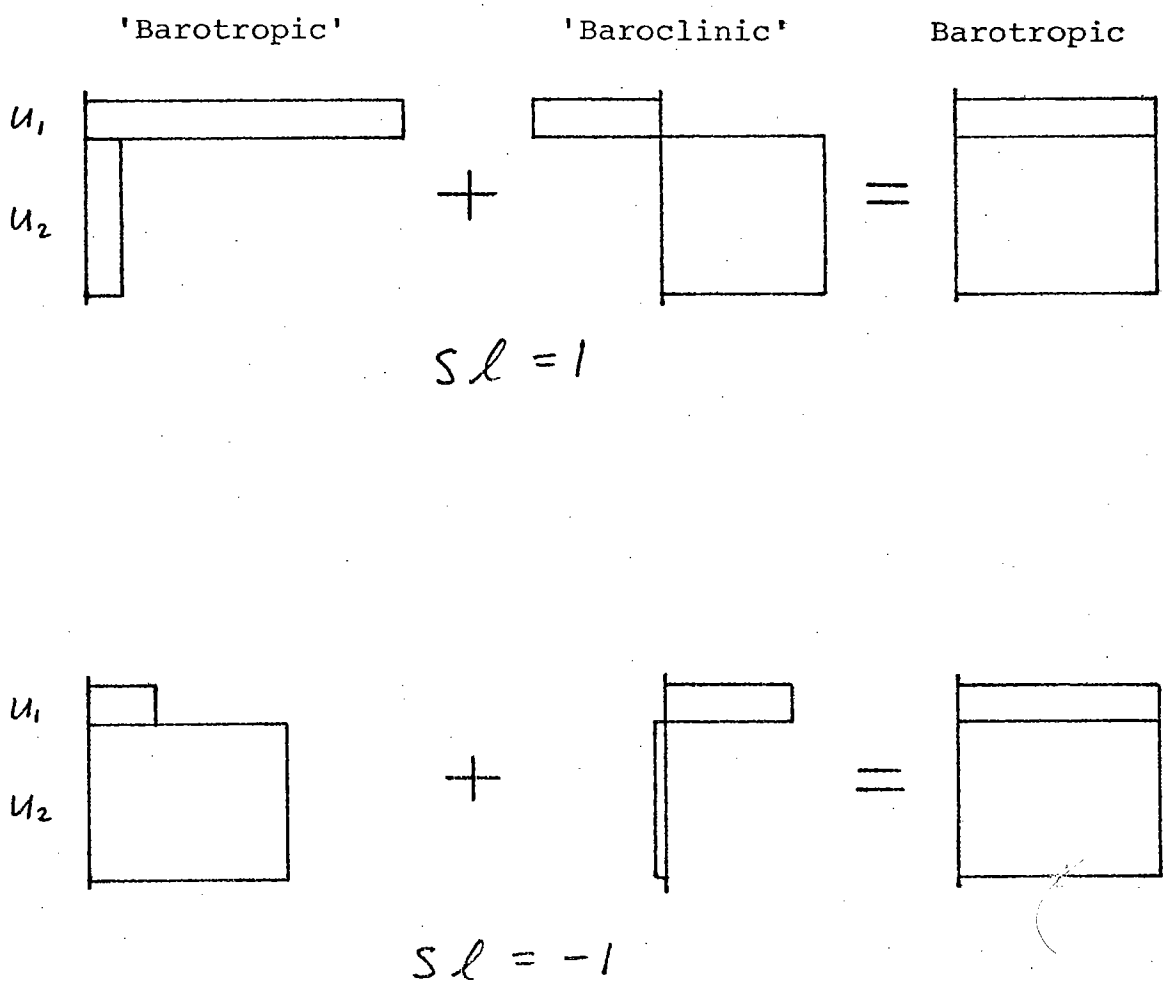

Figure 3.C-7

Sketch of the translation of a barotropic flat-bottom mode into a sum of 'barotropic' and 'baroclinic' slope modes.

upper layer waves that carry much of the upper layer flow over the slope. The second tendency is a bit more complicated. The upper layer flow in region I is the sum of two parts of comparable magnitude and a phase difference of $\pi/2$. One part comes from the Sverdrup balance and the second part comes from the baroclinic directly forced motion. (We are neglecting the baroclinic wave from the eastern boundary in these calculations.) The baroclinic part is relatively unchanged over the slope, while the Sverdrup part is increased in amplitude when $\ell = 1$ and decreased when $\ell = -1$ as explained in the previous paragraph. The addition of a larger Sverdrup component at roughly zero relative phase to a constant baroclinic component with phase $\pi/2$ gives a sum with an earlier phase than if the Sverdrup component were smaller. Hence the phase of I_{Ru} is earlier for $\ell = 1$ than for $\ell = -1$. This explanation neglects other factors, such as the larger value of p_{IF} for $\ell = 1$ than for $\ell = -1$, that may also affect I_{Ru}.

Comparison of Tables 3.C.-12 with 13 and 14 with 15 shows that even the large amount of dissipation represented by $\delta = .5$ has almost no effect on I_{Ru} and little effect on I_{RT}. The phase of I_{RT} for $\Delta h = 1$ and X = .1 in the ridge model is reduced by dissipation to be more in line with the phases for other ridge widths. Elsewhere there are no significant differences.

4. Summary

The main points of this section can be given in the form of answers to the three questions asked at the beginning of the section.

The model of a slope at the eastern boundary indicates that the slope plays little role in determining the overall response of the basin to large scale annual forcing. The only slopes that were found to have an appreciable effect were those of X = .8 and 1.6, Δh = .5 and 1. Even in these examples the maximum phase change of the barotropic response was .4 radians, or less than one month.

Comparison of the barrier model to the ridge and ridge-barrier models shows that the simple barrier model is quite good for ridges with a half-width of about 200 km or less. The effects of the slopes become increasingly important for wider ridges. A wide slope may nearly double the upper layer flow at the crest of the ridge, but the phase change in the most extreme case (for which flow over the ridge is decreased) is less than a month and a half. For more realistic ridges the changes are insignificant.

The ridge model with Δh = .5 and X = .8 is a reasonable first approximation of the Mid-Atlantic Ridge. Its effect on the barotropic response is under 15% in amplitude and under two weeks in phase.

D. The eight-layer barrier problem

The thin barrier model developed at the beginning of this chapter is highly idealized. In the previous section we saw that making the model more realistic by adding slopes of moderate width has little effect on the behavior of the model. In this section we will return to the thin barrier but will consider the effect of more realistic stratification. The mathematical structure of the two-layer problem can immediately be generalized to treat any number of layers with a barrier extending to any of the interfaces. Hence we can use a multi-layer model to approximate a continuously stratified fluid with a barrier of any height.

The multi-layer model used here is that of Lighthill (1969). All variables in this section will be dimensional. Superscripts will label layers, subscripts will label modes. Suppose there are N layers with densities and thicknesses ρ^i and H^i respectively, with the layers numbered starting with $i=1$ at the top. Define the matrix

$$A_{jk} \equiv \begin{cases} H^k \rho^k / \rho^j & k < j \\ H^k & k \geq j \end{cases} \qquad (3.D.1)$$

Then the eigenvalues H_i are the "equivalent depths" and the eigenvectors, when arranged as the columns of the matrix C_{ij}, specify the vertical normal modes of the system. Mode variables are related to layer variables by

$$p^i = \sum_{j=0}^{N-1} e_{ij}\, p_j \qquad (3.D.2)$$

For convenience the modes are ordered by decreasing value of H_i, starting with the barotropic value $H_0 \simeq \sum_{j=1}^{N} H^j$.

As in the two layer problem, the velocity is related to the pressure by the geostrophic balance, all variables are proportional to $e^{-i\omega t}$, and the limit $\omega \ll f$ is taken. The lowest order beta plane model then gives the familiar vorticity equation for each pressure mode,

$$-i\omega\left(\nabla^2 p_i - \lambda_i^{-2} p_i\right) + \beta p_{ix} = 0 \qquad (3.D.3)$$

with $\lambda_i^{-2} \equiv f^2/g H_i$. Plane wave solutions $p = e^{ik_j x} e^{ily}$ are governed by the dispersion relation

$$k_j^2 + \frac{\beta}{\omega} k_j + l^2 + \lambda_j^{-2} = 0 \qquad (3.D.4)$$

Subscripts W and E will again distinguish long from short waves.

The milti-layer barrier problem is solved in exactly the same way as the two-layer problem. Suppose that at the barrier at $x = 0$ there is some initial flow expressed as a superposition of vertical normal modes p_{Ii}. Let the

barrier extend to the interface between layer M and layer $M+1$, so there are M layers that are above the barrier. The matching conditions applied at $x=0$ are continuity of u and v above the barrier and $u=0$ on both sides below the barrier. Hence there are $2N$ conditions determining the amplitudes of $2N$ free waves. However, as we saw in the two-layer problem, the pressure amplitudes must be the same on both sides of the barrier, so we are left with only N conditions on N amplitudes:

$$\sum_{j=0}^{N-1} p_{Bj} C_{ij} \Delta k_j = 0, \quad 1 \le i \le M \tag{3.D.5a}$$

$$\sum_{j=0}^{N-1} p_{Bj} C_{ij} = -\sum_{j=0}^{N-1} p_{Ij} C_{ij}, \quad M < i \le N \tag{3.D.5b}$$

where

$$\begin{aligned} \Delta k_j &\equiv k_{jE} - k_{jW} \\ &= -\left[\left(\frac{\beta}{\omega}\right)^2 - 4\left(l^2 + \lambda_j^{-2}\right)\right]^{1/2}. \end{aligned} \tag{3.D.6}$$

Note that $\Delta k_j < 0$ if k_j is real, but $\mathrm{Im}(\Delta k_j) > 0$ if k_j is imaginary. The linear algebraic equations (3.D.5) are easily solved for any numerical example, and (3.D.2) can then be used to determine the flow over the barrier in each layer.

For all numerical examples we choose $N=8$ and a total depth of 4000 m. There are four types of stratification considered (Figure 3.D-2): 1) linear stratification, with both the layer thickness and the density difference constant; 2) exponential stratification, with constant layer thickness but larger density jumps toward the top; 3) exponential stratification, with constant density differences but thicker layers toward the bottom; 4) irregular stratification, with constant layer thickness everywhere, but with a small constant density difference at the lower five interfaces, a large difference at the sixth interface from the bottom, and an intermediate difference at the top interface, just below the free surface. The normal modes for each type of stratification are shown in Figure 3.D-1 and the equivalent depths and values of Δk are in Table 3.D-1. Not surprisingly, the details of the stratification are most evident in the higher modes. In particular, note that when exponential stratification is achieved through variable density jumps, the higher modes are bottom intensified, while the reverse is true when layer thickness is varied.

The barrier problem was solved with each type of stratification, with the barrier extending to each interface in turn. In one case the initial flow had a first baroclinic mode structure; in all the others a barotropic initial flow was used. All computations were made with a 1000 km meridional length

Table 3.D-1

H_j in meters and Δk_j in $10^{-4}m^{-1}$ for each example of stratification.

	Linear		Exponential-Density	
j	H_j	Δk_j	H_j	Δk_j
0	3998	-0.992	3398	-0.992
1	1.309	-0.906	1.347	-0.909
2	0.3404	-0.595	0.3476	-0.606
3	0.1615	0.586i	0.1675	0.544i
4	0.0996	1.081i	0.1049	1.029i
5	0.0722	1.409i	0.0722	1.409i
6	0.0587	1.633i	0.0488	1.846i
7	0.0519	1.773i	0.0307	2.449i

	Exponential-depth		Irregular	
j	H_j	Δk_j	H_j	Δk_j
0	3997	-0.992	3997	-0.992
1	1.279	-0.904	1.980	-0.936
2	0.3361	-0.589	0.3412	-0.597
3	0.1602	0.595i	0.2145	0.124i
4	0.0995	1.082i	0.0968	1.110i
5	0.0725	1.405i	0.0494	1.833i
6	0.0575	1.658i	0.0331	2.344i
7	0.450	1.944i	0.0267	2.656i

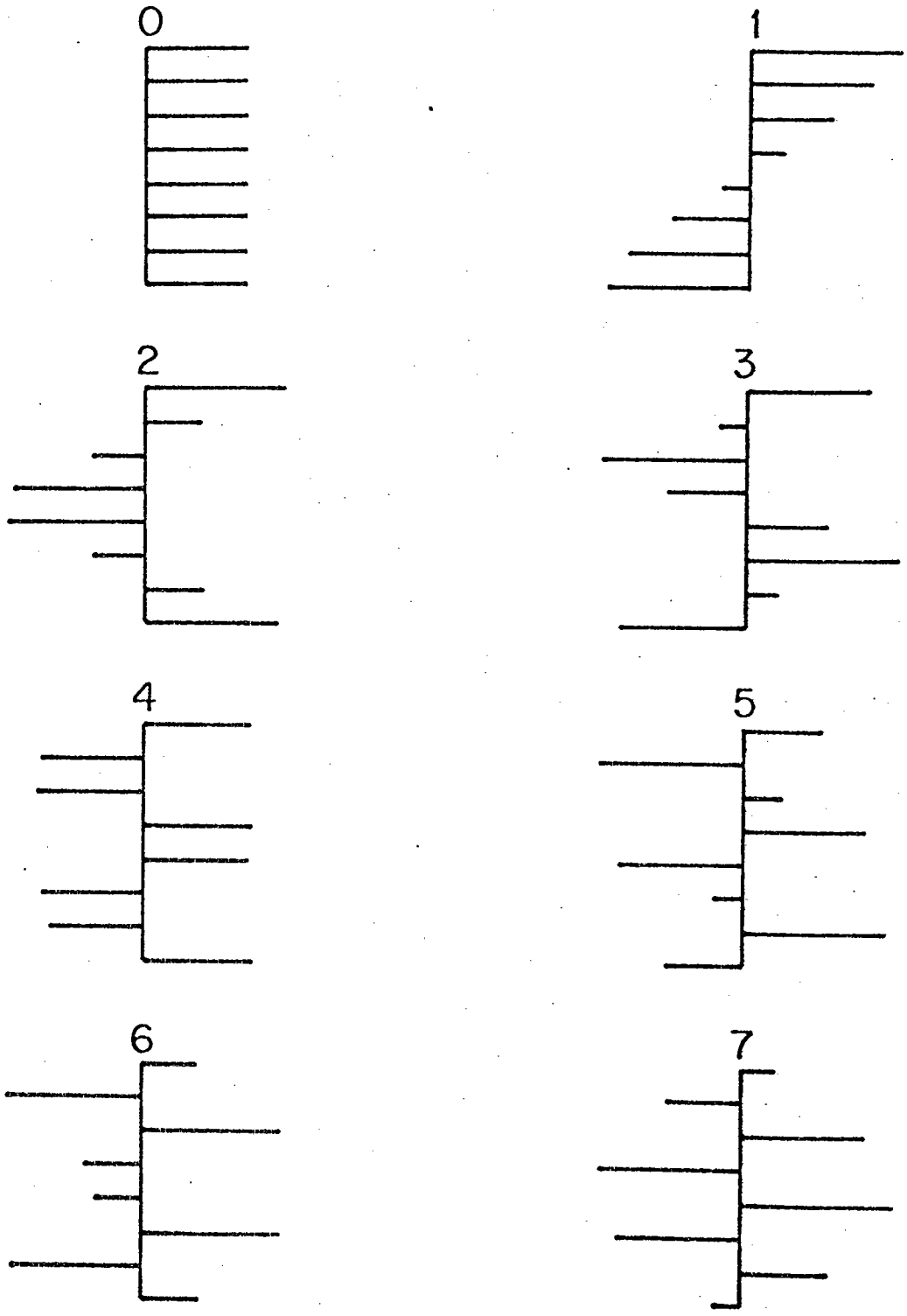

Figure 3.D-1a. Normal modes of eight-layer system with linear stratification.

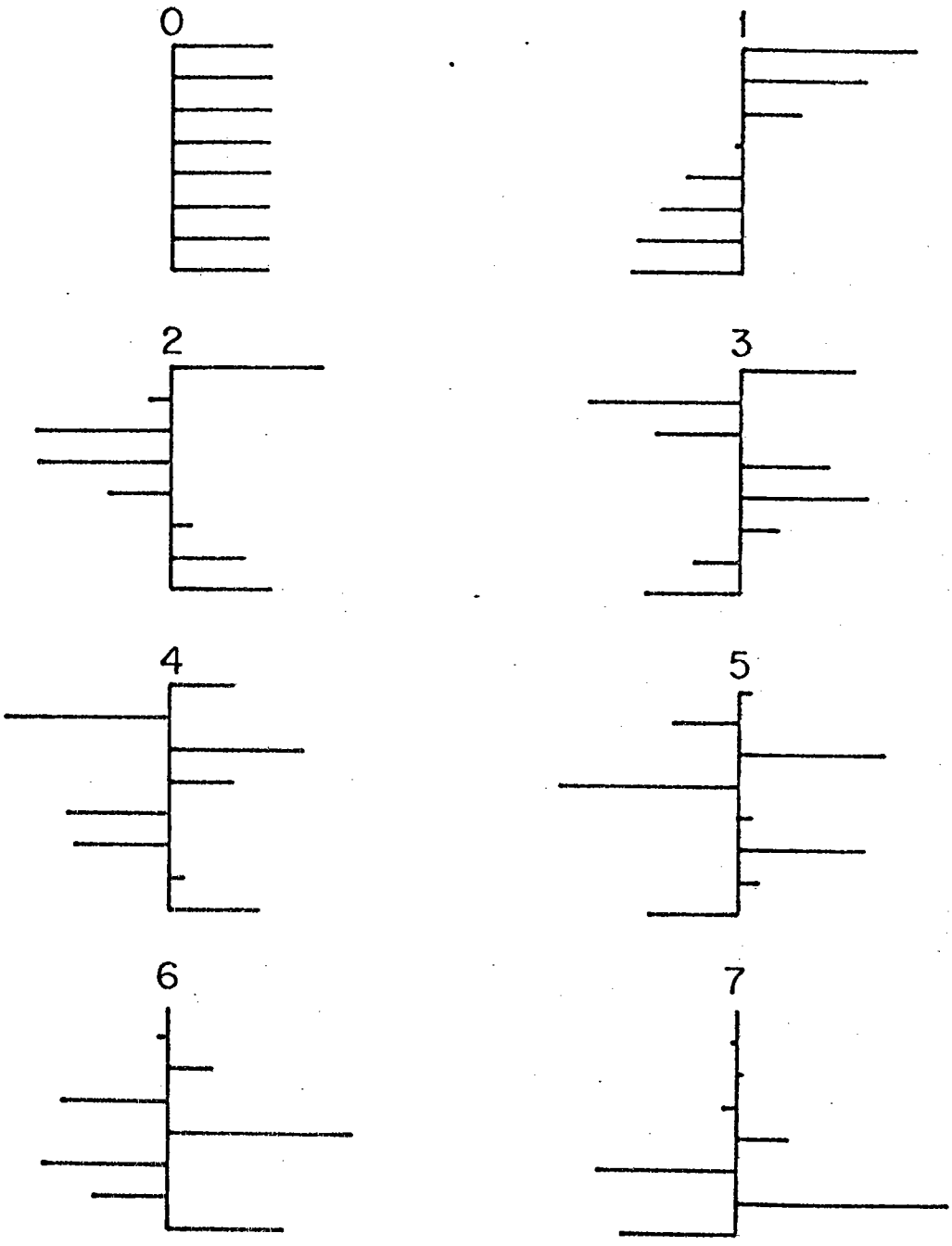

Figure 3.D-1b. Normal modes of eight-layer system with exponential stratification, equal layer depths.

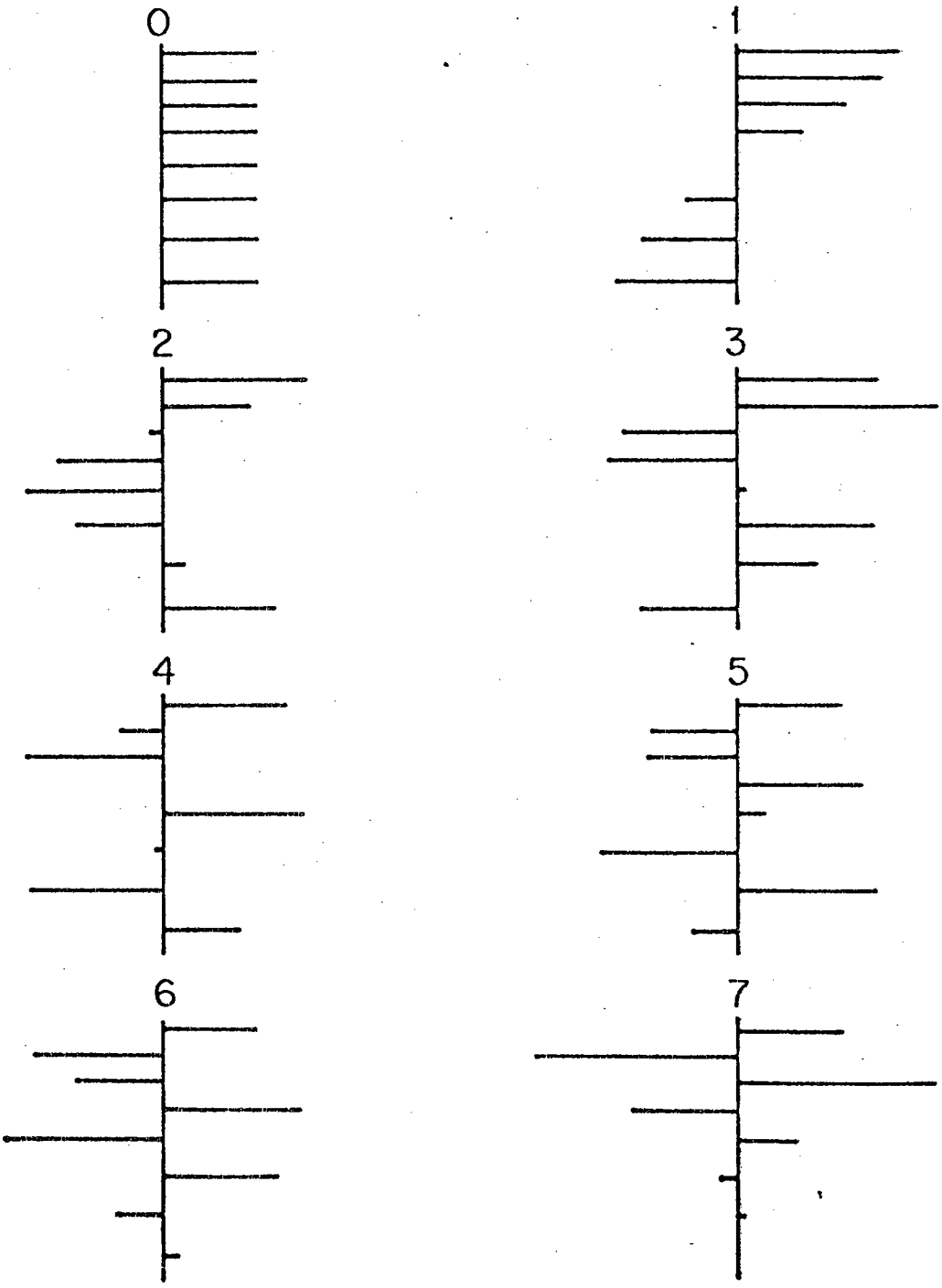

Figure 3.D-1c. Normal modes of eight-layer system with exponential stratification, equal density differences.

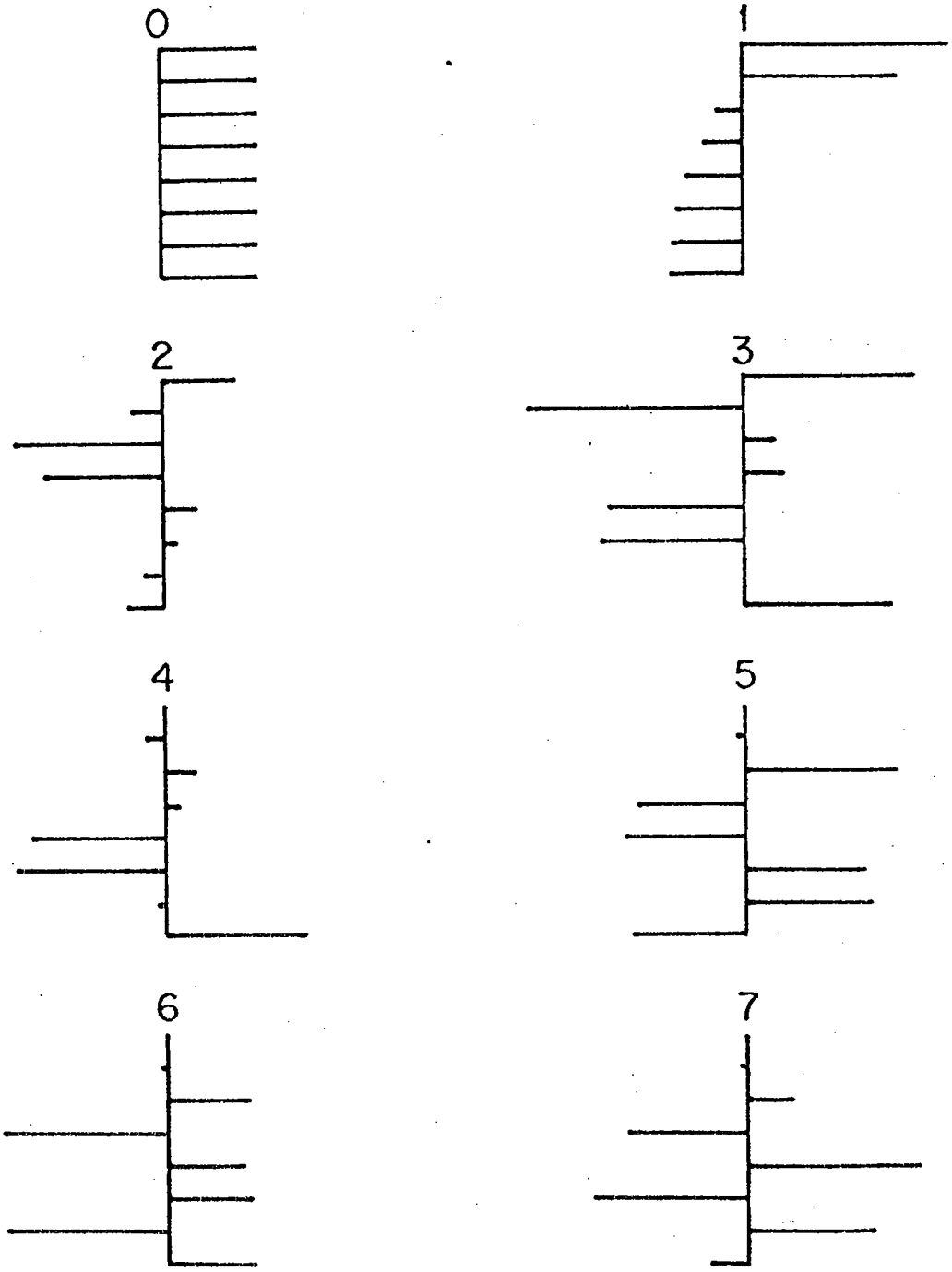

Figure 3.D-1d. Normal modes of eight-layer system with irregular stratification.

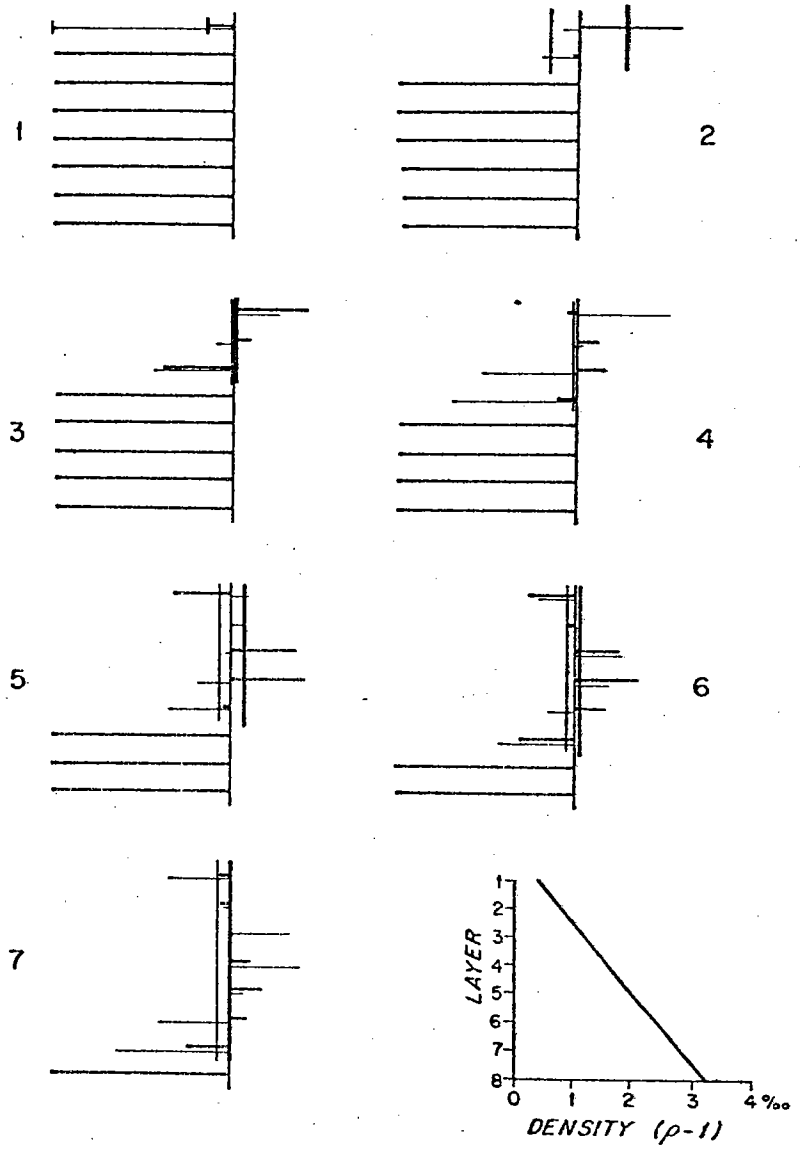

Figure 3.D-2a. Motion induced by barriers of various height due to an incoming barotropic wave. Heavy (light) horizontal lines are the pressure amplitudes in each layer induced by the barrier in phase (90° out of phase) with the incoming wave. A heavy line to the right augments the incoming flow. The heavy (light) vertical lines are averages of the in-phase (90° leading) flow over the barrier induced by the barrier. The number to the side is the number of layers above the barrier. Stratification is linear.

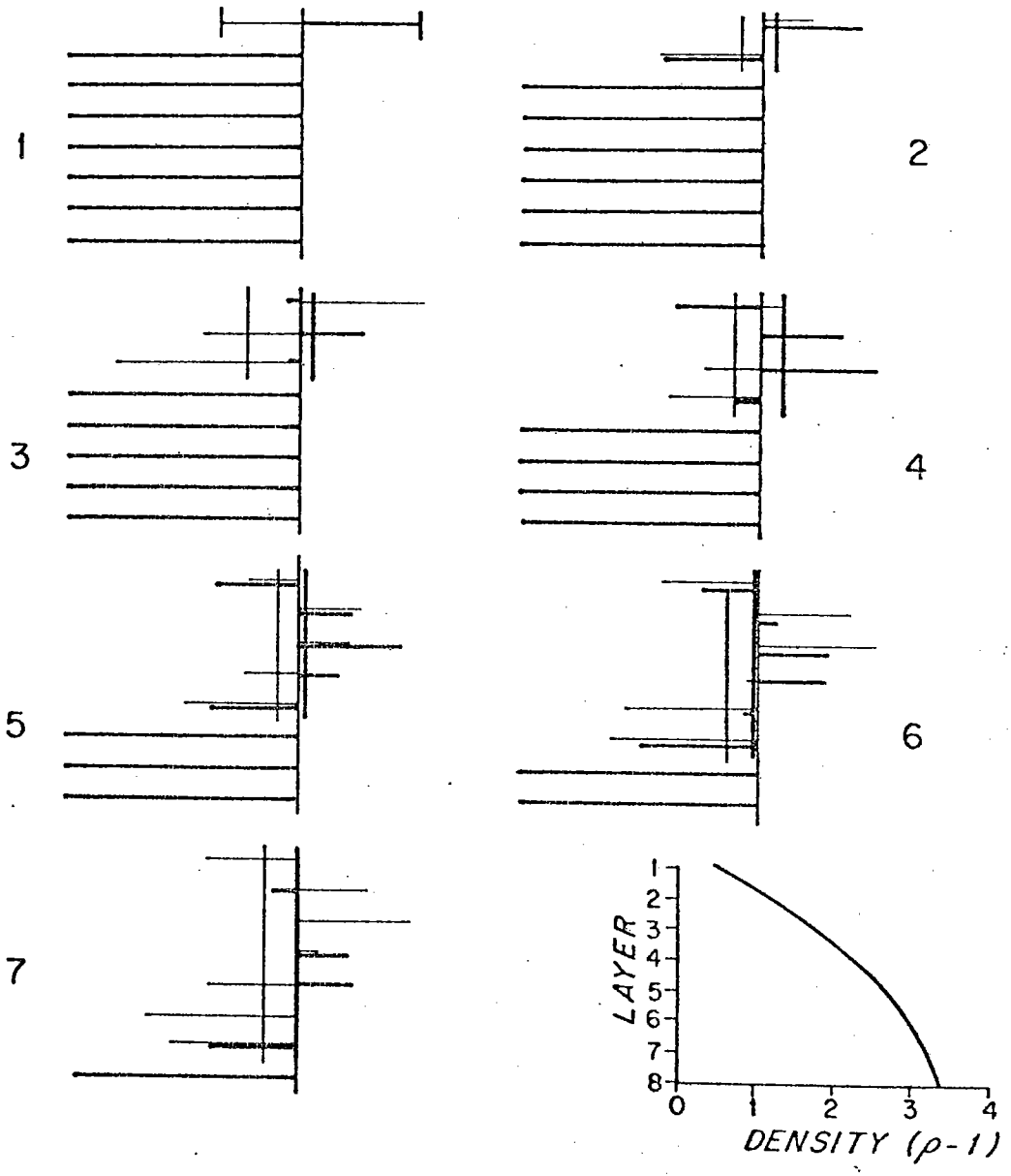

Figure 3.D-2b. Eight-layer barrier, exponential-density stratification, barotropic incident wave.

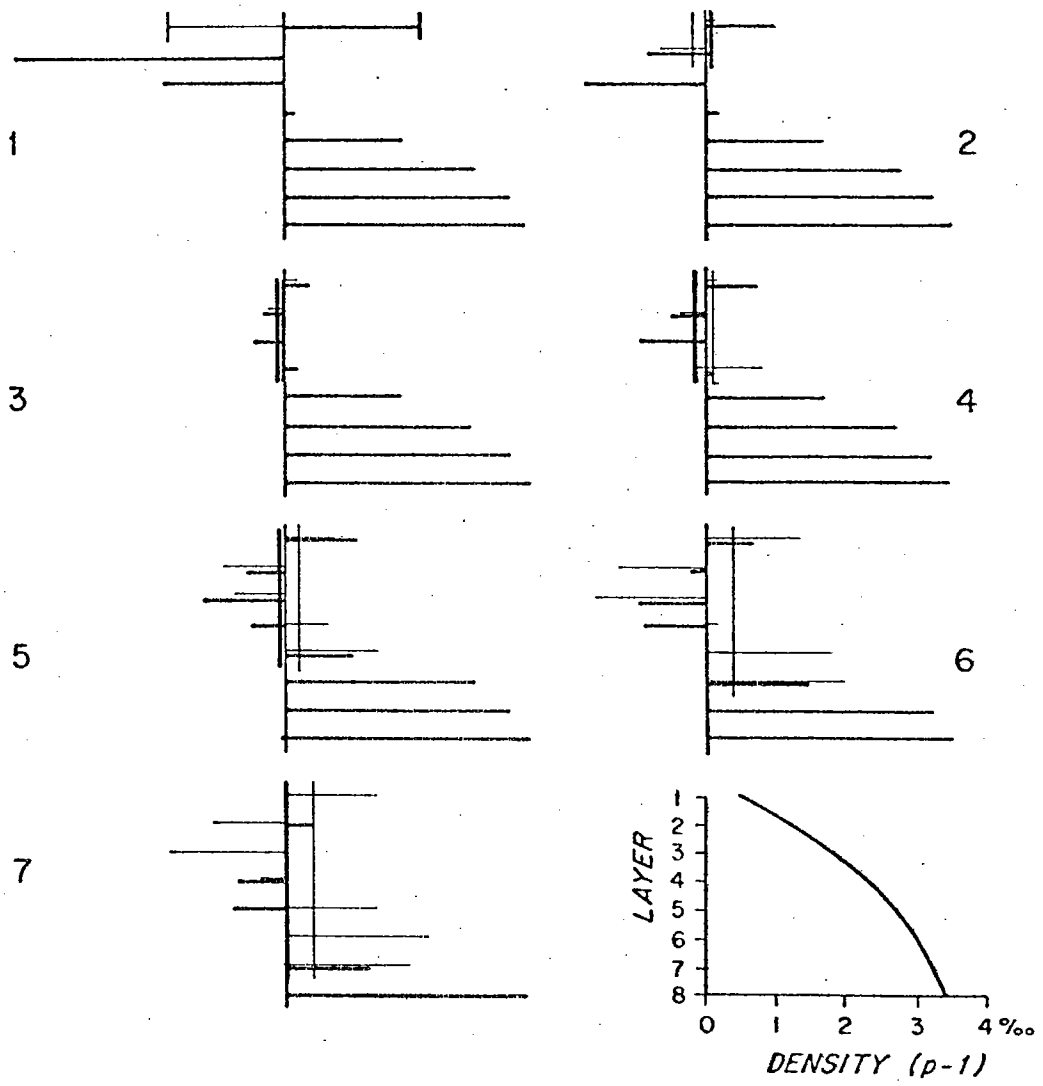

Figure 3.D-2c. Eight-layer barrier, exponential-density stratification, baroclinic incident wave.

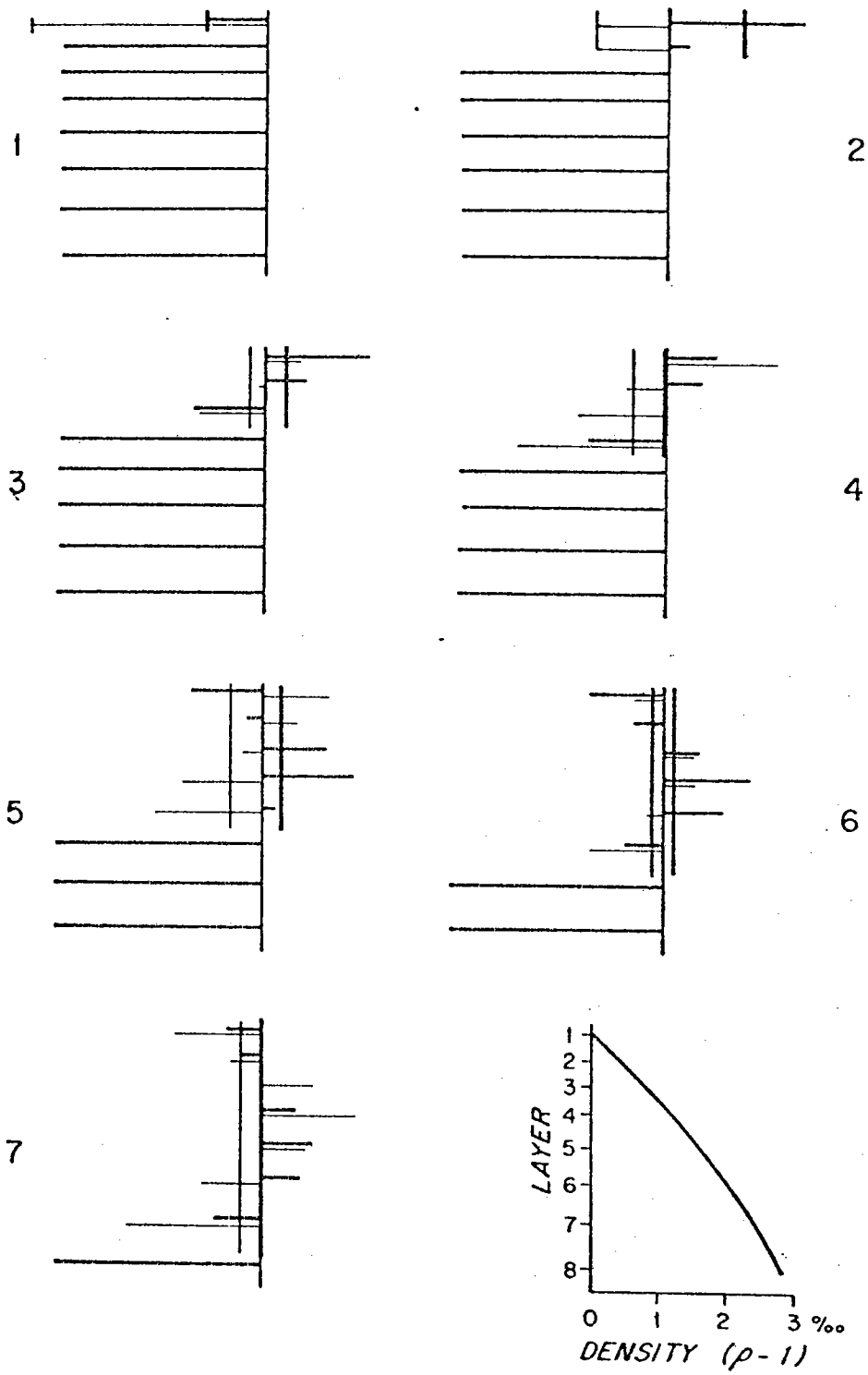

Figure 3.D-2d. Eight-layer barrier, exponential-depth stratification, barotropic incident wave.

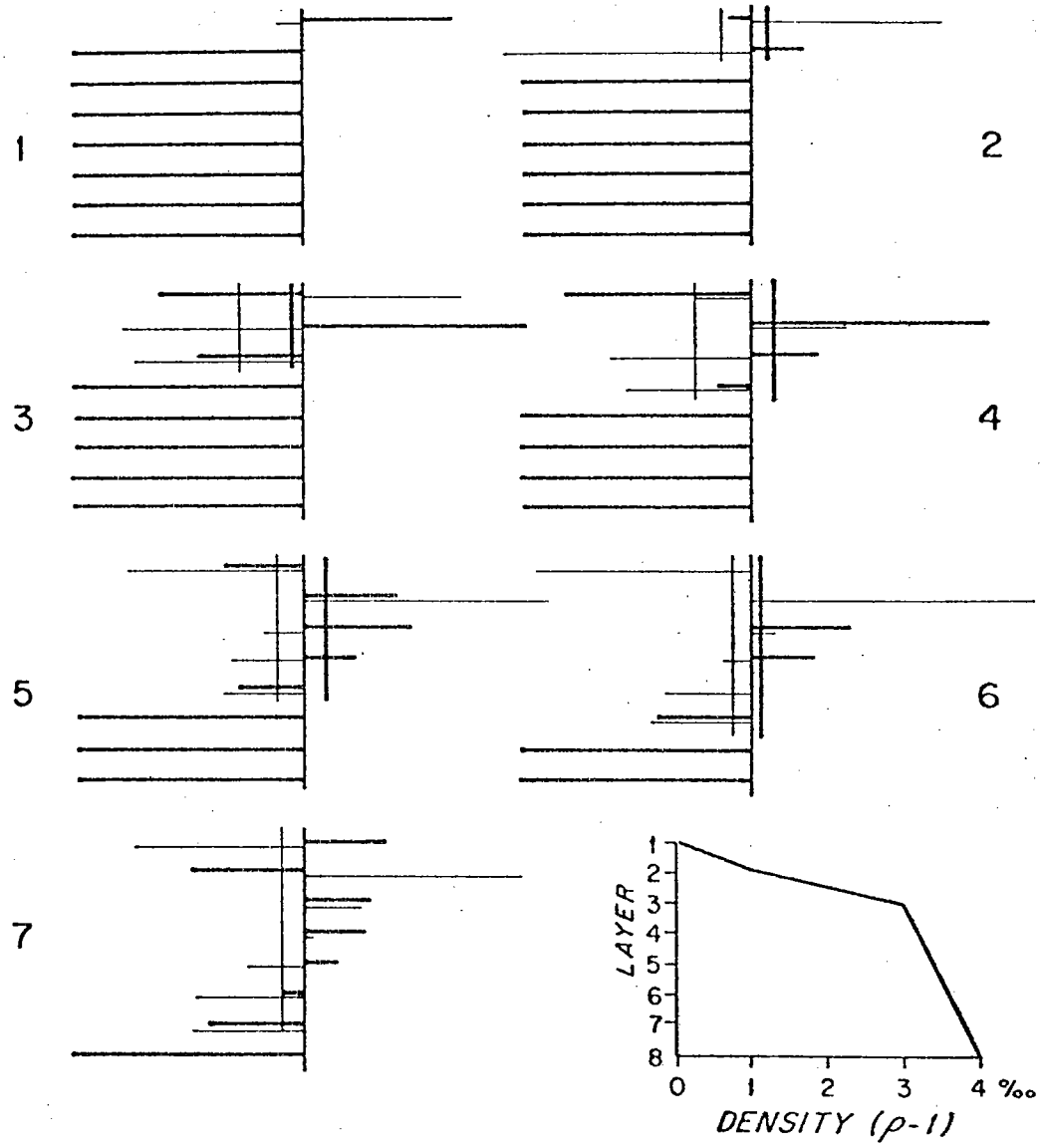

Figure 3.D-2e. Eight-layer barrier, irregular stratification, barotropic incident wave.

scale, annual period, and a central latitude of 20°N. The results of the computations expressed in terms of pressure in each layer due to the barrier, p_B^j , are given in Figure 3.D-2. The average pressure induced by the barrier on the layers over the barrier is also shown. This is a measure of the overall effect of the barrier in the zonal flux over its crest.

Figure 3.D-2 shows that although there is considerable barrier induced flow above the barrier, its average is rather small, usually less than a fifth of the initial flow. In most cases the average in-phase component augments the initial flow (if barotropic), while the out-of-phase component produces a phase lag. In other words, the barrier increases and delays the flow above the barrier. This is the same sort of behavior as was found in the two-layer model. There the flow was increased with no phase change so long as K was real, while a phase lag was introduced when K was imaginary. In the multilayer problem the solution is composed of low modes with real Δk and high modes with imaginary Δk, so the net result is both a phase lag and increased flow. However, when the initial motion is baroclinic and the barrier is lower than the zero crossing of the mode, a phase lag and decreased flow are found. This is to be expected, since the part of the initial flow that can influence the solution is the part below the barrier, which is opposite to the shallow flow.

Comparison of the results for different stratifications shows that the barrier has the least effect when the stratification is linear, and the most when it is irregular. This seems reasonable in view of the larger maximum layer velocities in the higher modes with irregular stratification, but the precise explanation is unclear.

In conclusion, the main result of the multi-layer barrier model is a confirmation of the two-layer result. Except when the barrier blocks all but the topmost layer, the flow induced by the barrier tends to average out to a small fraction of the initial flow. For the most part, the water column is sheared off by the barrier; the lower part is blocked but the upper part proceeds as if nothing had happened, at least in the immediate vicinity of the barrier.

Chapter IV

OBSERVATIONS

A. North Atlantic Winds

The theory presented in the preceding chapters relates primarily to motions forced by annual wind variations. We have assumed that these wind variations have a meridional length scale much larger than the internal Rossby radius of deformation, are fairly uniform in the zonal direction, and are of sufficient amplitude to be worth thinking about. To confirm the validity of these assumptions, let us briefly survey the characteristics of the annual cycle of wind stress in the mid-latitude North Atlantic. This will enable us to make specific predictions of some of the annual current variations forced by the winds.

The best currently available calculations of windstress are the work of Bunker (1976). He used a drag coefficient depending on wind speed and air-sea temperature difference to compute wind stress. Wind speed data came from ship reports collected by the National Climatic Center from 1941-1972. Monthly means were computed for an irregular grid of subdivisions of North Atlantic Marsden squares. The grid was designed to maximize resolution in regions of high gradient such as the Gulf Stream, and to reflect the variations in density of observations in different areas. Over

most of the area from 10°N to 40°N the grid consists of rectangles 2° latitude by 5° or sometimes 10° longitude. The errors involved in computing wind stress curl from these data are discussed by Leetmaa and Bunker (1978).

The annual cycle of wind stress curl was computed from Bunker's stress values through simple hand processing. Interpolation and averaging was used where necessary (interpolation being needed mostly east of 40°W between 10° and 30°N) to obtain monthly stress values on a regular grid of boxes 2° latitude by 10° longitude. Sine and cosine transforms of the monthly values yielded annual and semiannual harmonics. These were then smoothed meridionally using the filter $\tau_i' = \frac{1}{16}(\tau_{i-2} + \tau_{i+2}) + \frac{1}{4}(\tau_{i-1} + \tau_{i+1}) + \frac{3}{8}\tau_i$ where i is incremented for each 2° of latitude. A simple two-point difference was then used to compute the $-\tau^x_y$ component of the curl, which accounts for most of the total. The τ^y_x component of the curl was computed as an integral across the width of the ocean and added to the sum of the $-\tau^x_y$ components to get the total zonally averaged curl.

Some results of these calculations are shown in Figures 4.A-1 through 4. Comparison of Figure 4.A-1b with 4.A-3a,b shows that the amplitude of the annual harmonics of stress curl is typically about half of the mean. The semiannual harmonic is comparable to, but generally smaller than, the annual. It tends to be of greatest importance between about 28°N and 14°N. We see that although there is

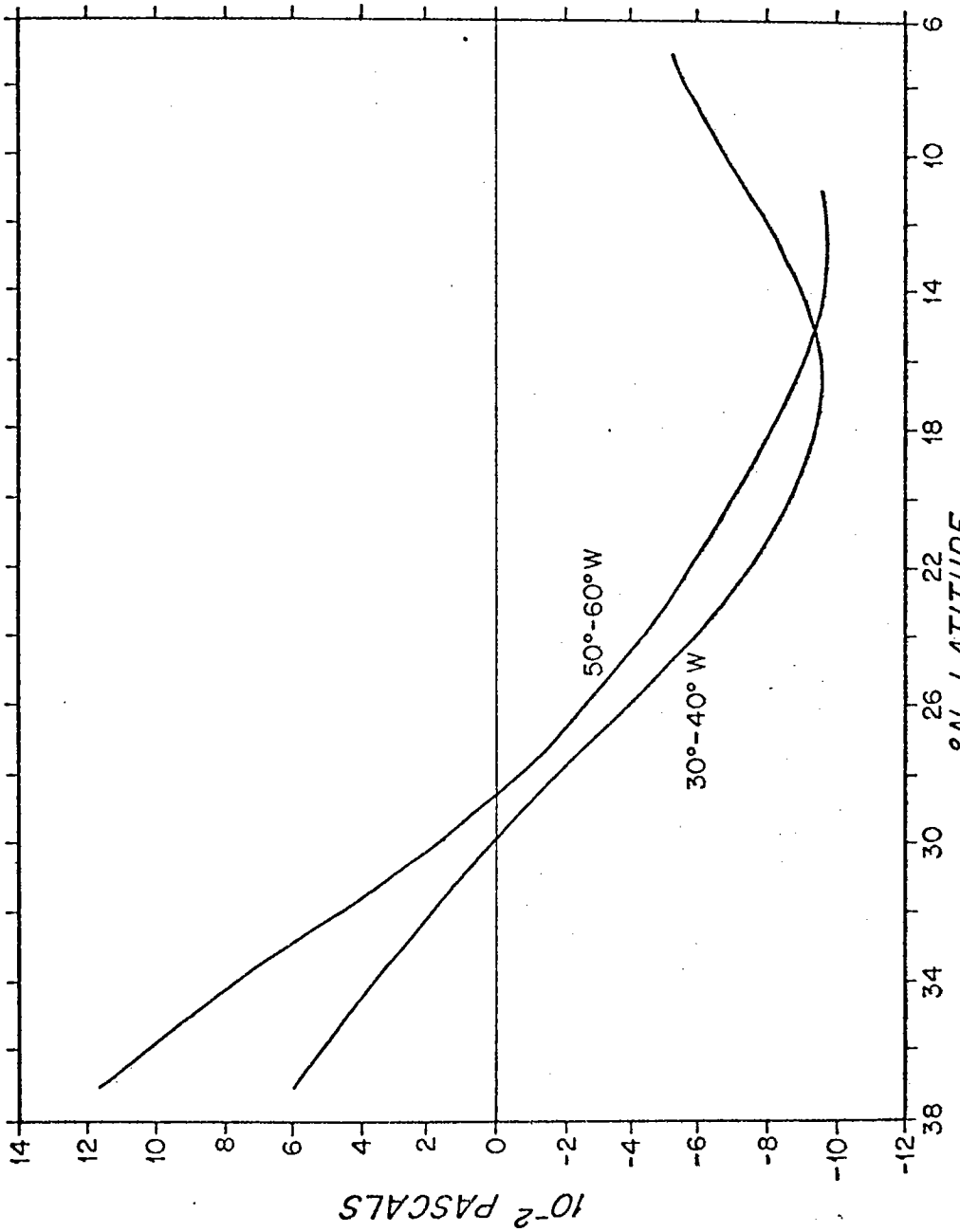

Figure 4.A-1a. Mean zonal wind stress between 30° and 40°W and between 50° and 60°W.

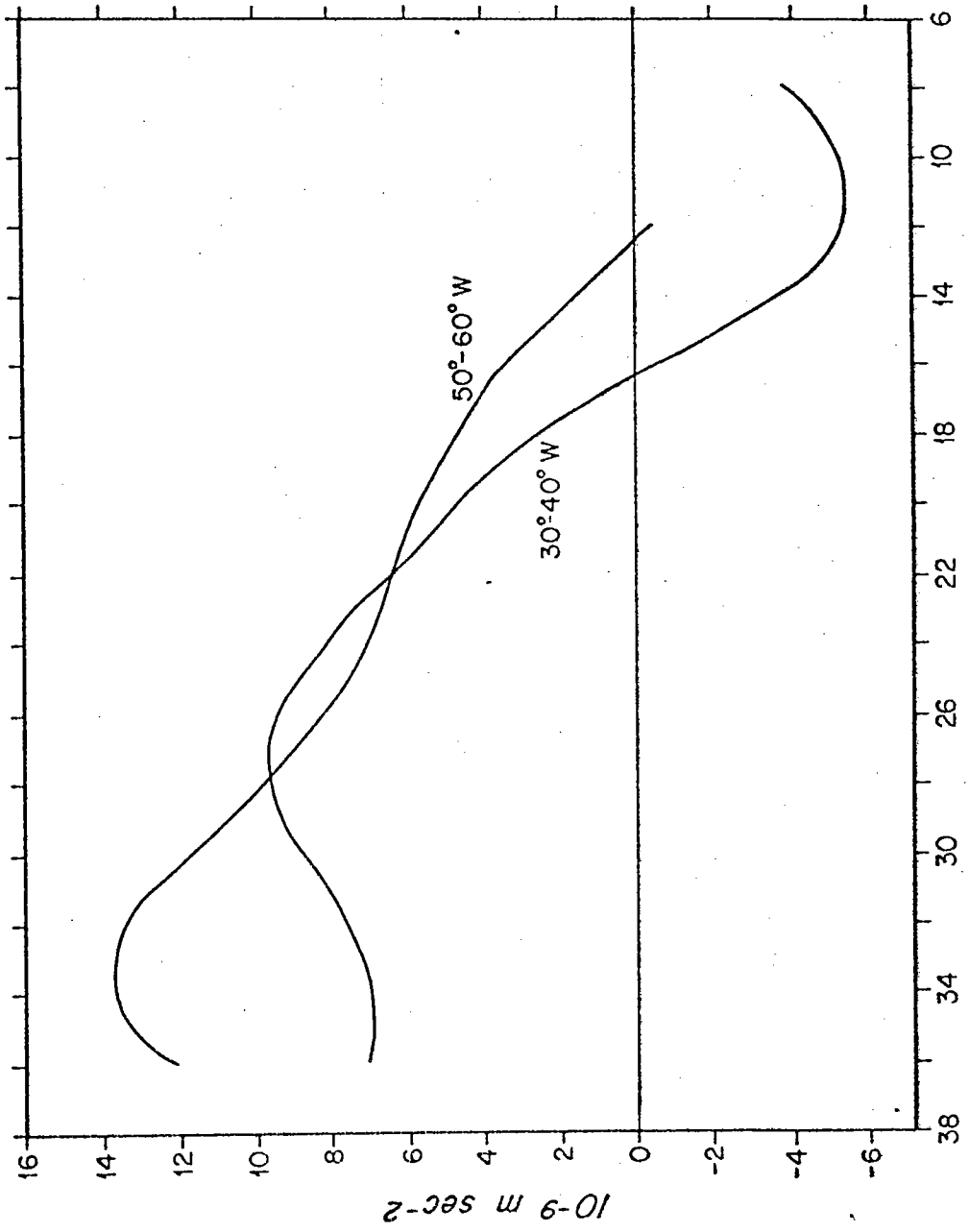

Figure 4.A-1b. Mean τ_y^x/ρ_o, 30°-40°W and 50°-60°W.

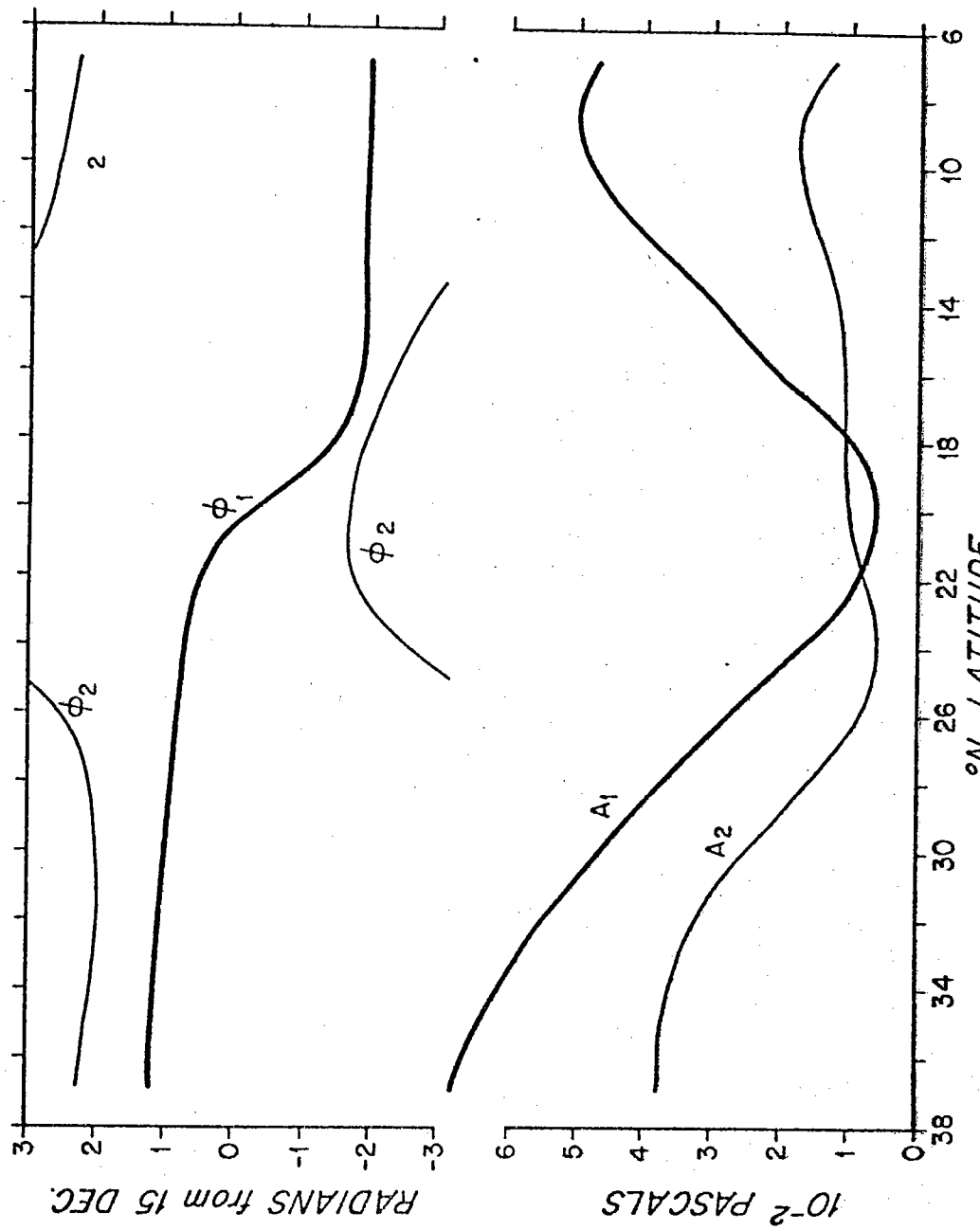

Figure 4.A-2a. Annual and semiannual components of zonal stress: $\tau^x = \overline{\tau^x} + A_1\cos(\omega t-\phi_1) + A_2\cos(2\omega t-\phi_2)$, $\omega = 2\pi/1$

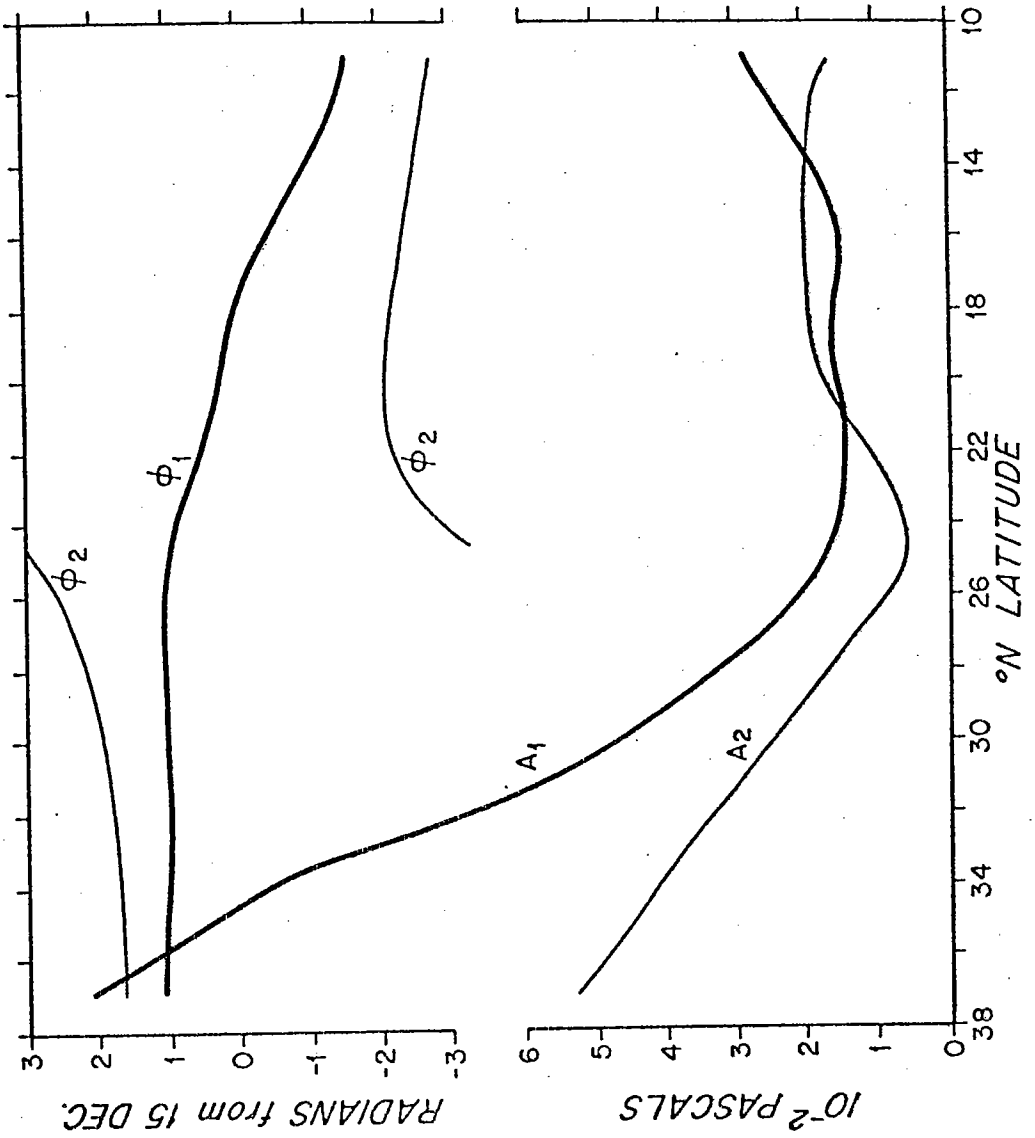

Figure 4.A-2b. Annual and semiannual components of zonal stress, 50°-60°W.

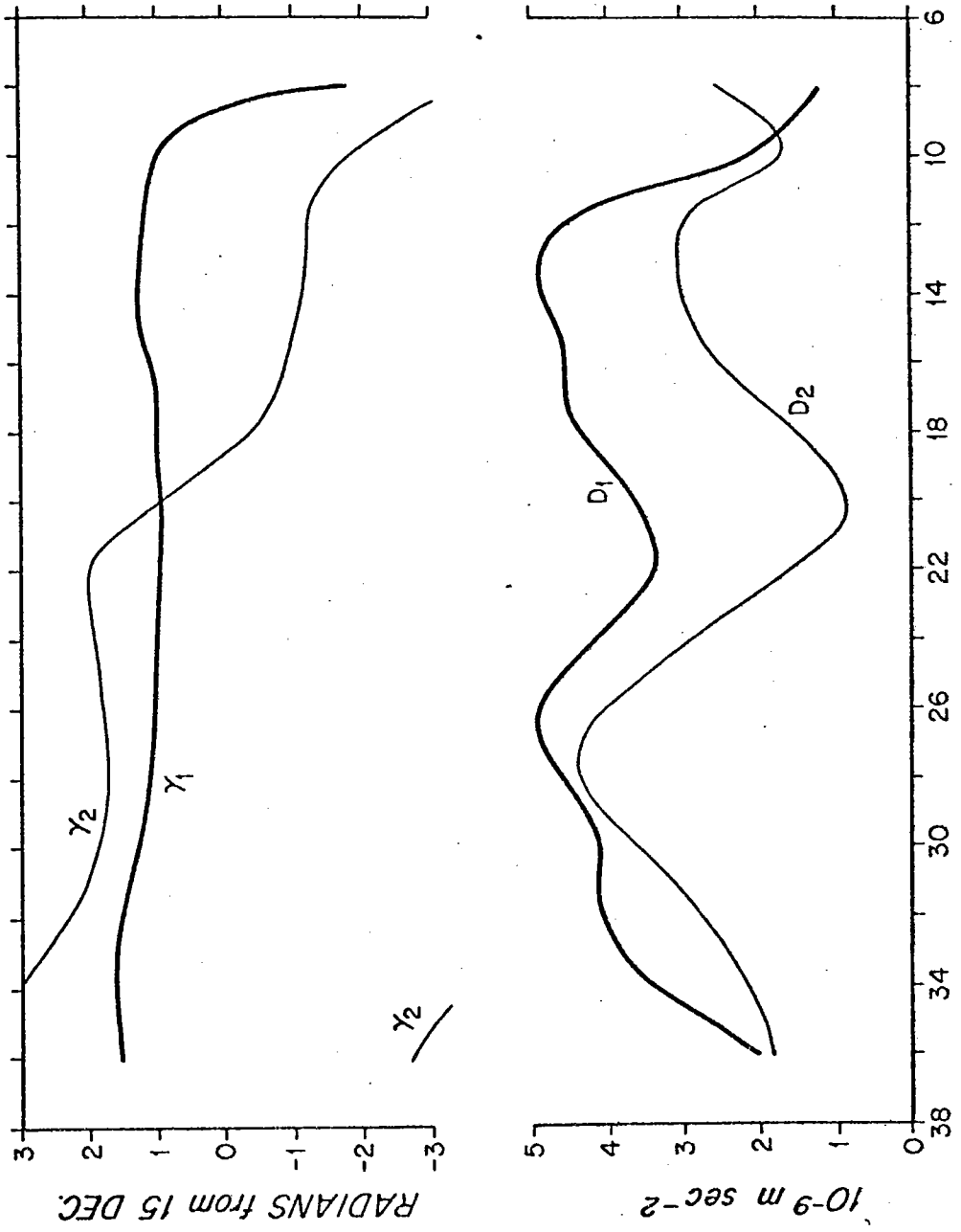

Figure 4.A-3a. Annual and semiannual components of $1/\rho_o \tau_y^x$ = $1/\rho_o \bar{\tau}_y^x + D_1 \cos(\omega t - \gamma_1) + D_2 \cos(2\omega t - \gamma_2)$, 30°-40°W.

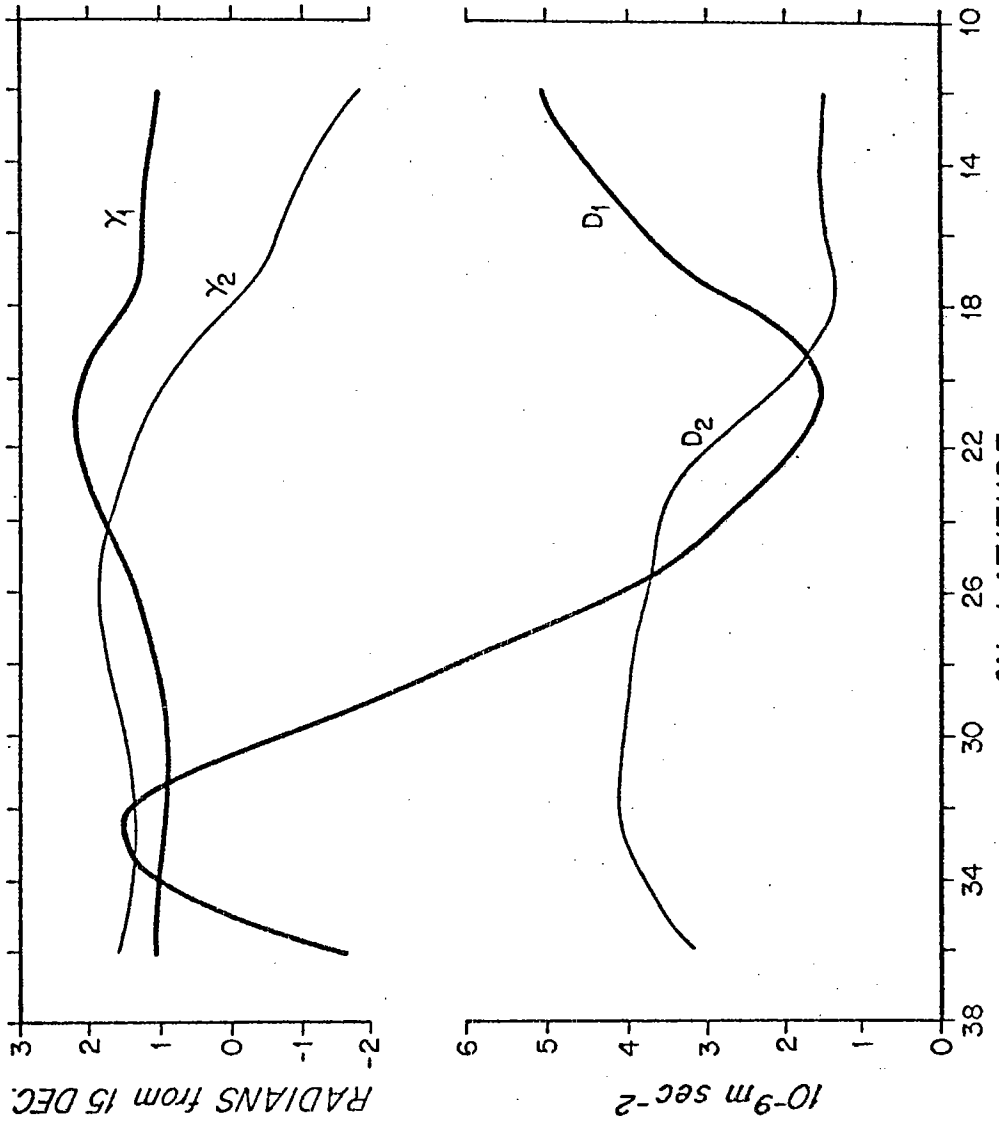

Figure 4.A-3b. Annual and semiannual components of $1/\rho_o\ \tau_y^x$, 50°-60°W.

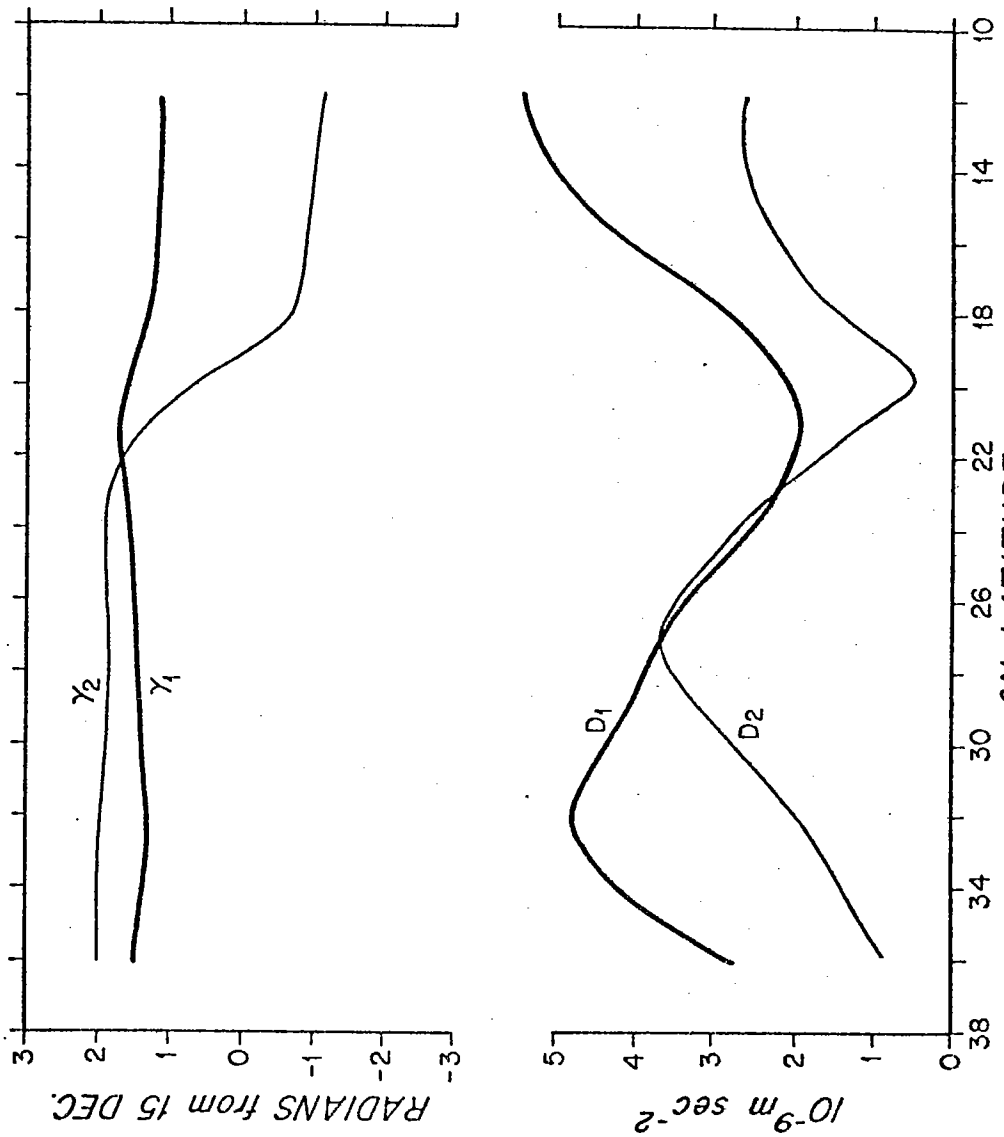

Figure 4.A-4. Annual and semiannual components of -∇xτ averaged from 20°-60°W.

some zonal variation in the mean stress and the annual and semiannual components, the general characteristics are independent of longitude. Note in particular the amplitude minimum of both the annual and semiannual harmonics of both τ^x and τ^x_y at around 20°N. The tradewinds are indeed remarkably steady. This feature is increasingly prominent toward the west, reaching its greatest intensity in the Caribbean.

In spite of the changes in amplitude, the phase of the annual component of τ^x_y is nearly constant over the entire North Atlantic from about 12° to at least 36°N. The annual forcing has a standing wave meridional structure with two main length scales: the larger scale of perhaps 1000 km over which the phase is constant; and the smaller scale of about 350 km over which the amplitude varies.

The results of Chapters II and III indicate that east of the Antilles the barotropic response of the ocean should be in accord with the Sverdrup balance. The annual cycle of Sverdrup transport calculated from the averaged stress curl (Figure 4.A-4) and the width of the North Atlantic is shown in Figure 4.A-5. The maximum southward interior transport occurs at roughly the same time, late February to mid-March, over the entire range of latitude for which the calculation was made. The amplitude varies from a maximum of 16 Sverdrups at 32°N to a minimum of 4.6 Sverdrups at 20°N. These are sizeable transports, but since they are

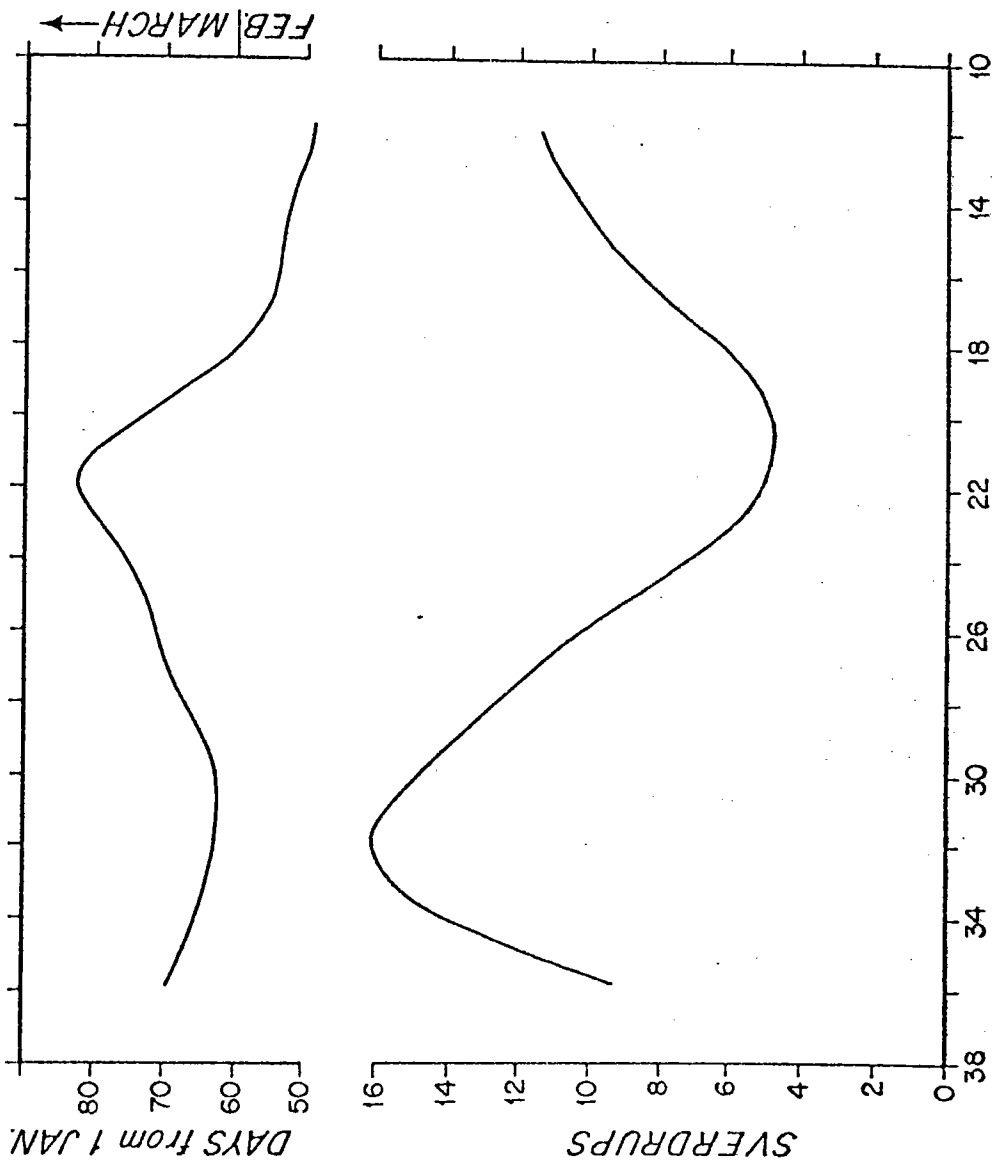

Figure 4.A-5. Predicted annual cycle of Sverdrup transport integrated across the North Atlantic. Phase given is the time of maximum southward interior transport.

barotropic they represent only small speeds. In the interior, 16 Sverdrups distributed over 4000 km width and 4000 m depth implies a mere 10^{-3}m sec^{-1} meridional speed. At the western boundary, if the scale of the variable boundary current were 10 km, the short wave scale, speeds of .4 m sec^{-1} would be found. However, it must be emphasized that the linear theory considered in this thesis cannot be expected to accurately predict the characteristics, other than total transport, of the periodic western boundary flow.

The predictable part of the baroclinic response to the wind stress curl is the thermocline deformation due to Ekman pumping. In Figure 4.A-6 we see the zonally averaged amplitude and phase of the annual Ekman pumping. The phase of thermocline displacement is three months later than the phase of w. Hence the thermocline is deepest everywhere in late May to early June. However, the amplitude increases southward from 20°N, so the maximum predicted strength of the North Equatorial Current down to 12°N is in late November to early December. The amplitude of the current speed predicted at 15°N is $.8 \times 10^{-2}$ m sec^{-1}. This amplitude increases rapidly to the south and quickly becomes negligible to the north. Indeed, since the thermocline displacement at 20°N is only about 2 m, it is clear that this baroclinic response is of no importance there. South of 15°, where the

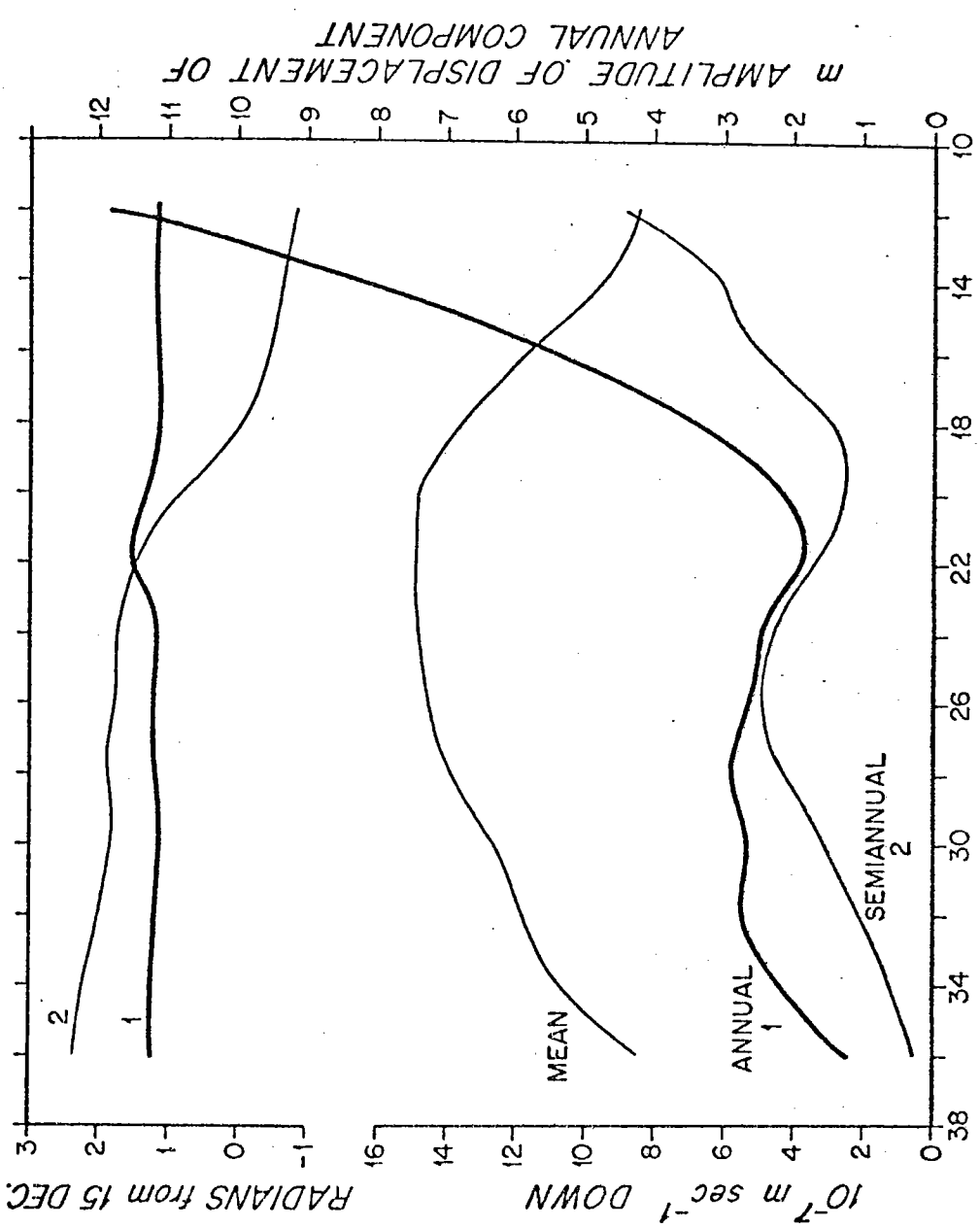

Figure 4.A-6. Mean, annual, and semiannual components of Ekman velocity averaged from 20°-60°W. Phases are times of maximum downward velocity. The phase for the maximum downward displacement (right hand amplitude scale) is $\pi/2$ radians (3 months) later than the annual velocity phase.

response becomes substantial, the baroclinic free wave length becomes comparable to the ocean width, so the free wave is an important part of the complete baroclinic response to the wind variations.

The barrier model of Chapter III applied to the Antilles Arc implies that the barotropic flow indicated in Figure 4.A-5 is not the transport one should expect to find in the Florida Straits. The transport of the Florida Current must equal the transport of primarily warm water over the Antilles Arc. The barrier model predicts that this transport should have the same phase as the Sverdrup transport but should be reduced to a quarter or less of its original amplitude. Furthermore, since the northernmost major passage into the Caribbean is the Windward Passage at about 20°N, it is the upper layer transport at this latitude that can be expected to pass through the Florida Straits. Hence we expect the annual cycle of North Atlantic windstress curl to result in a Florida Current transport cycle with an amplitude of the order of one Sverdrup and a maximum northward flow in early March. In the deeper water outside the Antilles Arc we expect to find an annual western boundary transport of up to ten Sverdrups below the thermocline with the same early March phase. North of the Florida Straits we expect the depth-integrated annual transport amplitude to reach as much as 16 Sverdrups with essentially the same phase as elsewhere.

This transport should be distributed uniformly with depth but might occur in different places at different depths due to topography, mean currents, and nonlinearity.

Having used wind observations and theory to predict annual current cycles, let us survey the observations of annual North Atlantic current variations.

B. North Atlantic Currents

The only direct observations of the annual cycle of western boundary current transport are the work of Richardson, Schmitz, and Niiler (1969) and Niiler and Richardson (1973), with additional more recent measurements by Brooks (1977). Transport of the Florida Current was measured directly by the free-drop method (Richardson and Schmitz, 1965) at 13 stations on a transect from Miami to Bimini. Niiler and Richardson (referred to as NR) analyzed 75 such transects made from 1964 to 1971 in which enough stations were successfully completed to allow calculation of the total transport of the Florida Current. The mean value was 29.5 Sverdrups. The least-squares fit to the annual harmonic yielded an amplitude of 4.1 Sverdrups with a maximum northward transport in early June. The transport variation was largely barotropic, although the variability was somewhat smaller in the thermocline than above or below it.

In Figure 4.B-1 we see the measurements of NR combined with those of Brooks (detided, taken from Figure 18 in

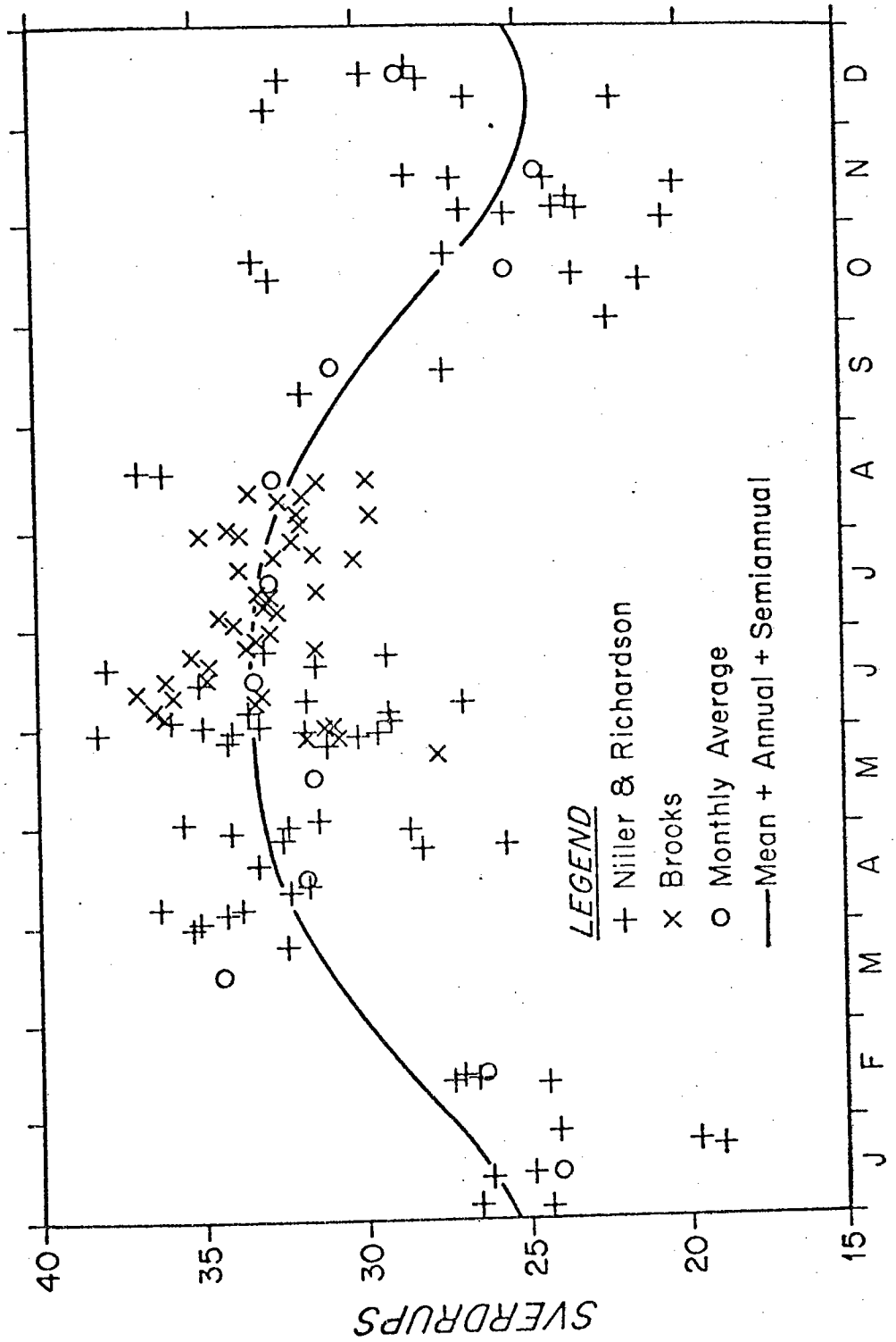

Figure 4.B-1. Florida Current transport observations. Solid line is the sum of the mean and the annual and semiannual harmonics of the monthly averages.

Wunsch and Wimbush, 1977). Monthly averages are also shown, along with the mean, annual, and semiannual harmonics calculated from the monthly means. The addition of the Brooks data, which fill a summer gap in the NR measurements, makes no significant difference in the calculated annual cycle. Here the cycle has amplitude 4.35 Sverdrups and phase 2.76 radians from 1 January, compared with NR's stated phase of 2.7 radians.

During most of a 26 month period from late 1972 to late 1974, a deep current meter mooring was maintained in the Florida Current near the edge of the Miami Shelf, due east of Miami. Düing, Mooers, and Lee (1977) computed a least-squares fit to the annual component of variation of meridional speed from this time series, and found an amplitude of 4.5 cm/sec with a maximum in late April. This is about 7 weeks earlier than NR's transport maximum, both for the current as a whole and for NR's station 5, which is near the current meter mooring. The phase difference might be due to the shortness of the current meter records; the time of maximum transport may vary widely from year to year. Error may have been introduced by variations in the depth and location of the mooring, which was reset 8 times during the experiment. On the other hand, there might be real phase differences within the current. The moored current meters were in the main thermocline where the annual current

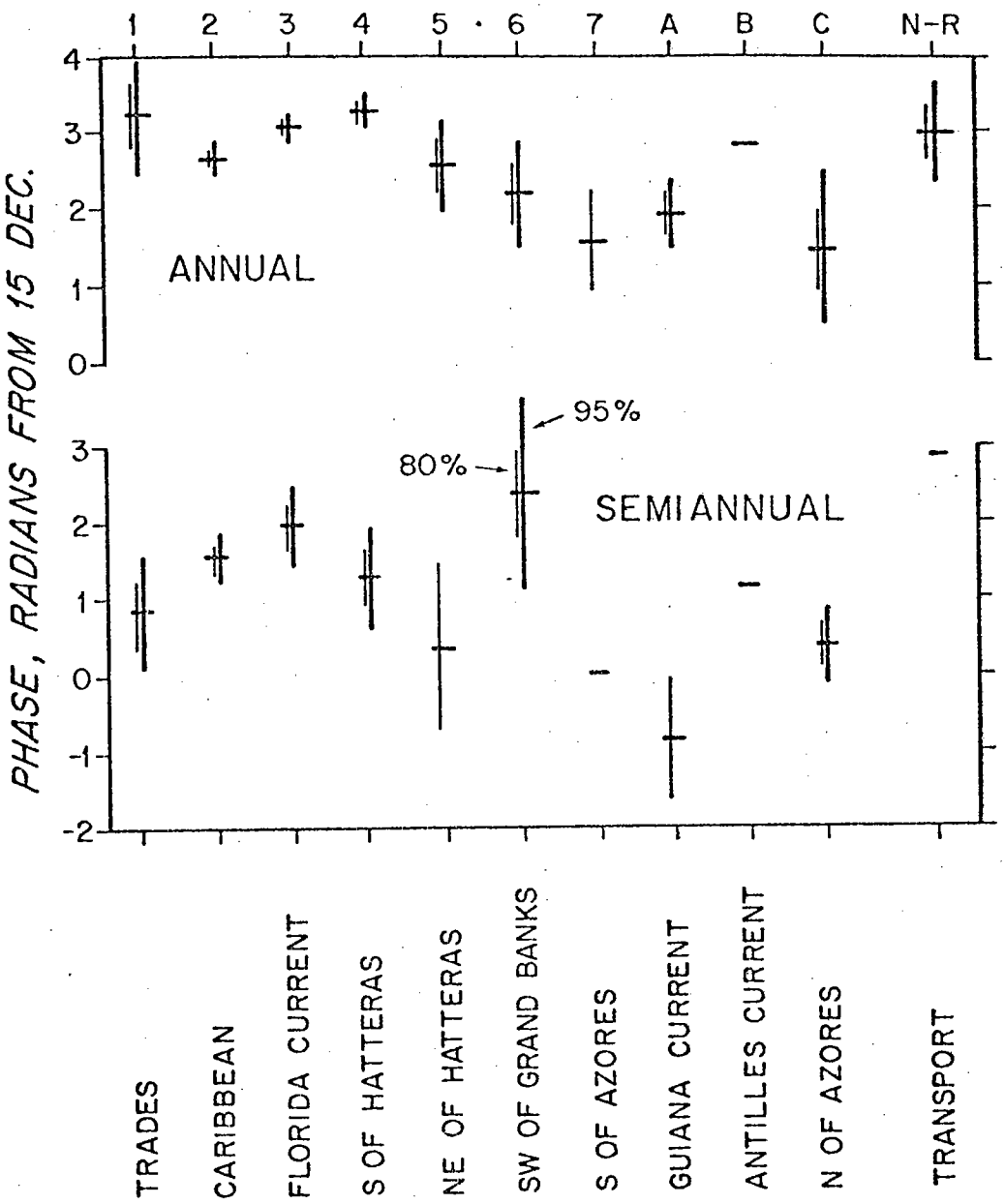

Figure 4.B-2. Times of maximum speed in various parts of the Gulf Stream System from Fuglister (1951), and Florida Current transport from Niiler and Richardson (1973).

speed variations are at a minimum, so a different phase there might have little influence on the phase of the total transport.

The work of Fuglister (1951) gives a valuable picture of the annual cycle of surface currents in various parts of the Gulf Stream System. Fuglister used ship drift reports to calculate monthly average surface currents in each of ten regions. Table 4.B-1 gives the mean and the annual and semiannual harmonics of the speed for each region. Figure 4.B-2 shows the phases of the harmonics with 80% and 95% confidence limits (calculated using Student's t distribution with the total noise variance estimated from the sample variance at periods shorter than semiannual). The location of the regions are also indicated in Figure 4.B-2.

The surface current variations form a rather coherent pattern. In most of the regions the annual amplitude is about 10% of the mean, a bit less than the 14% ratio found in the Florida Current transport. The exceptions are the Guiana Current, with a 31% ratio, and the Antilles Current, with a very small mean and a probably insignificant annual variation. From the Tradewind region outside the Caribbean to the area south of Cape Hatteras the maximum occurs in early summer. With the exception of the Tradewind region, the phase becomes progressively later downstream from the Guiana Current to south of Hatteras. Measuring distances

along the stream, we find phase speeds of about 40 km/day from the Guiana Current to the eastern Caribbean, 120 km/day from there to the Florida Straits, and 60 km/day to south of Hatteras. The meridional phase speed between the Caribbean and the Florida Straits is also 60 km/day. Progressing from south of Hatteras to north and south of the Azores, the phases become earlier again. These phase differences, to the extent that they are real, could arise in any of a number of ways: they could represent local response to a traveling forcing pattern; local forcing in one region could produce a wave-like disturbance propagating away from the source; or two large-scale responses with different phases and varying amplitudes could be summed to give a varying phase.

Since ship drift estimates are not ideal measures of surface currents, one might question the significance of Fuglister's results. As was pointed out by Fuglister, there is some correlation between the downstream wind component and the current speed in the Tradewind and Caribbean regions, although not in most of the other areas. However, the annual wind amplitude is about the same on either side of the Antilles, while the surface current amplitude is larger by a factor of three in the Caribbean, and the mean current is larger by a factor of two. Hence the ship drifts cannot easily be attributed to the windage of the ships or similar errors, and must be supposed to represent the actual surface currents.

Table 4.B-1

Mean, annual, and semiannual components of Fuglister's surface currents, with phase measured in radians from Dec. 15. Speed in miles/day (1 mile/day = 2.14×10^{-2} m sec^{-1}) is $\bar{A} + A_1 \cos(\omega t - \theta_1) + A_2 \cos(2\omega t - \theta_2)$ where $\omega = 2\pi/1$ year.

Region	$\bar{A}$	A_1	θ_1	A_2	θ_2	A_1/A_2	$A_1/\bar{A}$
1	7.6	0.65	-3.0	0.72	0.82	0.9	0.09
2	16.6	2.04	2.69	0.66	1.52	1.2	0.12
3	59.0	6.51	3.07	2.91	1.93	2.2	0.11
4	43.2	5.19	-3.02	1.82	1.26	2.9	0.12
5	22.2	1.56	2.57	0.57	0.36	2.7	0.07
6	12.1	0.97	2.21	0.63	2.35	1.5	0.08
7	3.8	0.30	1.57	0.13	0	2.3	0.08
A	22.2	6.86	1.95	2.27	-0.84	3.0	0.31
B	4.4	0.17	2.84	0.24	1.11	0.6	0.04
C	4.2	0.39	1.49	0.70	0.36	0.6	0.09

Another indication of a seasonal cycle in the Gulf Stream System is the variation in path length of the Loop Current reported by Maul (1977). Sometimes the Loop bulges nearly 1000 km into the Gulf and at other times it flows almost directly from Yucatan Strait to the Florida Straits. Shortening of the path length is often accomplished through the detachment of a warm eddy that drifts west into the Gulf. Eddy formation has been observed at various times during the year. However, on the basis of historical data and a one year series of measurements Maul suggests that on the average the eddy formation is part of an annual cycle that is in phase with the Florida Current transport variation. The maximum growth rate of the area enclosed by the Loop is concurrent with the maximum Florida Current transport. Furthermore, Maul calculates that the excess flow of warm water into the Gulf through the Yucatan Strait required while the Loop is growing is about 4 Sverdrups. Since the sill depth of the Florida Straits is 800 m while that of Yucatan Strait is 2000 m, one would expect the compensating cold water outflow to go primarily into the Caribbean. However, part of it may go northeast through the Florida Straits, accounting for NR's observation of increased annual transport variability below the thermocline.

The currently available observations of the Loop Current are inadequate to establish the phase of the annual cycle

with any certainty. It is important to note that the growth and decay of the Loop Current can affect the temperature distribution of the Florida Current outflow, but, given some particular flow through the Antilles into the Caribbean, the Loop cannot affect the total transport of the Florida Current. In other words, at annual periods the western boundary current system is barotropically nondivergent; but features such as the Loop Current can lead to divergence, and consequent phase changes, in the baroclinic boundary transport.

C. Relation of Observations to Theory

The general picture that emerges from the observations discussed in the previous section is of an annual current cycle that is fairly similar over a large portion of the Gulf Stream System. The amplitude of the fluctuations as a fraction of the mean is roughly constant, and the phase varies slowly from place to place. The maximum anticyclonic circulation occurs in late spring to early summer. The fluctuations are observed in the surface currents and must be largely confined to the warm water; at least in the latitudes south of Cape Hatteras the surface currents in deep water would imply enormous transports if they were barotropic.

The theory that has been presented predicts a barotropic western boundary transport varying from 4 to 16

Sverdrups with maximum anticyclonic circulation in late winter to early spring. The surface currents and Florida Current transport implied by this barotropic flow are modest. Hence, the observations neither confirm nor refute the theory. Some fraction, perhaps 20%, of the observed currents might be due to the predicted barotropic transport. With the data now available there appears to be no way to test this idea. It is consistent, however, with the observation that the phases of Fuglister's surface currents become earlier downstream of Hatteras as the predicted Sverdrup transport increases.

Although we discussed (in section 2.B) the physics of baroclinic western boundary current generation by longshore windstress, we are unable to make a definite prediction based on this theory. A crucial constant of integration cannot be determined, and there is also an unknown contribution from a baroclinic free wave. However, the theory suggests that western boundary transport generated by longshore windstress must eventually leave the coast as Ekman transport. Now, the annual amplitude of meridional windstress in the North Atlantic is about .05 Pascals, so with a mean $f = .7 \times 10^{-4} sec^{-1}$, a coastline of 5600 km would be required to distribute the annual transport variation of the Florida Current. Therefore, although meridional windstress may play a role in forcing the observed seasonal

variations, it seems unlikely that it can directly account for all of the Florida Current transport cycle.

Chapter V

Conclusion

In the introduction we stated that this thesis was concerned with two related questions: the annual cycle of currents driven by the annual cycle of the winds, and the influence of major topographic features on this annual cycle of currents. Let us now review the progress we have made toward answering these questions.

In Chapter II we developed a consistent set of scaled equations for a linear two-layer model with topography. These equations were then solved for the special case without topography. The model reproduces the quasi-steady barotropic Sverdrup response predicted by Gill and Niiler (1973) and the forced and free baroclinic response found by White (1977). It is shown that the western boundary current produced by frictional damping of short Rossby waves is of sufficiently small zonal scale to be nearly nondivergent horizontally in each layer. This implies that the transport in each layer depends only on the interior zonal transport into the boundary in that layer. However, as we noted in Chapter IV, this may not always be true in the ocean; indeed the Loop Current is a counterexample in which the complications of geography, nonlinearity, and mean flow lead to behavior far from the predictions of our simple theory.

In the first part of Chapter III we present a simple model of a high steep ridge. We find a striking result in

the limit of low frequency: the lower-layer barrier does not affect the upper layer flux across the barrier. This is due to the properties of short Rossby waves. At low frequencies their zonal scale becomes so short that the vorticity equations are dominated by a balance between the beta effect and the relative vorticity term. The coupling term is relatively small, so the upper layer east of the barrier does not "feel" the presence of the barrier.

Section B of Chapter III is devoted to the dynamics of flow over a constant east-west slope. We find that the vertical mode structure is the same for both long and short waves of a given frequency and meridional scale. As slope increases, the barotropic and baroclinic modes evolve into upper layer and lower layer modes. When the slope is down to the east, the barotropic mode becomes an upper (lower) layer mode if phase propagation is to the north (south). The reverse is true if the slope is down to the west. The upper layer mode acts much like a baroclinic mode over a flat bottom. The lower layer mode acts like homogeneous flow with total depth equal to the lower layer depth; in the lower layer long wave the flow is quasi-steady along geostrophic contours.

In Section C of Chapter III we model topographic features as sequences of regions of constant slope. The appropriate free waves are used to meet matching conditions at the

junctions. Unless the slope is very steep, so that the lower layer undergoes an O(b) change in thickness in a distance comparable to the short wave scale, the amplitudes of the short waves are small. At each junction the long waves are translated from one set of modes to another but continue to travel as long waves. Scattering of barotropic energy into baroclinic energy and vice versa can result from the different phase speeds of the different types of long waves. On the other hand, when the slope is steep and short waves are excited, a junction reflects wave energy. A steep ridge therefore can act as a lower layer barrier even if it does not extend to the interface.

Section D of Chapter III consists of a straightforward extension of the two-layer barrier model to a multilayer fluid. It is found that a barrier extending to an intermediate interface produces a small increase in amplitude and lag in phase in the average flow over the barrier due to a barotropic incident motion. Hence, the behavior found in the two-layer model is also found with more general stratification, with minor modifications.

The models of topography suggest that outside the island arcs the predictions of the simplest flat bottom theory are adequate. Neither the eastern boundary slope nor the mid-ocean ridge model makes a significant difference. The barrier model, on the other hand, implies that only a

small fraction of the interior annual Sverdrup transport should be returned through the Florida Straits. This prediction serves to make the theory more nearly consistent with the Florida Current observations; the predicted transport variation of a Sverdrup or less, with maximum in March, could be part of the observed four Sverdrups with maximum in June. The overall conclusion to be drawn from a comparison of theory and observations is that although the theory may be correct as far as it goes, it does not go far enough. It is inadequate to explain the observations. The inadequacy may be of two sorts. It may be that a better model of the circulation driven by the wind is needed; or it may be that the observed current cycle is driven by something other than the winds, presumably thermohaline forcing.

Let us survey the limitations of the theory that has been presented:

Some of the calculations of topographic effects were done by stretching the approximation of constant coefficients beyond its validity. However, we argue that although the calculations are inaccurate in detail they give useful qualitative information. Note also that in the case of the eastern boundary and ridge-barrier models, the place where the approximation of constant h is worst is near the boundary and near the barrier, respectively. But there the lower layer upslope flow goes to zero anyway, so the error introduced by the approximation is reduced.

The model is linear. This simplification should lead to no significant errors in the interior regions where the zonal scales are those of long waves or of topogrpahy such as the Mid-Atlantic Ridge. The particle velocities due to annual oscillations in the ocean interior are of the order of .5 cm sec^{-1}, so advective effects there are minimal. On the other hand, in the western boundary region the zonal particle velocities would be of the same order as the zonal phase speed of the short waves, so nonlinearity would play a role in the dynamics. In regions of steep slope and at a lower layer barrier, where short waves are generated, nonlinearity would likewise be expected. However, the main result of the lower layer barrier model depends on the scales of the short waves rather than in the details of the dynamics. As long as that scale is small compared to the radius of deformation, the upper layer will be only weakly disturbed above and immediately to the east of the barrier. It remains to be determined whether realistic nonlinearity would so drastically alter the short wave scale as to alter the behavior of the barrier model.

There is no mean flow. A mean flow would not alter the physics of the essential interior response. It might be important at the barrier and at the western boundary. Note, however, that a mean westward flow over the barrier would help prevent short wave "information" from propagating east

in the upper layer, so the behavior of the barrier model should remain about the same.

The model is periodic in the north-south direction. It cannot take very large-scale phenomena into account, and there is no equatorial region. The seriousness of this limitation is unclear.

The effect of longshore winds cannot be calculated explicitly. There is some indication from numerical experiments (Anderson, 1978; Bryan, 1978) that meridional winds may account for the surface currents observed by Fuglister (1951), although we have argued that they probably cannot account for the Florida Current transport observations.

The stratification is two-layer rather than continuous. This limitation is probably not very important. Hall (1976) has shown that scattering by topography is similar in continuous and two-layer systems; and the momentum and vorticity equations for the barotropic and first baroclinic modes without topography are identical in continuous and two-layer systems.

Only one class of topographic effects has been considered. The effect of rough topography needs further investigation. Also, the flow in regions of closed geostrophic contours such as the Azores may be qualitatively quite different from the regime in regions of open contours that have been considered here. We argue, however, that due to the predominantly zonal

group velocities of annual Rossby waves, the remote effects of the circulation in closed contour regions should be largely confined to the latitudes of the closed contour regions.

The geography is highly idealized. There may be important effects of the actual configuration of the Antilles, the Caribbean, and the Gulf of Mexico.

There is no thermal forcing. In view of the large seasonal heat flux in the decay region of the Gulf Stream, this may be the most important limitation of the theory.

The above list of limitations of the present theory serves also to suggest areas where work might be done in the future. Many areas will be accessible only through numerical modeling. Examples are realistic geography and topography, and probably nonlinearity. Some aspects of the effects of mean flows and rough bottom topography may be found analytically. Progress may also be possible in analytic modeling of the effect of thermohaline forcing in the Gulf Stream decay region. Such work should include a theory of the propagation of annual disturbances along the western boundary in the presence of mean flow.

There is one prediction of the present theory that may be subject to observational verification. The deep oscillating western boundary transport, both outside the Antilles and along the continental slope, could involve substantial velocities (over .1 m sec^{-1}) and might be detected by a

monitoring program lasting many years. The velocities would be large only if this current were of small lateral dimension (as it is in simple linear theory) in which case the placement of current meters becomes critical. Hence we cannot expect to see this observational test of the theory in the near future.

References

Anderson, D. L. T. (1978) Seasonal adjustment in the equatorial Atlantic, unpublished abstract.

Anderson, D. L. T., and A. E. Gill (1975) Spin-up of a stratified ocean, with applications to upwelling Deep-Sea Res. 22, 583-596.

Brooks, I. H. (1977) High frequency fluctuations in the transport of the Florida Current, in preparation.

Bunker, A. F. (1976) Computations of surface energy flux and annual air-sea interaction cycles of the North Atlantic Ocean, Mon. Weather Rev. 104, 1122-1140.

Bryan, K. (1978) Personal communication.

Düing, W. O., C. N. K. Mooers, and T. N. Lee (1977) Low-frequency variability in the Florida Current and relations to atmospheric forcing from 1972-1974, J. Mar. Res. 35, 129-161.

Foo, E.-Chien (1976) M.Sc. Thesis, University of Miami, unpublished manuscript.

Fuglister, F. C. (1951) Annual variations in current speeds in the Gulf Stream System, J. Mar. Res. 10, 119-127.

Gill, A. E., and P. P. Niiler (1973) The theory of the seasonal variability in the ocean, Deep-Sea Res. 20, 141-178.

Greenspan, H. P. (1969) The Theory of Rotating Fluids, Cambridge University Press.

Hall, R. E. (1976) Scattering of Rossby Waves by Topography in a Stratified Ocean, Ph.D. thesis, U.C.S.D.

Leetmaa, A. (1978) Fluctuating winds: an energy source for mesoscale motions, J. Geophys. Res. 83, 427-430.

Leetmaa, A., and A. F. Bunker (1978) Updated charts of the mean annual windstress, convergences in the Ekman layers, and Sverdrup transport in the North Atlantic, J. Mar. Res. 36, 311-322.

Lighthill, M. J. (1969) Dynamic response of the Indian Ocean to the onset of the Southwest Monsoon, Phil. Trans. Roy. Soc. London A 265, 45-92.

Lighthill, M. J. (1971) Time-varying currents, Phil. Trans. Roy. Soc. London A 270, 371-390.

Longuet-Higgins, M. S. (1964a) On group velocity and energy flux in planetary wave motions, Deep-See Res. 11, 35-42.

Longuet-Higgins, M. S. (1964b) Planetary waves on a rotating sphere I, Proc. Roy. Soc. London A 279, 446-473.

Longuet-Higgins, M. S. (1965a) The response of a stratified ocean to stationary or moving wind-systems, Deep-Sea Res. 12, 923-973.

Longuet-Higgins, M. S. (1965b) Planetary waves on a rotating sphere II, Proc. Roy. Soc. London A 284, 40-68.

Maul, G. A. (1977) The annual cycle of the Gulf Loop Current Part I: Observations during a one-year time series. J. Mar. Res. 35, 29-47.

Meyers, G. (1975) Seasonal variation in transport of the Pacific North Equatorial Current relative to the wind field, J. Phys. Ocean. 5, 442-449.

Munk, W. H. (1950) On the wind-driven ocean circulation, J. Meteor. 7, 79-93.

Niiler, P. P., and W. S. Richardson (1973) Seasonal variability of the Florida Current. J. Mar. Res. 31, 144-167.

Pedlosky, J. (1965a) A study of the time-dependent ocean circulation, J. Atmos. Sci. 22, 267-272.

Pedlosky, J. (1965b) A note on the western intensification of the ocean circulation, J. Mar. Res. 23, 207-209.

Phillips, N. A. (1966) Large-scale eddy motions in the western Atlantic, J. Geophys. Res. 71, 3883-3891.

Rhines, P. B. (1969) Slow oscillations in an ocean of varying depth, Part I: Abrupt topography, J. Fluid Mech. 37, 161-190.

Rhines, P. B. (1970) Edge, bottom, and Rossby waves in a rotating stratified fluid, Geophys. Fluid Dyn. 1, 273-302.

Richardson, W. S., and W. J. Schmitz (1965) A technique for the direct measurement of transport with application to the Straits of Florida, J. Mar. Res. 23, 172-185.

Richardson, W. S., W. J. Schmitz, and P. P. Niiler (1969) The velocity structure of the Florida Current from the Straits of Florida to Cape Fear, Deep-Sea Res. 16, 225-231.

Rooth, C. (1978) Personal communication.

Suarez, A. A. (1971) The Propagation and Generation of Topographic Oscillations in the Ocean, Ph.D. Thesis, MIT-WHOI.

Veronis, G. (1970) Effect of fluctuating winds on ocean circulation, Deep-Sea Res. 17, 421-434.

Veronis, G., and H. M. Stommel (1956) The action of variable wind stresses on a stratified ocean, J. Mar. Res. 15, 43-75.

Welander, P. (1968) Wind-driven circulation in one- and two-layer oceans of variable depth, Tellus 20, 1-16.

Welander, P. (1969) Effects of planetary topography on the deep-sea circulation, Deep-Sea Res. Supp. to 16, 369-391.

White, W. B. (1977) Annual forcing of baroclinic long waves in the tropical North Pacific Ocean, J. Phys. Ocean. 7, 50-61.

Wunsch, C., and M. Wimbush (1977) Simultaneous pressure, velocity, and temperature measurements in the Florida Straits, J. Mar. Res. 35, 75-104.